COMPARISON OF ALUMINIUM GRAIN REFINED AND VANADIUM GRAIN REFINED SPRING STEELS FOR THE MANUFACTURE OF HIGHLY STRESSED AUTOMOTIVE COIL SPRINGS

Firoz Limalia

A dissertation submitted to the Faculty of Engineering and the Built Environment, University of the Witwatersrand, in fulfillment of the requirements for the degree of Master of Science in Engineering

Johannesburg, 2005

Declaration

I declare that this dissertation is my own, unaided work. It is being submitted for the Degree of Master of Science in Engineering in the University of the Witwatersrand, Johannesburg. It has not been submitted before for any degree or examination in any other University.

_____

_____ day of _____ of _____

Abstract

The selection of a particular steel grade for an application is extremely important to ensure that the final components have a long serviceable life. The chemical compositions of the steels are critical, and minor changes in chemistry can make substantial differences. Aluminium and vanadium are used in heat treatable steels as grain refining agents. These elements affect the properties of the steels.

Two steels with identical chemical composition except for the aluminium and vanadium additions were comparatively tested to determine the better steel for a particular automotive coil spring. The tests included mechanical testing and on site fatigue testing. Fatigue resistance is extremely important especially for automotive coil springs. The mechanical properties revealed superior tensile strength in the vanadium grain refined spring steel while the aluminium grain refined spring steel had superior ductility and fatigue resistance.

Dedication

For my wife Fathima, Thank you for being there.

TABLE OF CONTENTS

8

9

LIST OF FIGURES

17

LIST OF TABLES

LIST OF SYMBOLS

Absolute temperature	T
Activation energy	Q
Activity of the dissolved microalloy	$a_{[M]}$
Activity of the constituent phase	$a_{(MX)}$
Activity of the dissolved interstitial	$a_{[X]}$
Aluminium present as Al_2O_3	$Al_{Al_2O_3}$
Austenite	γ
Austenite-ferrite boundary	γ/α
Austenite grain boundary area/unit volume	S_V
Compressive residual stress	$-\sigma_r$
Equilibrium constant	k_s
Equilibrium constant for aluminium/nitrogen combination	$K_{[Al][N]}$
Friction stress	σ_I
Ferrite	α
Gas constant	R
Grain size	d
Growth distance	S_o
Hardness Rockwell C	HRc
Intersheet spacing	λ_{is}
Lower yield stress	σ_y
Nano-metres	nm
Nitrogen present as aluminium nitride	N_{AlN}
Number of stress cycles	N
Number of cycles at crack nucleation	N_c
Number of cycles for propagating a nucleated crack	N_p
Number of cycles at slipband formation	N_s
Number of cycles to failure	N_f
Parts per million	ppm
Proportionality factors	K_2, K_1
Reduction in Area	R/A
Strengthening coefficient	k_y
Stress amplitude	σ_a
Tensile residual stress	$+\sigma_r$
Total Aluminium	Al_{Tot}
Total Nitrogen	N_{Tot}

CHEMICAL SYMBOLS AND ACRONYMS

Alumina	Al_2O_3
Aluminium	Al
Aluminium nitride	AlN
Carbon	C
Hertz	Hz
Hexagonal close packed	HCP
High strength low alloy	HSLA
Manganese Sulphide	MnS
Mega-Pascals	MPa
Niobium	Nb
Niobium carbide	NbC
Niobium carbonitride	Nb(C,N)
Niobium nitride	NbN
Nitrogen	N
Original Equipment Manufacturer	OEM
Scanning electron microscopy	SEM
Sodium chloride	NACl
Thermo-Mechanical Treatment	TMT
Titanium	Ti
Titanium carbide	TiC
Titanium-vanadium nitride	(Ti,V)N
Vanadium	V
Vanadium carbide	VC
Vanadium carbonitride	V(C,N)
Vanadium nitride	VN
Yield Strength	YS
Ultimate Tensile Strength	UTS
Zirconium	Zr

1   INTRODUCTION

A significant use of spring steels is in the suspension system of automobiles. With the advent of aggressive mass reduction in the automotive industry, there has been emphasis on designing lightweight, high strength chassis system components. Suspension coil spring design has been no exception to this trend, and higher spring operating stresses are being utilised. In terms of size and weight, smaller springs translate into a steel bar of generally decreased diameter and length. An important aspect of automotive coil springs is their fatigue resistance because in their application, the springs are constantly subjected to loading and un-loading.

Spring steels are typically identified by their ability for spring back after loading. The high stress application of automotive springs requires that the steel be forgiving to defects as the manufacturing process is not perfect. The control of grain size is important in spring steels since the processing requires heat treatment by hardening and tempering.

Grain size is typically controlled by rolling practice or by addition of alloys, which through precipitation are able to limit grain growth at elevated temperature. These alloys, often referred to as microalloys, apart from influencing the microstructure and hence the properties of steel through precipitation of carbides and nitrides, also influence the microstructure by other means particularly through their presence in solid solution.

The alloys usually considered, as microalloys are niobium (Nb), vanadium (V) and titanium (Ti). Aluminium (Al) however should be included because aluminium nitride (AlN) was the first nitride to be used to control grain size. In the early days of Al grain

refinement, problems were experienced during continuous casting of these steels. The Al was responsible for clogging of the nozzles in the tundish.

The easiest way to avoid this problem was to substitute Al with another grain refiner such as V. The use of V fine-grained spring steel posed no problem for the manufacture of automotive coil springs. This however changed when the need for weight reduction arose. A coil spring with smaller diameter and length was designed. Stress analysis of the coil showed that the inherent stresses in the coil was much higher than before.

The V fine-grained steel actually became notch sensitive for the new application. Minor surface imperfections in the coil usually resulted in failure while performing fatigue testing on the coils. These surface imperfections are typical of the manufacturing process. The steel was referred to as "brittle" for the application.

An Al fine-grained spring steel with identical composition except for the addition of Al instead of V was investigated to determine if the notch sensitivity was better.

The aim of this work may be summarised as follows:
- Determine the differences in mechanical properties between the two steels.
- Assess the metallurgical properties of the steels under different heat treatment conditions.
- Produce coil springs and conduct fatigue testing.

2   LITERATURE REVIEW

2.1   ALUMINIUM IN STEEL

Over the past three decades, significant progress has been made in the development of high strength low alloy (HSLA) or microalloyed steels [1,2,3,4]. The properties attained depend on the presence of small additions Nb, Ti or V. These elements react in different ways with the carbon (C) and nitrogen (N) in the steel to form precipitates which increase strength by precipitation and inhibit grain growth. These elements are typically called microalloying elements.

Of all the elements used for austenitic grain size control, Al is the most effective. The mechanism of controlling the inherent grain size of steels by Al additions is in the formation of AlN precipitates, which act as a grain boundary filament and thus restrict the growth of primary austenite (γ) grains. The effect of the AlN precipitates is at least as significant as that produced by Nb, Ti or V additions. However, Al is not classified as a microalloying element for historical reasons.

For over 50 years, Al was used primarily as a deoxidizing agent in steel. However, Al-killed steels have long been known to show improved strain-aging resistance and enhanced deep drawability, and for many years the term 'aluminium grain refined' has been synonymous with grain size control. Aluminium is used extensively as a deoxidant for steel, combining with the oxygen of soluble iron oxide to form alumina (Al_2O_3), insoluble particles of which often remain as a dispersion in the steel. Aluminium is typically used in steels for inclusion control and grain refinement. It is in this respect that the importance of Al is emphasised for spring steels.

31

Aluminium hardens α considerably by solid solution and, if dissolved in γ, increases the hardenability mildly. It has no carbide forming tendencies. By removing dissolved gases from the melt, Al helps to ensure freedom from blowholes and segregation.

Plain carbon steels, rendered fine-grained by addition of Al, have increased resistance to strain ageing and improved impact strength. Also, the more uniform structure improves machinability. However, creep resistance is impaired [4].

2.2   GRAIN   REFINEMENT   AS   A   STRENGHTENING MECHANISM

The awareness of the effect of adding small amounts of Al to plain carbon steels is reflected in many old specifications for plain carbon and alloy steels [5]. It is well known that Al treated steels have higher yield strengths and superior toughness. The quantitative relationship between yield strength and grain size in metals was first described by Hall, based on experimental observations, and by Petch, based on both experimental and theoretical approaches. The relationship between yield strength (YS) and grain size is now commonly known as the Hall-Petch equation:

$$\sigma_y = \sigma_i + k_y d^{-1/2}$$ ....(2.2.1)

where, σ_y is the lower yield stress, σ_I is the friction stress, k_y is the strengthening coefficient and d is the grain size.

In practice, grain refinement can be achieved during hot rolling by the interaction between microalloying elements Nb, V, or Ti and hot deformation. During the allotropic transformation, α nucleates

on austenitic grain boundaries. Maximum grain refinement can be achieved by increasing the austenitic grain boundary area.

This can be accomplished by either producing fine grains of γ through repeated recrystallisation between rolling passes, or by flattening of non-recrystallised γ grains into "pancakes" [6]. Accelerating cooling after completion of hot rolling can further enhance grain refinement. The undercooling of γ enhances the rate of α nucleation and slows down the rate of growth. A combination of these two factors contributes to the formation of smaller grains.

Chikushi *et al* [7] investigated the effect of grain size on the ultimate tensile strength (UTS) and YS for three steel grades, Figure 2.2.1. Findings were that the finer the grain size, the higher the mechanical properties.
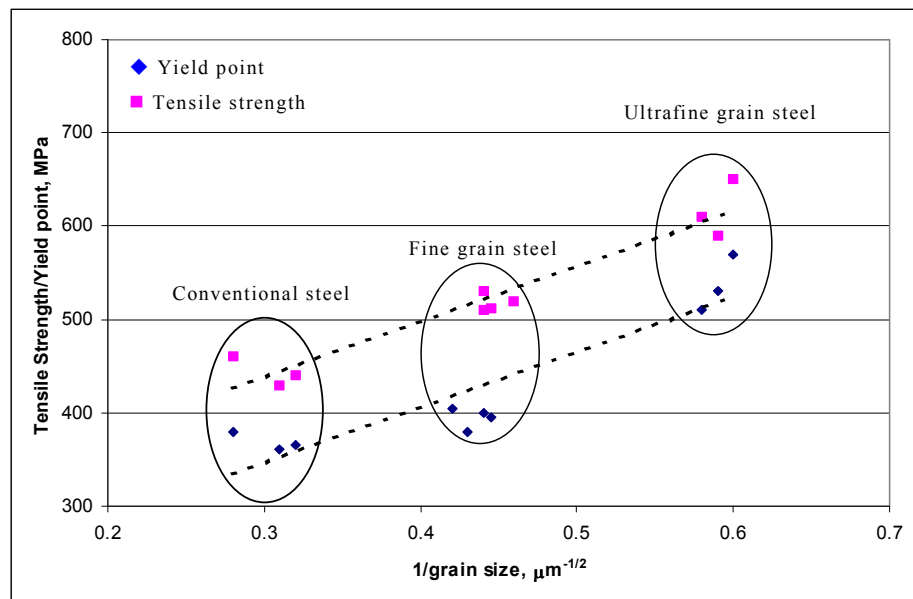
Figure 2.2.1: Relationship between ferrite grain size and mechanical properties
(After reference 7)

Control of grain size is particularly important when the steel is subjected to subsequent heat treatment processes such as hardening and tempering. Grain growth inhibitors such as precipitates of carbides, nitrides, or carbonitrides in the γ phase hamper recrystallisation of the γ [8].

This leads directly to α refinement after transformation of un-recrystallised γ. The effect of steel chemical composition on the transformation kinetics has obvious importance in relation to both α nucleation and growth. Precipitates in γ can accelerate the γ-α transformation because they act as potential nucleation sites and raise the transformation start temperature.

2.3   NITROGEN IN STEEL

Nitrogen, either present as residual in an electric arc furnace (EAF) steel or enhanced through N additions, exhibits a high affinity for Al or V and promotes precipitation of nitrogen rich AlN, vanadium nitrides (VN) or vanadium carbonitrides (V(C,N)) [9]. Free N in solution in α, has serious detrimental effects such as ageing and brittleness. These harmful effects can be neutralized by binding the N with elements, which act as scavengers, and thus remove N from solid solution in α.

Aluminium and Ti are effective scavengers. Vanadium has a unique dual effect on N. Vanadium not only neutralises N by forming VN compounds, but also uses N to optimise the precipitation reaction. Enhanced N increases the supersaturation in α and promotes a more active nucleation of V(C,N) particles as shown in Figure 2.3.1 [6]:
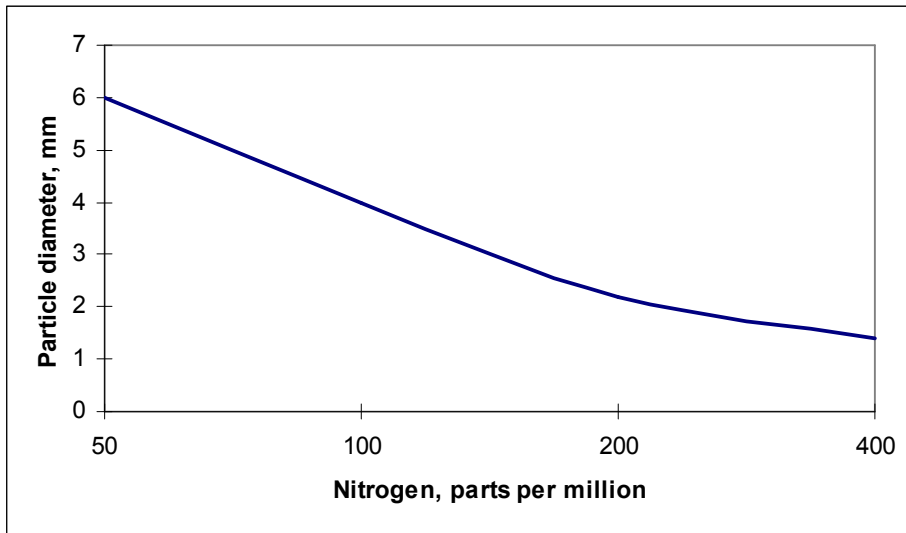
Figure 2.3.1 Effect of nitrogen content on the precipitated particle size.

As the nitrogen content increases, the precipitated particles become smaller and their number increases [10,11,12]. Higher N contents also promote particle nucleation and retard coarsening as shown in Figure 2.3.2. It is well known that the effectiveness of precipitation strengthening is increased at smaller interparticle distances. This is the mechanism whereby N optimises precipitation reactions in steel.
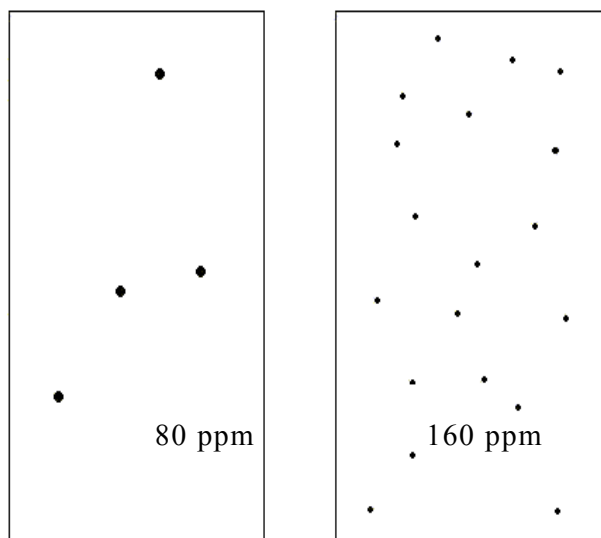
Figure 2.3.2 Effect of reducing the particle diameter.

2.4   MICROALLOYING ELEMENTS IN STEEL

The primary effect of microalloying elements is through their carbides, carbonitrides or nitrides, which can influence the properties of a steel through the various mechanisms shown in Figure 2.4.1: [2]
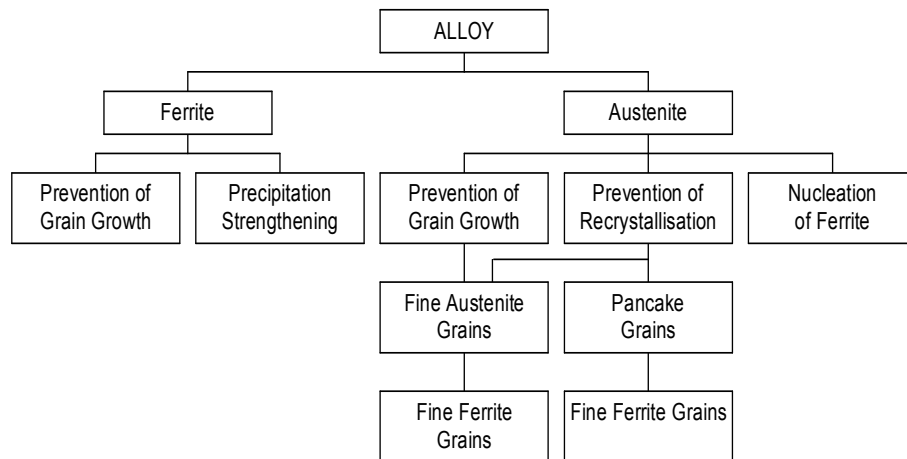
Figure 2.4.1: Effect of microalloy precipitates on microstructure of steel

The role of a microalloy precipitate depends on the temperature at which it forms in relation to the transformation temperature of the steel and the recrystallisation temperature of the austenite or ferrite. The temperature at which the simple nitrides and carbides form in relation to transformation temperatures as a steel cools during and after processing is illustrated in Figure 2.4.2: [2]

Microalloys in solution can play an important role in determining the microstructure and properties of steel. Apart from strengthening the ferrite lattice they also lower the transformation temperatures and can suppress the formation of bainite or α [2].
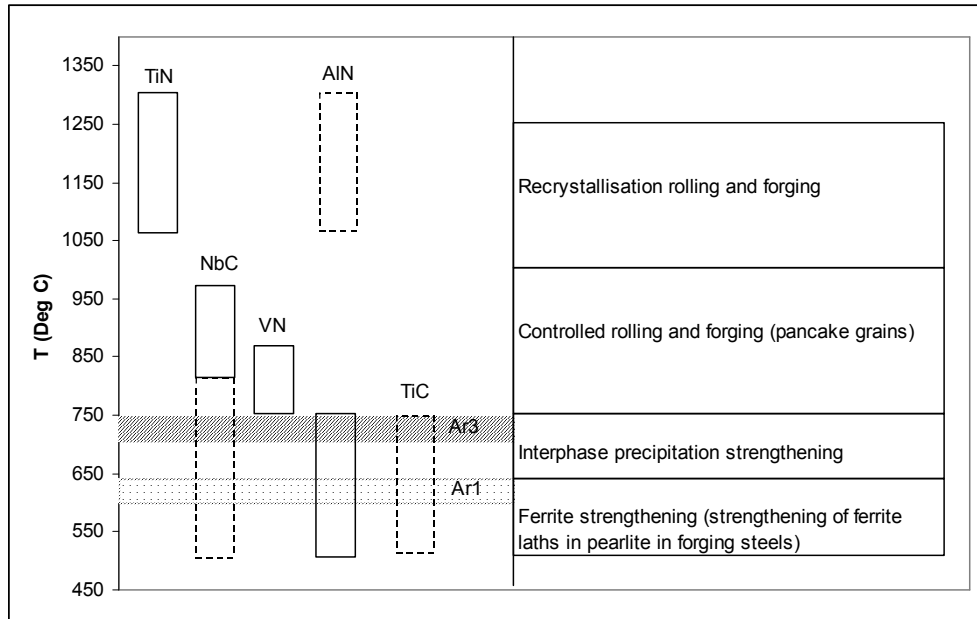
Figure 2.4.2: Temperature of formation of microalloy nitrides and carbides in relation to transformation temperature during cooling. (After reference 2).

These data are based on equilibrium conditions and give an indication of the relative temperatures at which the various compounds form. In practice, the rate at which a steel cools will determine the actual temperature at which precipitates and transformation occur. The higher the cooling rate, the lower the temperature at which the precipitates form. The rate of cooling can in fact determine whether a precipitate forms in γ or α.

When more than one alloying element is present, the element whose carbide or nitride precipitates at the highest temperature has the dominating influence in as rolled or forged steel because:

a) Its compounds have opportunity to influence the microstructure as the steel cools.

b) The formation of nitrides or carbides of the alloying elements will reduce the probability or lower the temperature at which nitrides or carbides of the other microalloying elements form and this may modify the influence of the alloy forming compounds at the lower temperature.

c) Alloys, which alone form carbides or nitrides at a low temperature, may form complex carbides or nitrides with an alloy forming a carbonitride at the higher temperature and so the quantity of the alloy forming compounds at the lower temperature and hence its effect may be reduced.

d) The formation of nitrides will reduce the N in solution and so reduce or remove any effect that the N may have on hardenability or embrittlement.

In addition to influencing the structure of steel as it cools, the precipitates can influence the microstructure and hence the properties when a steel is reheated for normalising or heat treatment. During the initial processing (rolling or forging) some undercooling occurs and the formation of some carbonitrides may be repressed.

On reheating the steels tends to revert to equilibrium conditions and precipitates, which were suppressed during processing, may precipitate during reheating. This is particularly important for AlN. Further, under practical rates of reheating, precipitates take time to go into solution and the final solution temperature is usually higher than the precipitation temperature.

This is particularly significant for steels which are heated rapidly for processing, such as steel blocks reheated by induction for forgings where nitrides which would be expected to be in solution at a temperature much below the forging temperature remain and

prevent grain growth during processing giving rise to a fine grained product.

The approximate temperatures through which precipitates are considered to exist during normal and rapid reheating are shown in Figure 2.4.3: [2]
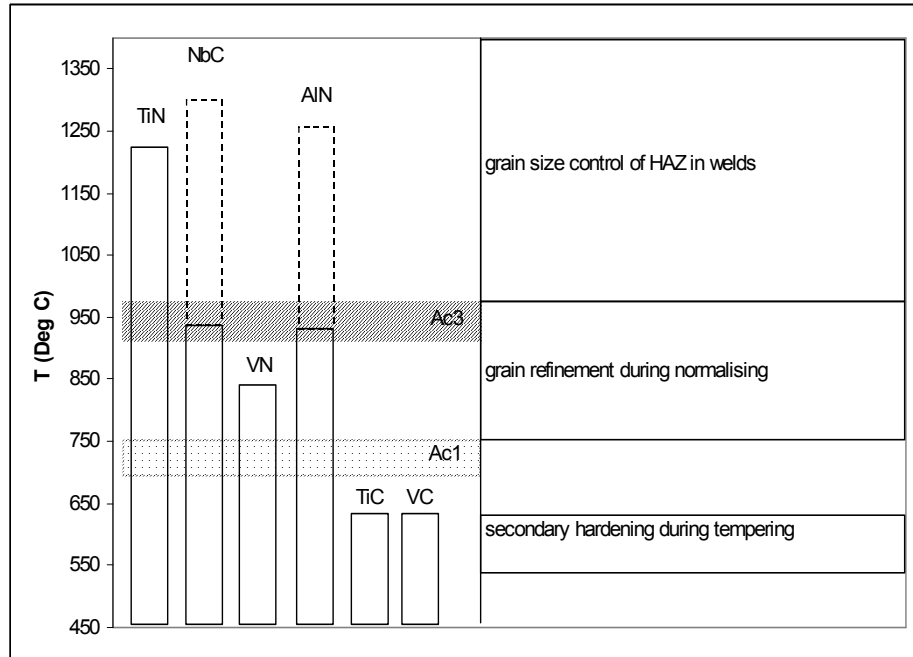
Figure 2.4.3: The presence of microalloy carbides and nitrides in relation to transformation temperature during reheating. (After reference 2).

2.5   THE USE OF MICROALLOYING ELEMENTS
2.5.1 PRECIPITATION STRENGTHENING OF FERRITE

One of the most effective mechanisms for increasing the strength of steels is through fine precipitates, which form in α during or after transformation. The carbide and nitrides of the microalloys especially V are less soluble in α than in γ and the precipitates therefore form in typical rows as the γ-α boundary advances during transformation.

Excess of alloys precipitating in γ and used to control grain size may continue to precipitate in α and will contribute to the strengthening of the steel.

2.5.2 PREVENTION OF GRAIN GROWTH AND RECRYSTALLISATION OF FERRITE

In the same way that growth of γ grains can be inhibited by precipitates, which pin grain boundaries, so precipitates can pin the grain boundaries of α and prevent grain growth. In recent years, increasing use has been made of this to obtain a fine α grain size in as rolled steels, which can to some extent replace normalised steels with considerable cost saving [2].

The recrystallisation of α can also be prevented by precipitates at a lower temperature but little use is made of this in practice.

2.5.3 PREVENTION OF GRAIN GROWTH AND RECRYSTALLISATION OF AUSTENITE

Precipitates, which can exist at high temperatures above the recrystallisation temperature of γ while steel is being rolled or forged, may pin grain boundaries and ensure a fine grain size at transformation and hence a relatively fine ferrite grain size in the finished steel. Titanium nitride (TiN) is the only practically viable microalloy precipitate, which can exist in steels under normal processing conditions. The use of TiN to control the grain size of austenite during hot rolling has become known as recrystallisation rolling.

Aluminium nitride and niobium carbonitrides (Nb(C,N)) which under normal processing conditions would be in solution at high

temperatures can however remain out of solution for sufficient time to control grain growth during forging of the steel if the steel is rapidly heated by induction. Aluminium nitride can precipitate during reheating for normalising or full heat treatment.

Once formed it is stable at the reheat temperatures and is effective in preventing the grain growth of γ at heat treatment temperatures [2,3]. Recrystallisation of γ is prevented by precipitates, which form in the γ at relatively low temperatures or the drag, which they produce in a precipitation state [2].

2.5.4 EFFECTS OF MICROALLOYS ON RECRYSTALLISATION

One of the most essential features of microalloying additions is their influence on recrystallisation during controlled rolling. They prevent recrystallisation and thereby produce 'pancaked' γ grains during hot deformation and condition the γ to form fine α grains during transformation. They also minimise the effect on recrystallisation thereby allowing repeated recrystallisation to occur during multiple deformation and a gradual refinement of γ and the subsequent α [1].

The first case is the controlled rolling route for the Nb-bearing structural steels, and the second is the route, recrystallisation controlled rolling, adopted for the Ti-V structural steels. The effect of the microalloying elements on recrystallisation differs widely, especially so for V and Nb, as demonstrated in Figure 2.5.1, which shows the recrystallisation stop temperature as a function of dissolved microalloy content (atom %), when the hot deformation starts.
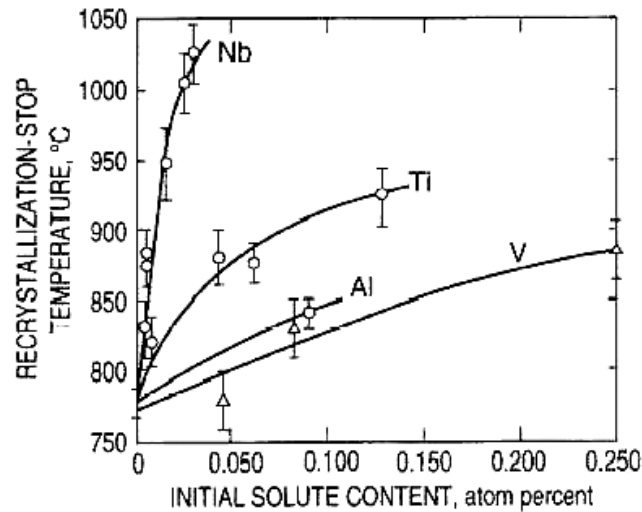
Figure 2.5.1: The increase in recrystallisation-stop temperature with increase in the level of microalloy solutes in 0,07C-0,25 Si-1,40Mn steel.

The mechanism by which the microalloying elements act to raise the recrystallisation stop temperature has been the subject of much debate throughout the history of microalloyed steels and numerous investigations have been performed. Mechanisms based either on solute drag or particle pinning has been proposed [1]. The view most commonly upheld today seems to be that strain-induced microalloy carbonitrides formed during the hot deformation suppress recrystallisation during the interpass time.

For Nb-steels convincing evidence has been presented that the pinning force created by the observed Nb-carbonitride dispersion at the recrystallisation stop temperature exceeds that of the driving force for recrystallisation. However, there is still doubt as to why the microalloy elements act so differently, Figure 2.5.1. A partial explanation could be gathered from which it can seen that most Nb can be precipitated in the temperature range 800-1000°C for a 0.03 % Nb steel whereas only a minor part of V can be precipitated between 800-900 °C for a 0.10 % V steel.

However, it appears that this alone cannot account for the large difference between the Nb and V curves. A detailed interpretation of the figure is more difficult, because of the complex experiments behind the results. In particular, the recrystallisation stop temperature has been determined by carrying out a multipass deformation in a temperature range of about 50°C above the recrystallisation stop temperature.

When considering the full temperature range for deformation, very little strain-induced V(C,N) precipitation can take place. The Nb steels, on the other hand, are open for Nb(C,N) precipitation during the full deformation cycle.

The particle pinning model and the varying precipitation characteristics of the different elements could possibly explain the large differences between the microalloy elements in suppressing recrystallisation. However, a full quantitative explanation of the differences in impact on recrystallisation is still lacking.

2.6   SOLUBILITY OF MICROALLOYING ELEMENTS
2.6.1   THE SOLUBILITY PRODUCT

The solubility of carbides and nitrides in γ and α is usually expressed as a solubility product in terms of weight % microalloy element and C and/or N. Consider a reaction between a microalloying element, M, with an interstitial, X, both being dissolved in the γ, to give a compound, MX, at a temperature T [5].

$$[M] + [X] \leftrightarrow (MX)………………………(2.6.1)$$

Where [M] represents the concentration of M dissolved in austenite, [X] represents the concentration of X dissolved in

austenite, and (MX) represents the constituent. The equilibrium constant can be written as:

$$k_s = a_{[M]} \cdot a_{[X]}/a_{(MX)} \dots \dots \dots \dots \dots (2.6.2)$$

Where $a_{[M]}$ is the activity of the dissolved microalloy, $a_{[X]}$ is the activity of the dissolved interstitial and $a_{(MX)}$ is the activity of the constituent phase.

It should be noted that the convention for the equilibrium constant used by chemists is the inverse of that given in equation (2.6.2), but the equation given is widely used by the metallurgist, the equilibrium constant, k_s, being referred to as the solubility product. The temperature dependence of the solubility product is generally expressed by the Arrhenius relationship in the form [1],

$$\log k_s = \log[M][X] = \log A - B/T \dots \dots \dots \dots \dots (2.6.3)$$

where [M] is the dissolved microalloy (wt%), [X] is the content (wt%) of N or C, A and B are constants and T is absolute temperature.

Several authors [1,10,11,13,14,15,16] have attempted to establish the solubility of carbides, nitrides and carbonitrides in γ. All of these investigators expressed their results in a form of solubility products. However, the results proposed by various authors as the "best-line" relationships sometimes differ considerably. An analysis of published data concerning the solubility of VC, VN, NbC, NbN, TiN and AlN, Figures 2.6.1 to 2.6.4, has shown that there exist more than ten different solubility equations for each carbide/nitride, and the spread between them is significant, in most cases greater than 150 ^{o}C.
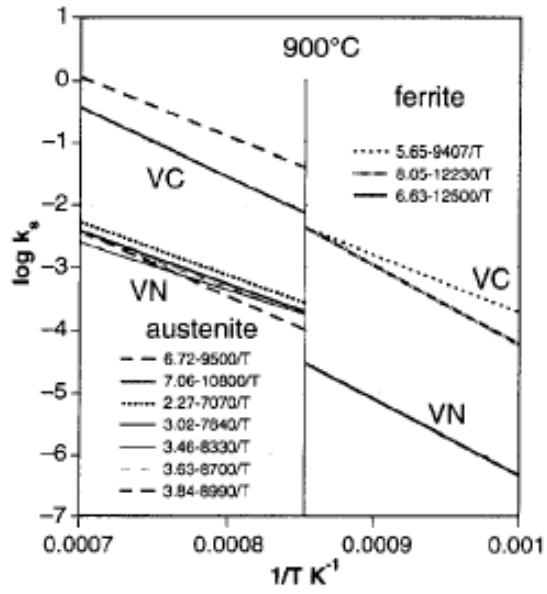
Figure 2.6.1: Solubility data for VC and VN in austenite and ferrite.
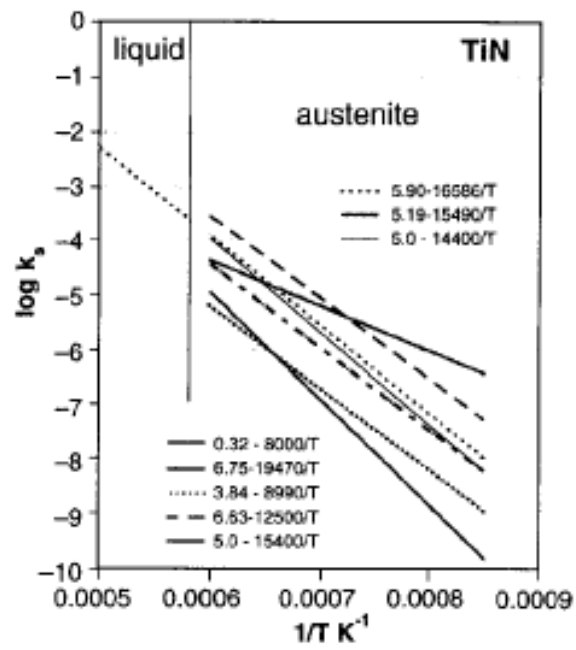
Figure 2.6.2: Solubility data of TiN in austenite and liquid steel.
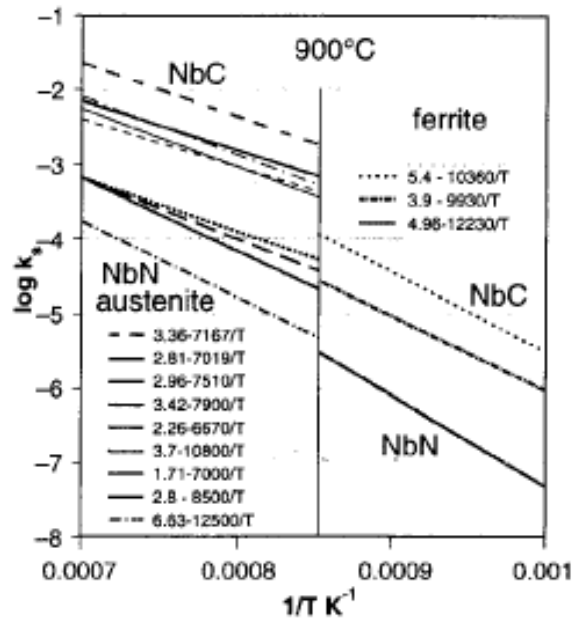
Figure 2.6.3: Solubility data of NbC and NbN in austenite and ferrite.
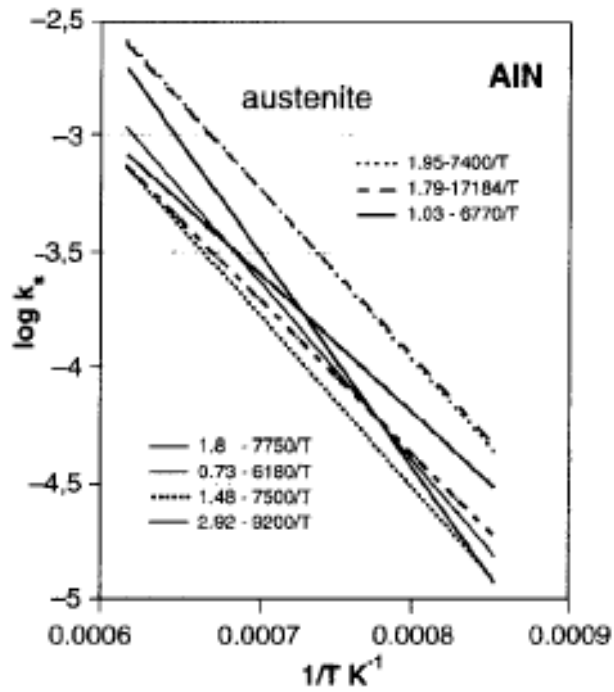
Figure 2.6.4: Solubility data of AlN in austenite.

It should be pointed out that the situation is even more complicated when more than one microalloy element is present and when the ratio of C to N is changed. The analysis of the solubility data in terms of solubility products implicitly assumes that the activity coefficients of microalloying elements as well as C and N are equal to unity and the microalloying additions are treated as a dilute solute and any interactions between solutes in the system are neglected.

Therefore the individual solubility equations apply only to a particular composition investigated and are not capable of predicting the solubility at different compositions, where the effects of solute interactions become significant. The carbides and nitrides are also non-stoichiometric and, hence, their composition can vary when precipitated in steels.

2.6.2   SOLUBILITY OF CARBIDES AND NITRIDES

The strengthening effect of microalloying additions may be produced by the dispersion strengthening effect of fine carbonitride particles or by grain refinement, i.e. inhibition of grain growth by carbonitride particles, or by a combination of these two effects [1]. In order to maintain a fine γ grain size prior to transformation, particles that remain undissolved in the γ, or particles that will precipitate during hot rolling are required.

To produce the very fine particles that are responsible for dispersion strengthening (i.e., particles that are 2-5 nm in diameter), it is necessary that these should be freshly precipitated during or after transformation to α. To achieve the desired metallurgical states, a detailed knowledge of the solubilities of the microalloy carbides and nitrides is required, together with knowledge of their precipitation behaviour.

An understanding of the role of different microalloying elements can be gained from the solubility product data summarised in Figure 2.6.5 from recent thermodynamic evaluation [3]. Despite a simplification, the individual solubilities of the microalloyed carbides and nitrides offer clear directions for the selection of microalloying additions for specific purposes.

It is seen that TiN is extremely stable and can withstand dissolution at high temperatures during reheating prior to rolling or during welding. Niobium nitride and carbide have relatively low solubilities and may precipitate out in the later stages' of rolling. Vanadium on the other hand, has a rather high solubility in γ even at temperatures as low as $1050^{o}C$.

Nitrides are substantially less soluble than the corresponding carbides. This is especially true for Ti and V where the differences are particularly pronounced. In normal circumstances the solubility relationships shown in Figure 2.6.5 represent a simplification, as steel may contain more alloying elements with high affinity for C and N, which alter the solubility of the microalloyed carbides and nitrides.
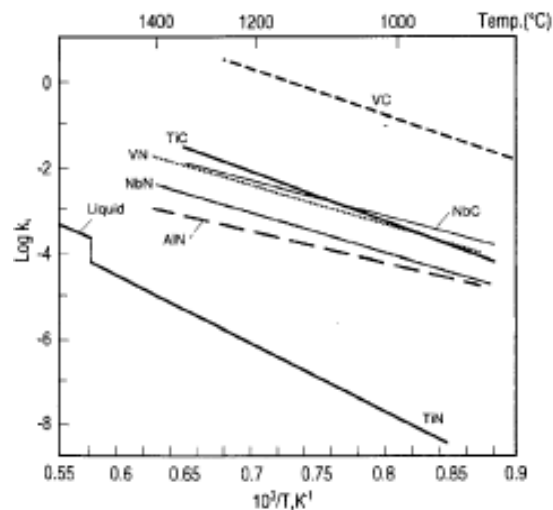
Figure 2.6.5: Solubilities of microalloy carbides and nitrides

2.7 PROPERTIES OF ALUMINIUM NITRIDE

2.7.1 PRECIPITATION OF ALUMINIUM NITRIDE

Significant strengthening is obtained by the precipitation of carbonitrides, carbides or nitrides in α. The solubility of these precipitates in α is much less than in γ [6]. This results in a strong supersaturation, which provides the driving force for precipitation.

The precipitation process proceeds at a perceptible rate only if there is a driving force, i.e. a free energy different between product and parent phases [1]. This driving force enters the steady state nucleation rate in a central way and must be known with some accuracy if nucleation rates are to be calculated, or even estimated.

It is necessary to emphasise that Al differs from other grain refining elements such as V, Nb and Ti because it does not form carbide in steel. Instead it forms a nitride, AlN, with HCP structure, which is different. Therefore, there is no mutual solubility between AlN and the carbides or nitrides of V, Nb and Ti, all of which have NaCl (Sodium chloride) cubic crystal structure. Aluminium is normally dissolved in γ at high temperature prior to rolling but the nitride phase is thermodynamically stable at lower temperatures.

The precipitation of AlN is sluggish and the particles formed are relatively coarse. Accordingly, AlN has little influence on the structures or properties of hot rolled steels although it contributes to grain refinement after normalising. However, AlN nucleates with some difficulty in steel and has a widely different morphology from other nitrides [4,16]. AlN precipitation in α has been extensively studied in connection with the development of favourable crystallographic textures.

Blum [15] studied the features of AlN precipitation on disintegration of γ in a low-carbon Mn-V steel containing N, as a function of Al and V. Two laboratory melts were produced with residual Al ranging from 0.006 to 0.13 %. The chemical compositions of the melts was: 0.1 % C, 1.7 % Mn, 0.35 % Si, 0.035 % N and 0.07 % V, while in the second melt their was 0.15 % V.

The casts were forged to bars and annealed. After bringing up to 920^0C and 1050^0C with 30 minutes soaking, one part of the specimens was normalised and the other quenched in water. The hardness and mechanical properties were measured in the normalised specimens. The AlN concentration of the steel was determined after different heat treatments.

To ascertain the phase composition and size of the nitrides, electron microscope and electron diffraction studies were made using carbon extraction replicas. The results are given in Figure 2.7.1:
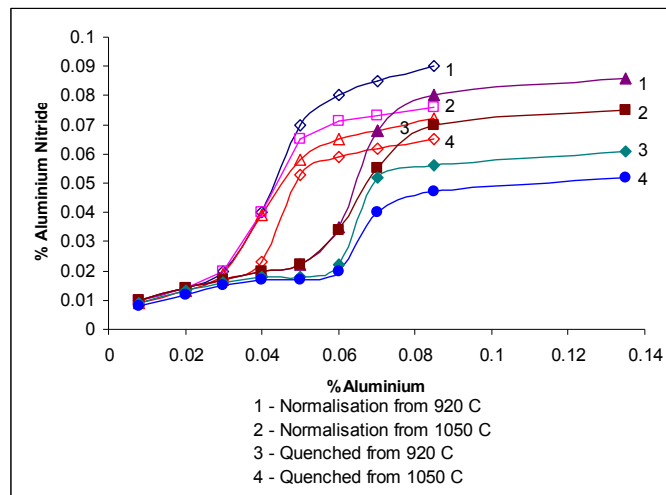
Figure 2.7.1: Amount of aluminium nitride as a function of the aluminium concentration and heat treatment of the steel. 0.07 % V steel (unfilled points), 0.15 % V steel (filled points). (After reference 15).

Above a certain level of Al concentration, the strength characteristics are independent of the normalisation temperature. In this case, the N is combined in barely soluble AlN; there is hardly any finely dispersed VN, which would strengthen the steel. As can be seen in Figure 2.7.2, the deflection on the hardness curves corresponds to the Al concentration at which the amount of AlN increases suddenly.
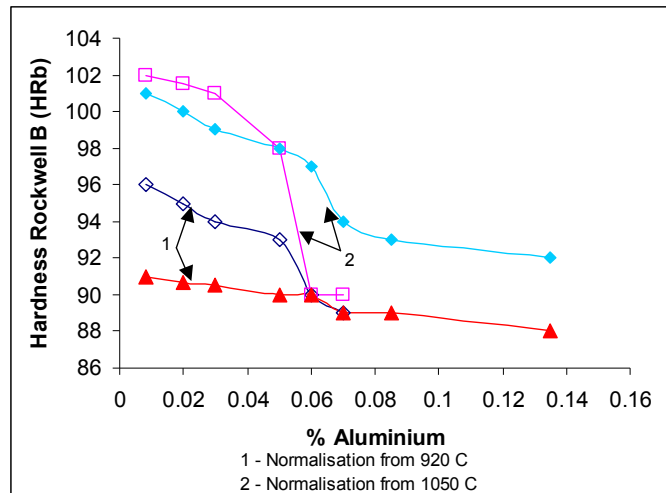
Figure 2.7.2: Hardness as a function of the aluminium concentration. 0.07 % V steel (Unfilled points), 0.15 % V steel (Filled points). (After reference 15).

The hardness of steels with fairly low Al content rises when normalised at higher temperatures. The UTS and YS vary in a similar manner. The improvement of the strength characteristics is attributed to dissolution of VN on heating and its subsequent precipitation in a finely dispersed form on cooling. These were confirmed by electron microscope and electron diffraction analyses.

2.7.2 SOLUBILITY OF ALUMINIUM NITRIDE IN AUSTENITE

The solubility of AlN in steel conforms to the normal solubility product equation derived from equation 2.7.1 [4,5]:

$$\ln k_s = \ln[Al][N] = C - Q/(RT) \quad \dots\dots\dots\dots\dots\dots(2.7.1)$$

where, [Al] and [N] represent the metallurgically soluble Al and N, respectively, K_s is the solubility product, Q is the activation energy, R is the gas constant, T is the absolute temperature, and C is a constant.

Under equilibrium conditions, precipitation of AlN will occur when the solubility product is exceeded. A more accurate definition of the above solubility product was defined by Gladman [4]:

$$K_s = \left(Al_{Tot} - Al_{Al_2O_3} - \frac{27}{14} \times N_{AlN} \right)\left(N_{Tot} - N_{AlN} \right) \dots\dots\dots\dots\dots(2.7.2)$$

where, Al_{Tot} an N_{Tot} represent the total Al and N levels, respectively, N_{AlN} is the N present as AlN, and $Al_{Al_2O_3}$ is the Al present as Al_2O_3. Wilson and Gladman [4] did a complete review of AlN in steel and quote the following values in Table 2.7.1 and Figure 2.7.3 from various references:

Table 2.7.1 Solubility of AlN in austenite (See Figure 2.7.3).

Reference on Figure 2.7.3	Temperature Range, Deg C		$LogK_{[Al][N]}$	Calculated temperature of complete solution, Deg C		
				0.005%N, 0.02 % Al.	0.01%N, 0.02 % Al.	0.02%N, 0.04 % Al.
A	1050	1350	-7400/T + 1.95	977	1042	1206
B	810	1260	-6770/T + 1.03	1076	1155	1373
C	800	1300	-7184/T + 1.79	961	1025	1192
D	900	1350	-7750/T + 1.80	1060	1139	1320
E	900	1200	-6180/T + 0.725	1034	1125	1353
F	900	1200	-6015/T + 0.309	1106	1208	1493
G	950	1300	-7500/T + 1.48	1042	1186	1393
H	800	1250	-5675/T + 0.18 +2.4 (wt % Al)	1034	1115	1301
K	850	1300	-10020/T + 3.577	1049	1104	1228
L	850	1300	-9200/T + 3.079	1055	1116	1255

52
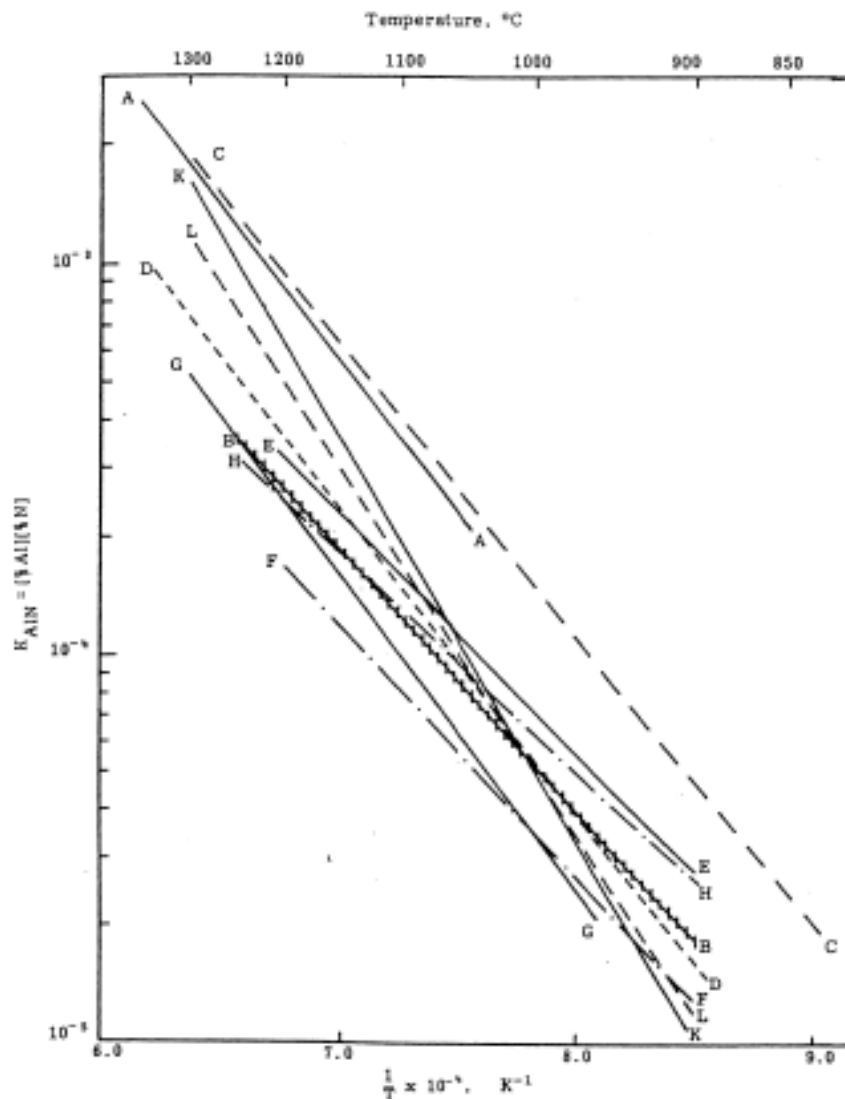
Figure 2.7.3: Solubility of AlN in austenite. (See table 2.7.1).

It is also possible to use the above data to trace the extent of the precipitation of AlN in a given steel as a function of temperature, provided that the cooling rate is slow enough to give a reasonable approach to equilibrium [4]. Figure 2.7.4 shows such precipitation curves for selected Al and N levels. Increasing the Al content increases the precipitation temperature range, and with 0.05 % Al, 0.015 % N, the bulk of the precipitation (more than 70 %) occurs above 1100 $^{\circ}$C.
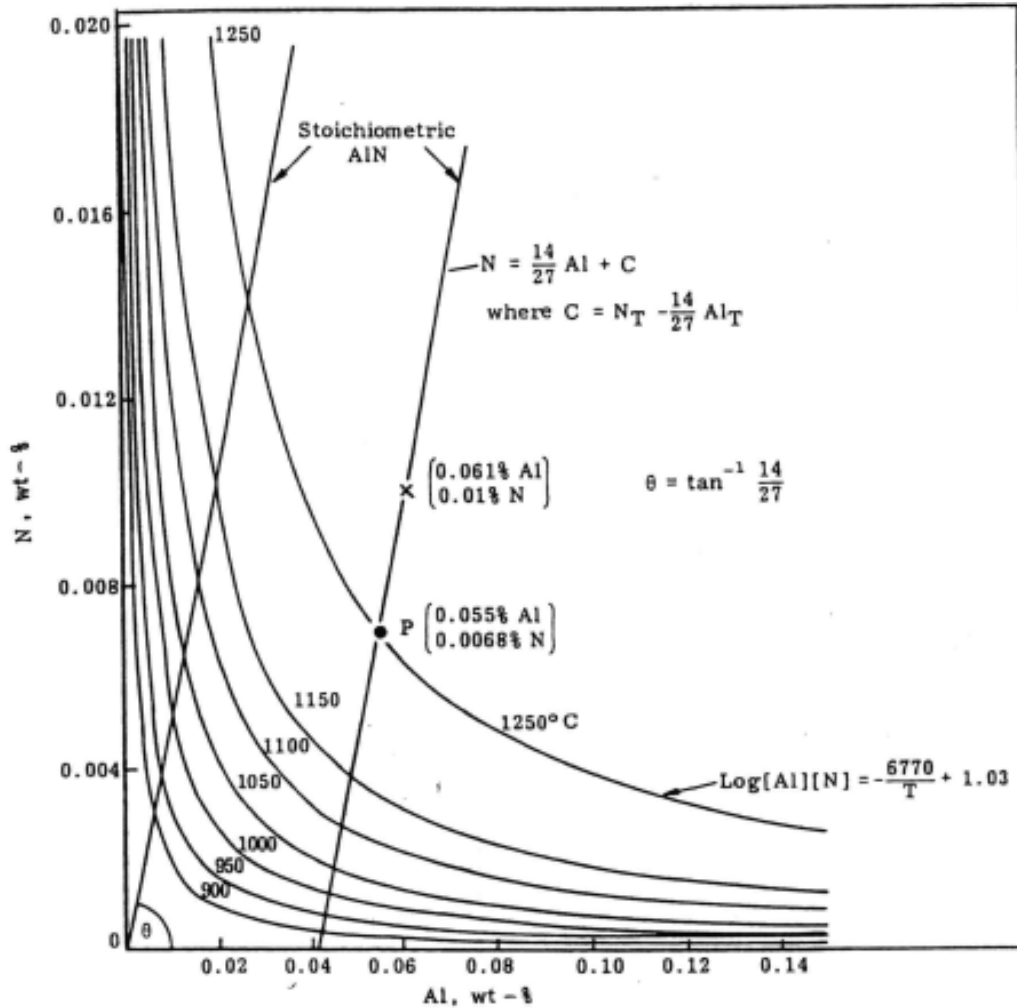
Figure 2.7.4: Effect of temperature on equilibrium solubility of AlN in steel.

Solubility diagrams provide no information on the morphology, size distribution, and location of AlN precipitates. These can only be derived from direct metallographic observation.

2.7.3 PRECIPITATION KINETICS OF ALUMINIUM NITRIDE

The rate at which precipitation of AlN occurs in steel is dependent on: [4]

(i) The chemical driving force. This is governed by the prevailing Al-N supersaturation, which is dictated by the steel analysis, $K_{[Al][N]}$, temperature, and the matrix structure (α or γ).

(ii) The prevailing rate of diffusion of Al, which, for a given temperature, is significantly higher in α-iron than γ-iron. Thus the γ-α transformation, which is dependant on the steel analysis and the cooling rate, has an important effect on the precipitation kinetics.

(iii) The nucleation energy barrier.

(iv) The time spent at a given temperature.

(v) Partitioning effects: N, like C stabilizes γ in which it shows extensive solubility. In α, N shows restricted solubility (maximum of $\approx$0.1 % at 520 ^{o}C in equilibrium with Fe and N) and is mainly held to be responsible for strain ageing effects. Aluminium is a powerful stabiliser of α to which it partitions in the $\alpha + \gamma$ range. (See Figure 2.7.5).

The relative contribution of these factors is determined by the steel composition and thermo-mechanical history.
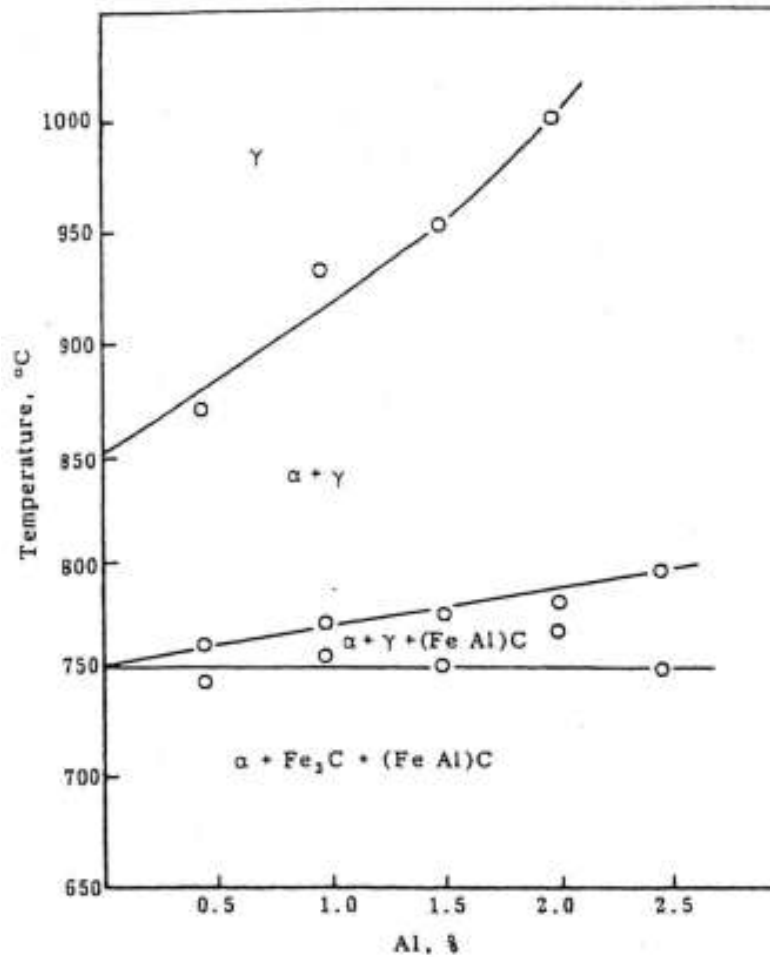
Figure 2.7.5: Section through ternary diagram Fe-Al-0.3 %C.

2.7.4 EFFECT OF DEFORMATION ON PRECIPITATION KINETICS OF ALUMINIUM NITRIDE

The hot deformation of γ supersaturated with Al and N results in a complex interaction between dynamic and static recovery and recrystallisation with dynamic and static precipitation of AlN. The effects on the kinetics of precipitation depend on the strain rate, the temperature of deformation, and the steel analysis [4]. It is generally acknowledged that the hot deformation of Al-killed steels results in a marked increase in kinetics of precipitation of AlN.

It has been reported that the kinetics of the dynamic precipitation (during deformation) of AlN were increased by more than an order of magnitude over the corresponding static precipitation rates.

2.7.5 MORPHOLOGY OF ALUMINIUM NITRIDE PRECIPITATES

The form and morphology of AlN precipitates in steel are determined by the steel analysis, especially Al and N levels and the prior thermal history. Thus, depending on the heat treatment and processing conditions, AlN precipitates can be dendritic, large plates, rod shaped, needle shaped, rectangular/cuboidal or prismatic.

2.8   VANADIUM IN STEEL

Vanadium was discovered by the Swedish scientist and doctor Nils Gabriel Sefström in 1830 [1]. In his studies of ductile iron originating from iron ore of the Taberg mine, he obtained a residue, which contained a compound with a previously unknown element, vanadium. At this point, Sefström's master, the famous Swedish chemist Jöns Jacob Berzelius, took interest in the new element.

He announced Sefström's discovery internationally and also initiated a large research programme on vanadium salts. Sefström and Berzelius' work was however confined to chemical studies of a large number of vanadium compounds. It was only some 30 years later that vanadium was isolated as a metal due to work by the English chemist, Sir Henry Roscoe.

Hot-rolled plain carbon steels are the most popular material used in construction. Raising the carbon content can increase strength. In fact, strength is proportional to carbon equivalent, (CE), which is essentially the combined effect of the carbon and manganese content of steel. While raising the carbon equivalent increases strength, it also drastically reduces other engineering properties such as ductility, toughness and weldability.

The strengthening mechanisms of hot rolled steel can be differentiated into five fields shown in Figure 2.8.1: [6]
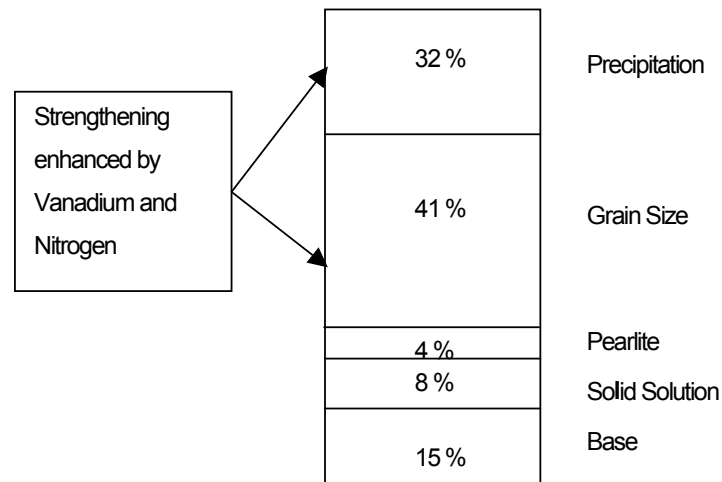
Figure 2.8.1: Strengthening mechanisms in hot-rolled steels.

As shown in Figure 2.8.1, the addition of V in conjunction with N, enhances the strength of steel by grain refinement and precipitation hardening. Precipitation hardening increases strength but may contribute to brittleness. Grain refinement increases strength but also improves toughness.

As a result, grain refinement counteracts any embrittling caused by precipitation hardening. In steel, V forms stable compounds with both C and N and it is in the way that these elements interact with V, which determines many of the properties of V containing steels.

2.9 PRECIPITATION CHARACTERISTICS OF VANADIUM COMPOUNDS

2.9.1 PRECIPITATION OF VANADIUM COMPOUNDS IN AUSTENITE

The reduction in solubility with decreasing temperature and on transforming from γ to α leads to the possibility of precipitation of V compounds in steel. However, because of their relatively high solubilities, V compounds tend not to precipitate in γ until relatively low temperatures are reached, usually in the presence of high levels of V and N (or C) and normally in the presence of deformation.

The start of precipitation can be enhanced by the presence of a suitable substrate and Figure 2.9.1 shows an example where VN has been precipitated as a cap on a MnS (manganese Sulphide) inclusion.
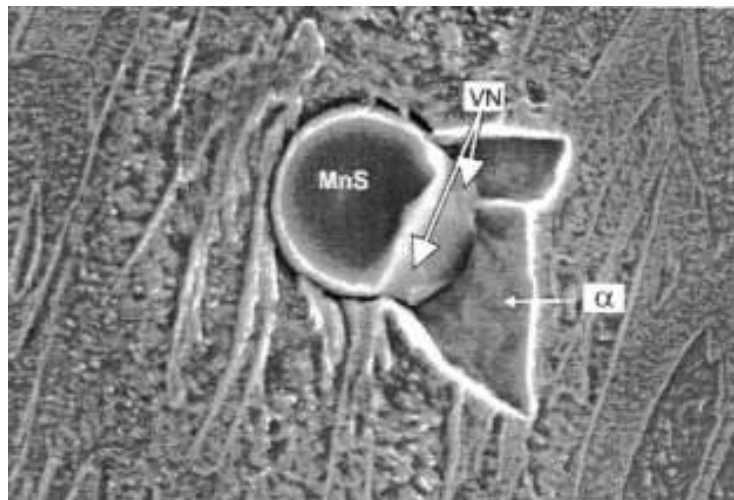
Figure 2.9.1: SEM micrograph showing VN precipitated as a cap on MnS.

Vanadium does not readily precipitate in γ [1]. Since V(C,N) has high solubility in γ it hardly affects the hot deformation process but rather precipitates during cooling in α, thereby increasing the strength level of the steel by precipitation hardening. For hard precipitates such as V(C,N), bypassing of dislocations is expected to occur by bowing between the particles (Orowan-mechanism) under all practical conditions.

This means that there is only one parameter, which determines the precipitation strengthening namely the inter-particle spacing. The smaller the inter-particle spacing, the larger the strengthening effect. In precipitation reactions, the decisive factor, which minimises the inter-particle spacing and maximises the precipitation strengthening is the rate of nucleation since it determines the particle density.

In turn, the most important parameter controlling the nucleation frequency is the chemical driving force for precipitation. Hence, the strong effect of N in increasing this driving force. Figure 2.9.2.a shows the driving force for VC and VN precipitation. It should be noted, however, that the driving force can also be raised by V addition but the effect per concentration unit is much less. Figure 2.9.2.b.
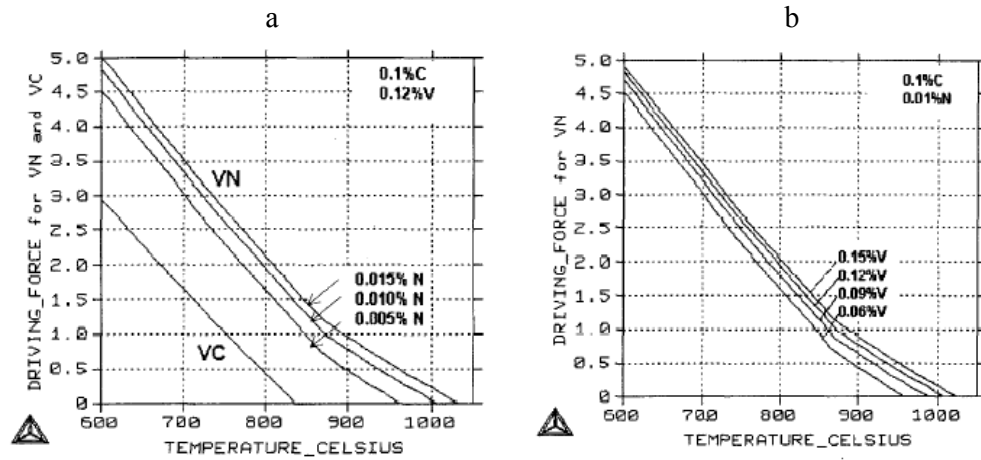
Figure 2.9.2: Chemical driving force, $\Delta G_m/RT$, for precipitation of VC and VN in 0.12 % V steel.

A combination of V with other elements in the same steel can naturally lead to interactions since they compete for the same interstitial elements and may also form mixed compounds with one another. For example, the stable TiN phase may incorporate a significant amount of V and even AlN has sometimes been detected in complex TiN particles.

Since the titanium-vanadium nitrides ((Ti,V)N) particles are rather coarse such an effect reduces to some extent the contribution, which the V can be expected to make towards precipitation strengthening.

Lagneborg *et al* used a computer program (Thermo-Calc) for calculations of the precipitation of V(C,N) in steels microalloyed with V [1]. These calculations are shown in Figure 2.9.3. Also shown in this figure is the mole fraction of N in carbonitrides at various temperatures and for various N contents from hyper-

stoichiometric levels to zero. This shows that V starts to precipitate in γ as almost pure nitride, until practically all the N is consumed.
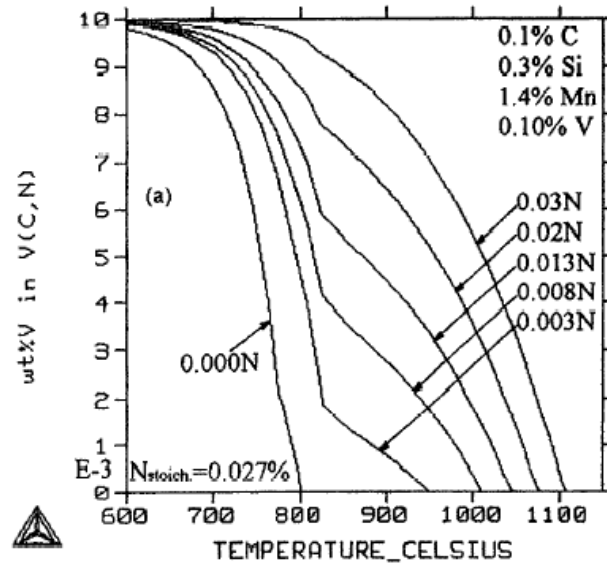
Figure 2.9.3: Calculated precipitation of V(C,N) as a function of temperature in 0.10% V steel at various nitrogen contents.

When the N is about to be exhausted there is a gradual transition to form mixed carbonitrides, Figure 2.9.4. Nitrogen rich V(C,N) may precipitate during or subsequent to the γ-α transformation. Precipitation during the transformation is a result of the solubility drop of the V(C,N) associated with the transformation from γ to α at a given temperature.

A significant feature of the solubility of VC in γ is that it is considerably higher than those of the other microalloy carbides and nitrides, suggesting that VC will be completely dissolved even at low austenitising temperatures.
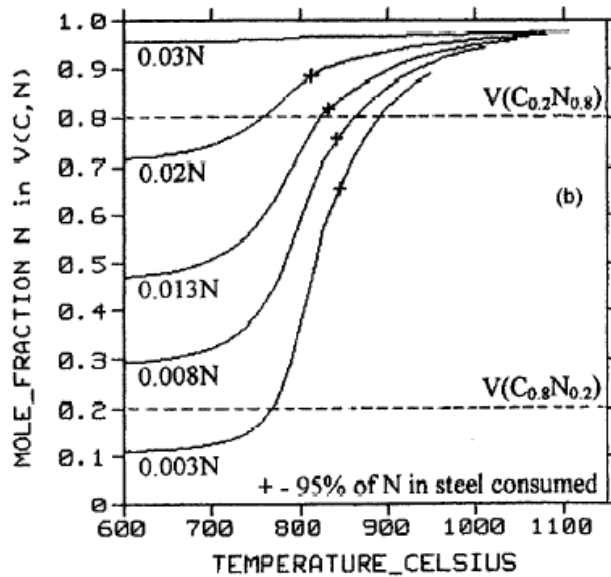
Figure 2.9.4: Calculated mole fraction of N in V(C,N) as a function of temperature in a 0.10% V steel at various nitrogen contents.

Vanadium offers no effective resistance for austenite recrystallisation during hot rolling since its larger solubility produces no impeding precipitates [1]. The absence of hindering particles on the other hand offers a new opportunity for grain refinement: Repeated austenite recrystallisation after each rolling reduction generates, after a sufficient number of passes, a very efficient austenite grain refinement which after transformation can produce a fine ferrite grain size.

2.9.2 PRECIPITATION OF VANADIUM COMPOUNDS IN FERRITE

As regards strengthening, the effective V(C,N) particles are those formed in α during the last passage through the γ-α transformation [10]. At equilibrium the circumstances are such that a certain, small portion of the V should precipitate in γ, especially if the contents of V and N are high.

However, the kinetics of V(C,N) formation in γ are sluggish and for processing at finishing temperatures higher than 1000°C and for normal steel compositions virtually all V will be available for precipitation in α. Some solute V can be forfeited during controlled rolling as a result of strain induced V(C,N) precipitation, or by the formation of alloyed Ti(V,N) particles during casting and reheating of Ti-V microalloyed steels.

However, compared to the other microalloying elements V has a higher solubility and therefore remains in solution to a much larger extent during processing in the γ range. Accordingly, in steels where especially efficient precipitation strengthening is wanted, V is the preferred choice.

Precipitation of V(C,N) can occur randomly in α in the wake of the migrating γ/α boundary, general precipitation or by interphase precipitation characterised by the development of sheets of particles parallel to the γ/α interface formed repeatedly with regular spacing.

2.9.3   PRECIPITATION STRENGTHENING

Since normal contents of V in steels dissolve in γ at relatively low temperatures, unlike the other microalloying elements, and therefore can contribute fully to precipitation strengthening when the steel is cooled into the α-range, V is usually the preferred element when precipitation strengthening is required.

Roberts *et al* [17] investigated the additions of small amounts of V on C-Mn steel. A modest addition of 0.10% V can bring about a strength increase beyond 200 Mpa, and in special cases even up to 300 Mpa, Figure 2.9.5.
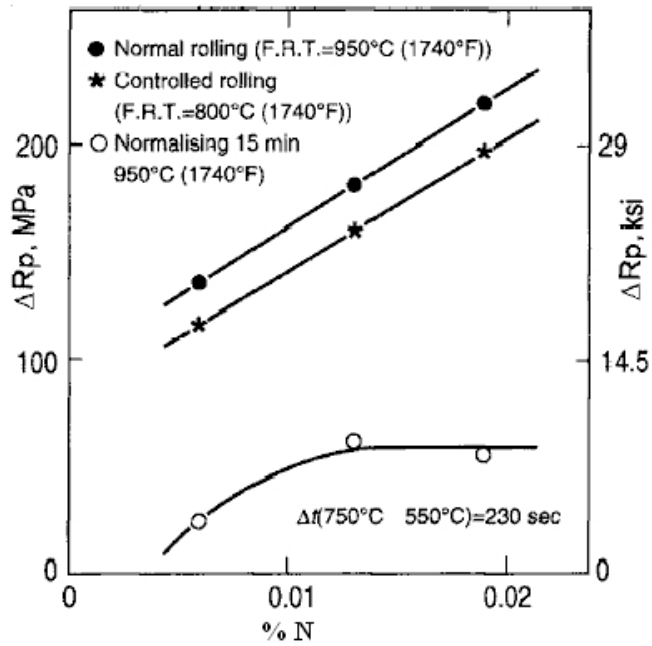
Figure 2.9.5: Effect of processing method on the precipitation strengthening derived from V(C,N). Base composition steel is: 0.12%C-0.35%Si-1.35%Mn-0.095%V-0,02%Al.
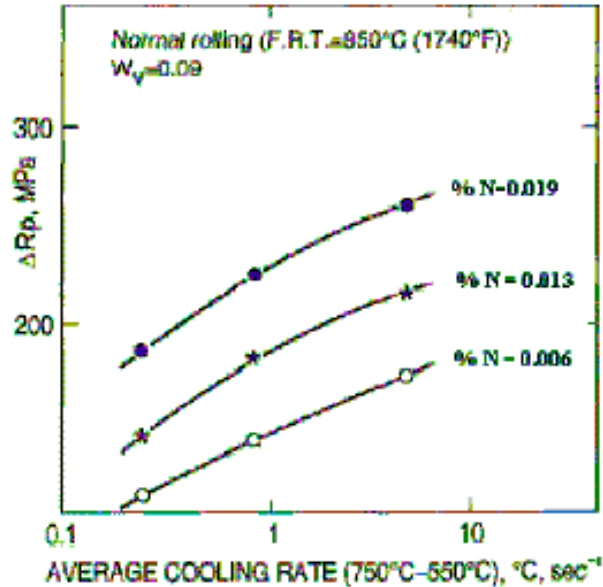
Figure 2.9.6: Influence of cooling rate on the strength contribution from V(C,N) precipitates. Base composition as for Figure 2.9.5.

66

Figures 2.9.5 and 2.9.6 show another essential feature of V-steels, i.e. that nitrogen in small contents adds significantly to precipitation strengthening. Precipitation strengthening of V steels is greatly improved by N. Similarly, enhanced cooling through the γ-α transformation and afterwards enhances the particle hardening, Figure 2.9.6. The results of Figure 2.9.5 show also that normalising at 950°C does not allow all V to go into solution completely and hence produces only modest strengthening. The technically very important effect of N on the strengthening of V steels is illustrated in Figure 2.9.7.
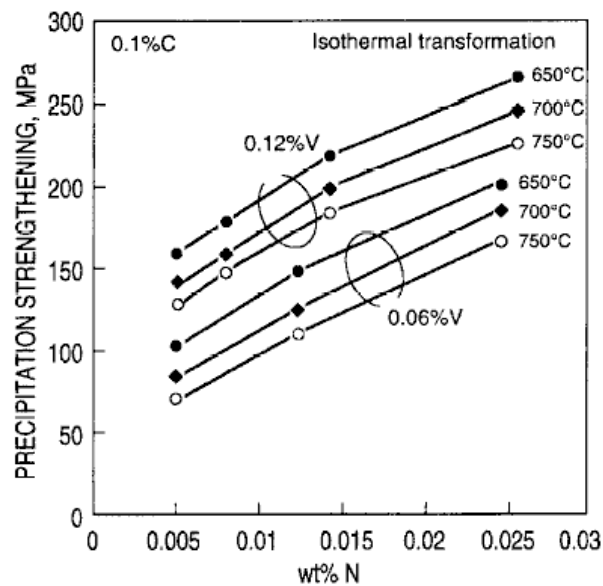
Figure 2.9.7: Effect of N, V and transformation temperature on the precipitation strengthening in 0,l %C-V-N steels after isothermal ageing at different temperatures for 500 s.

The effect of N on the strengthening of V steels has sometimes been interpreted such that only VN forms a precipitate, and that the remaining V does not combine with C, possibly due to the larger solubility and lower chemical driving force for VC [10]. However, this is a rather loose statement and is not an entirely correct description of the phenomenon.

A physically more correct account would be as follows. With hard non-penetrable V(C,N) precipitates, the particle strengthening occurs by the Orowan mechanism (bowing of dislocations between particles) and in that case the decisive parameter is the interparticle spacing in the slip plane.

In turn, that is determined by the density of the precipitates. This density is controlled by the nucleation frequency and the number of nuclei it creates until the supersaturation has diminished so that nucleation dies. The essential parameter governing the variation in nucleation is the chemical driving force for V(C,N) precipitation which depends on the available quantities of both C and N.

It is true, however, that it varies relatively strongly with the N content, but C may also significantly influence the chemical driving force. Precipitation strengthening in microalloyed steels benefits from the γ-α transformation because the chemical driving force for precipitation of microalloy carbonitrides increases suddenly and strongly as γ is transformed to α. This is also reflected in the widely different solubilities in the two phases and thereby gives rise to profuse precipitation in the α.

Vanadium microalloyed steels are particularly suited for generating large precipitation strengthening because of their ability to dissolve large quantities of V(C,N) at relatively modest temperatures in the γ range due to the larger solubility as compared to other microalloy carbonitrides. This again creates conditions for a high driving force and therefore dense precipitation.

2.9.4 INTERPHASE PRECIPITATION

The precipitation of V(C,N) in V-microalloyed steels can occur either randomly in α in the wake of the migrating γ-α interface (general precipitation) or by interphase precipitation characterised by the development of sheets of particles parallel to the γ-α interface formed repeatedly, with rather regular spacing [13,18].

The precipitate particles form in bands, which are closely parallel to the interface, and which follow the general direction of the interface even when it changes direction sharply. The bands are often associated with planar low energy interfaces, and the interband spacing is determined by the height of steps, which move along the interface.

Zajac *et al* investigated interphase precipitation [10]. Figure 2.9.8 shows the typical morphology of interphase precipitation of V(C,N) in 0.04 – 0.10 % C, 0.13 % V steels.
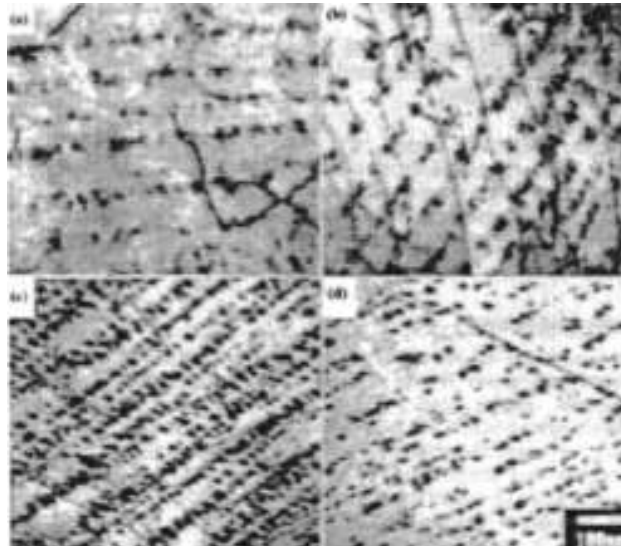
Figure 2.9.8: Electron micrographs of 0.04 – 0.10 % C, 0.13 % V steels, isothermally transformed at 750 ^{o}C for 500s. (a) 0.0051 % N, (b) 0.0082 % N, (c) 0.0257 % N, (d) 0.00295 % N, 0.04 % C.

It was concluded from Figure 2.9.8, that such a microstructure formed in sheets parallel to the γ-α interface by repeated nucleation of particles as the transformation front moves through the austenite. At high transformation temperatures of about 800 $^{\circ}$C, the interphase precipitation consists of irregularly spaced, and often curved sheets of V(C,N) particles. With decreasing temperatures the incidence of curved rows of precipitates diminishes and the dominant mode is regularly spaced, planar sheets of particles.

From about 700 $^{\circ}$C the interphase precipitation is commonly found to be incomplete, and random precipitation from the supersaturated ferrite after the γ-α transformation takes over progressively with decreasing temperature. A characteristic feature of interphase precipitation is that it becomes more refined at lower temperatures, Figure 2.9.9.a [10] and 2.9.9.b shows that the nitrogen content of the steel affects the intersheet spacing considerably.
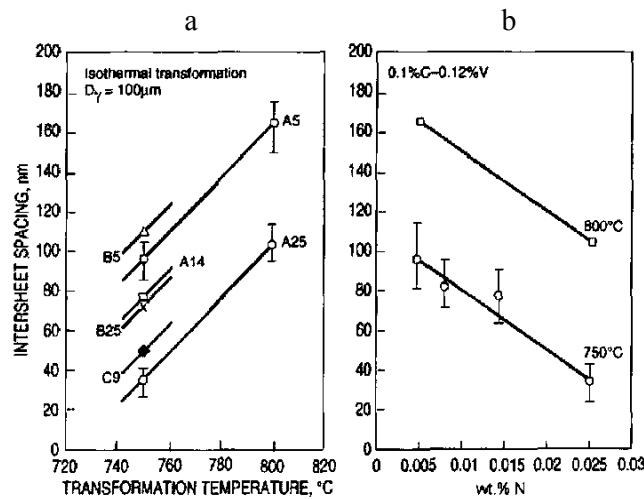
Figure 2.9.9: The effect of transformation temperature and N content on intersheet spacing of V(C,N) interphase precipitation. B5 (0.10 C − 0.12 V − 0.056 N), A5 (0.10 C − 0.12 V − 0.0051 N) A14 (0.10 C − 0.12 V − 0.014 N), B25 (0.10 − 0.06 V − 0.025N), C9 (0.04 C − 0.12 V − 0.0095 N), A25 (0.10 C − 0.12 V − 0.026 N).

2.9.5 THE MECHANISM OF INTERPHASE PRECIPITATION

The mechanism of interphase precipitation has been the subject of considerable discussions. The models that have been proposed to explain the phenomenon fall broadly into two categories: ledge mechanisms and models based on solute diffusion control. Honeycombe and coworkers were among the first to study interphase precipitation more profoundly [14,19,20]. They suggested that interphase particles form heterogeneously on γ/α boundaries thereby pinning their migration normal to the boundary. Local breakaway leads to formation of mobile ledges.

The ledges move sideways while the remaining part of the released boundary is stationary and enables repeated particle nucleation to occur, forming a new sheet. Hence, in this mechanism the intersheet spacing will be determined by the ledge height. From this follows one of the main drawbacks with the ledge mechanism, i.e. to produce a credible explanation of the observed variation of the intersheet spacing with temperature, and steel composition, especially N, V and C. It is hard to see how these parameters should generate a corresponding variation of the ledge height.

A model based on diffusion control, the solute-depletion model, proposed by Roberts [17] is the most prominent and promising. Zajac and Lagneborg [11] developed this model further. The quantitative description of the solute-depletion model considers a ferrite grain growing into austenite where the growth is controlled by carbon diffusion in austenite while maintaining local equilibrium at the interface, Figure 2.9.10.
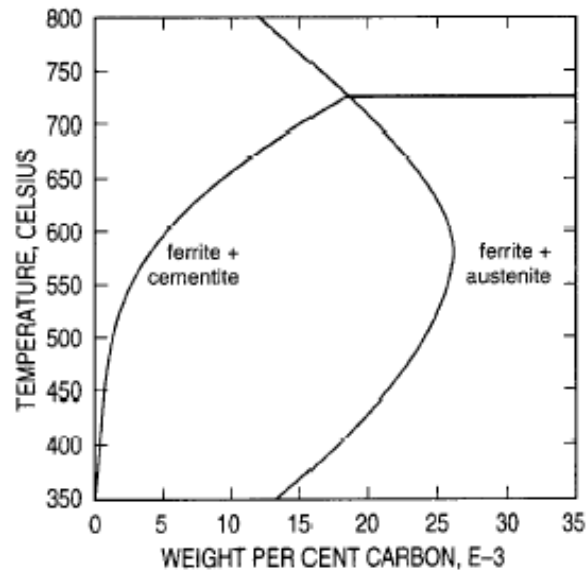
Figure 2.9.10: Solvus lines for C in ferrite calculated using Thermocalc for equilibrium with cementite and austenite.

At a given point of this growth the interplay is analysed between the nucleation of V(C,N) particles in the γ-α interface, the accompanying growth of V-depleted zones around the precipitates, and the continued migration of the γ-α boundary away from the precipitate sheet. The growth rate of a V-depleted zone is infinitely large directly after nucleation but declines gradually with time according to a parabolic growth law of type, particle radius $\propto$ $(time)^{1/2}$.

The growth of the ferrite obeys a similar parabolic time-law, but its rate can be considered constant for the short distance corresponding to the intersheet spacing relative to the size of the ferrite grain. The implication of this is that the moving γ/α interface will after nucleation initially be in a V-depleted zone, but will eventually catch up with the growing depleted zone.

The boundary has now returned into material with the original V-content, and nucleation of a sheet of particles will repeat itself. Hence, this gives the condition for calculating the intersheet spacing. Carrying out this quantitative analysis gives the following expression for the intersheet spacing [10]:

$$\lambda_{is} = 2S_0 \cdot \frac{K_2}{K_1} \dots\dots\dots\dots\dots\dots(3.1)$$

where, S_o is the distance grown by the ferrite at the point analysed, K_2 and K_1 are the proportionality factors in the parabolic growth laws for the V-depleted zone around the precipitate, and for ferrite, equations 3.2 and 3.3 apply:

$$r^2 = 2 \times 10^4 \cdot D_v^\alpha \frac{C_v^{\alpha\infty} - C_v^{\alpha/VCN}}{C_v^{VCN} - C_v^{\alpha/VCN} \cdot t} \dots\dots\dots(3.2)$$

where r is the radius of the depleted sphere at a point with 99% of the original V-content, D_v^α is the diffusion coefficient of V in α, $C_v^{\alpha\infty}$ the original V content in α, $C_v^{\alpha/VCN}$ the V content in α at the α/VCN interface, and C_v^{VCN} the V content of the V(C,N) particle.

$$S^2 = D_c^\gamma \frac{\left(C_c^{\gamma/\alpha} - C_c^{\gamma\infty}\right)^2}{\left(C_c^{\gamma/\alpha} - C_c^\alpha\right)\left(C_c^{\gamma\infty} - C_c^\alpha\right)} \cdot t \dots\dots\dots(3.3)$$

where S is the distance from the point of α nucleation to the location of the γ/α interface at time t. D_c^γ is the diffusion coefficient of C in austenite, $C_c^{\gamma/\alpha}$ the C content of γ at the γ/α interface, $C_c^{\gamma\infty}$ the original C content of γ, and C_c^α the C content of α in equilibrium with γ.
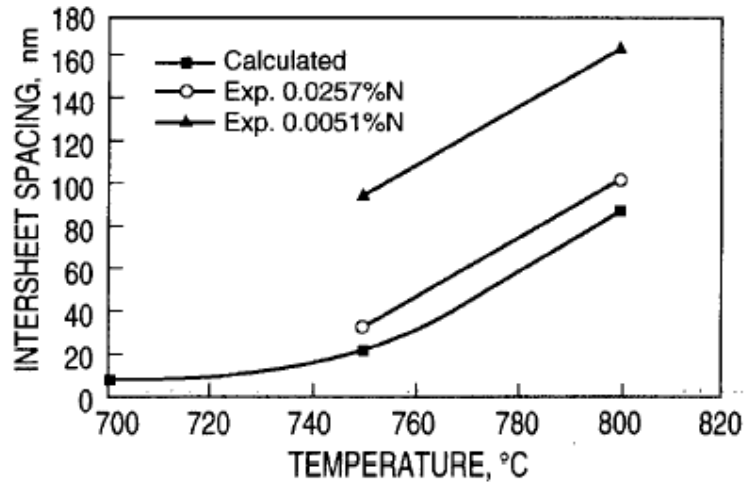
Figure 2.9.11: Experimentally measured and computed intersheet spacing in interphase precipitation of a 0.10 % C – 0.13 % V steel as a function of the transformation temperature.

Zajac and Lagneborg [11] used the model to predict the intersheet spacing, Figure 2.9.11. The agreement with observations of temperature dependence of the intersheet spacing is almost perfect. The noticeably smaller spacings observed for the high-N steel as compared to the low-N steel cannot explicitly be accounted for by the expressions above. However, we do know, also quantitatively, that the chemical driving force for VN precipitation is much larger than for VC.

This means that profuse nucleation occurs for lower V-concentrations, and thus we should expect that going from C-rich V(C,N) to N-rich will lead to smaller intersheet spacings. The computations shown in Figure 2.9.11, also predict that the intersheet spacing around 700°C will fall below the approximate size of observed precipitates. Physically, this implies that the growth rate of the γ-α interphase exceeds that of the V-depleted zone.

74

Hence, the γ/α boundary escapes, leaving the ferrite in its wake supersaturated with respect to V(C,N). In excellent agreement with experiments it is predicted that general V(C,N) precipitation occurs below about 700°C for steel compositions referred to in Figure 2.9.12. Above 800°C the V(C,N) precipitation becomes increasingly irregular and sparse for compositions typical of V-microalloyed structural steels, 0.10 % C - 0.10 % V. Again, this can be understood from the model.
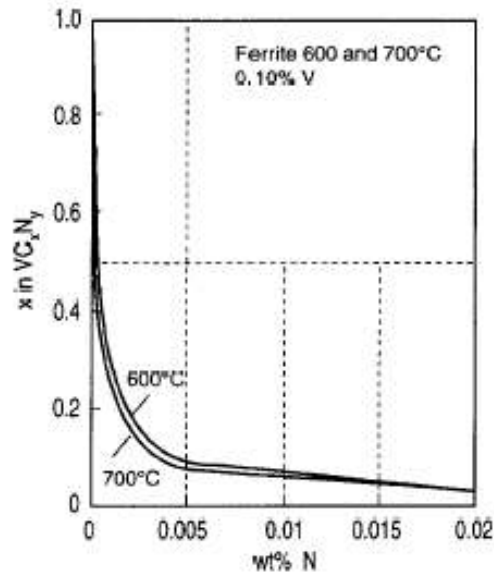
Figure 2.9.12: Thermodynamic calculations of the variation in the composition of V and N with content of N remaining in solution during precipitation in ferrite.

It predicts an accelerated increase of the intersheet spacing in this temperature range; at 850°C the predicted value for the steel examined in Figure 2.9.11 exceeds 500 nm. At the same time the spacing within the sheet will also increase. Under those circumstances it will be very difficult to perceive the observed microstructure as intersheet precipitation. To this should be added that around 850°C the solubility limit of V(C,N) is approached for the compositions considered.

2.10 EFFECTS ON THE AUSTENITE FERRITE TRANSFORMATION

2.10.1 TRANSFORMATION FROM AUSTENITE FERRITE IN VANADIUM CONTAINING STEELS

The transformation of austenite to ferrite and the changes, which accompany this transformation, are amongst the most important factors to be considered during steelmaking. In V containing steels, precipitation of V(C,N) can occur during this transformation. However, it is equally important to consider the effects of vanadium on the transformation and the transformation products, which result.

The primary parameters controlling the ferrite grain size produced in the γ-α transformation are the effective austenite grain boundary area, i.e. austenite grain boundary area/unit volume (S_V), and the cooling rate. However, for Nb-microalloyed steels, for a given S_V, the ferrite grain size is smaller when transformed from unrecrystallised, deformed and flattened austenite grains than from recrystallised, equiaxed grains [1].

Traditionally this difference has been accounted for by the additional ferrite nucleation that takes place in the deformation bands of heavily deformed austenite. Interestingly though when the same type of experiment is conducted for V and Ti-V microalloyed steels no difference is found. Deformed, unrecrystallised austenite grains transform to ferrite with virtually the same grain size as that produced from equiaxed, recrystallised austenite, Figure 2.10.1.

Thus, for the V steels the ferrite grain size is found to be independent of austenite grain shape and processing method. As can be seen from the figure, the V steels occupy an intermediate position between the lines for recrystallised and unrecrystallised Nb steels.
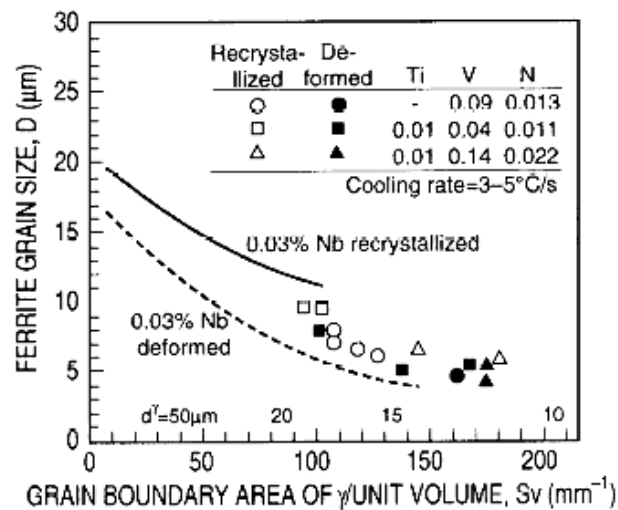
Figure 2.10.1: Dependence of ferrite grain size on the total area of austenite grain boundary per unit volume. Data points are for Ti-V and V microalloyed steels. Curves refer to Nb-microalloyed steels.

An essential result is that the same degree of ferrite grain refinement can be achieved for the V steels as for the Nb steels; about 4 μm, provided the effective austenite grain boundary area is large enough. An important and interesting feature of Ti-V and V steels is that additional N above a level of 0.003 % further refines the ferrite during the austenite-ferrite transformation, as shown in Figure 2.10.2 for recrystallisation controlled processing and in Figure 2.10.3 for normalising.

This behaviour has been explained partly as a result of interphase precipitation of V(C,N), which slows down the austenite-ferrite transformation and thereby gives more time for ferrite nucleation,

77

and partly as a result of more profuse ferrite nucleation along 'scalloped' γ grain boundaries.
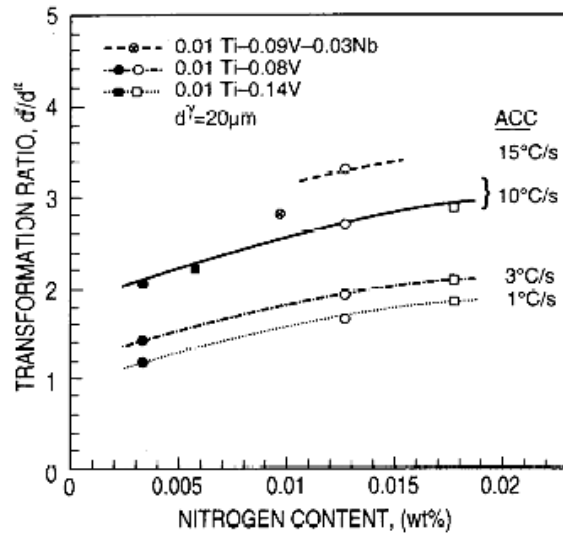
Figure 2.10.2: The effect of N on the refinement of ferrite during the γ-α transformation in Ti-V-(Nb)-N steels.
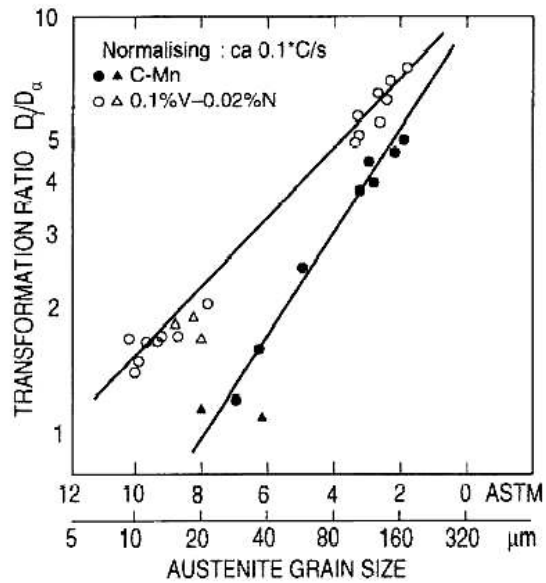
Figure 2.10.3: The effect of V and high N in refining the polygonal ferrite grain size produced during the γ-α transformation.

2.11 TEMPERING OF STEELS CONTAINING VANADIUM

Vanadium is usually added to steels to increase their tempering resistance in both the martensitic and bainitic conditions. Vanadium is a strong carbide former and, in steel with as little as 0.1 % V, the face-centred cubic vanadium carbide (VC) is formed [19]. It is often not of stoichiometric composition, being frequently nearer V_4C_3, but with other elements in solid solution within the carbide.

Normally, this is the only vanadium carbide formed in steels, so the structural changes during tempering of vanadium steels are relatively simple. Vanadium carbide forms as small platelets, initially less than 5 nm across and not more than 1 nm thick. These form on dislocations within the ferrite grains in the temperature range of $550 - 650^0C$ and produce a marked secondary hardening peak.

At 700 ^oC, the platelets coarsen rapidly and begin to spheroidise. The original martensite laths can still be recognized, and are only replaced by equi-axed ferrite grains after long periods at 700 ^oC.

2.12 MICROSTRUCTURE DEVELOPMENT DURING THERMO-MECHANICAL PROCESSING OF V STEELS

Knowledge of the microstructure development in association with hot rolling is very important for optimising rolling procedures with the aim of improving properties of steels [1]. Reheating has almost no effect on the final austenite grain size resulting from recrystallisation rolling, as long as the rolling procedure involves more than 3 to 4 passes.

After large reductions, recrystallisation takes place via copious nucleation of new grains and refinement of the structure can be achieved. The nucleation of recrystallisation decreases strongly as the level of strain is reduced, and hence small rolling reductions at high temperatures can cause abnormally large recrystallised grains. This is most serious at the end of the hot rolling sequence when a small 'sizing' pass applied for control of thickness or shape may destroy the fine-grained austenite structure. Coarsening of the austenite can occur as a result of grain growth at high temperatures or, at lower temperatures, from the 'critical strain anneal' phenomenon.

With small reductions in final sizing passes, nucleation of new grains takes place only infrequently at a few favoured sites followed by extensive growth. Instead of refinement, this process leads to a mixture of recovered pre-existing fine grains together with some very much coarser grains.

Holding time at temperature is also important for microstructure coarsening and a practical conclusion is that accelerated cooling applied rapidly after the final pass can be of great benefit in reducing the danger of structure coarsening.

Vanadium grain refined steels are prone to grain growth as most mills have finishing passes with small reductions (<10%) in the final stages of rolling. The finishing temperature after passing through the final rolls determines if any temperature related grain growth will occur.

2.13 THE EFFECT OF VANADIUM IN SPRING STEEL

More recent work has focused on the development of steel compositions which can be heat treated to higher hardness levels resulting in not only improved sag resistance, but in improved fatigue properties [21].   Spring sag is a relaxation phenomenon, which results in a reduced load carrying capability.

High silicon levels in spring steels are effective in refining carbides formed during tempering. As a result, high silicon levels significantly improve sag resistance. Additions of microalloying element have been found to be beneficial in improving both strength and sag resistance. An important aspect of the properties of these microalloyed steels is the type of heat treatment conducted.

Heitmann [21] *et al* investigated the effect of V additions to a medium C and high C spring steel in conjunction with alternative heat treatments for the use of short time induction heaters. The two steels that were used in the experiment is shown in Table 2.13.1.

Table 2.13.1: Experimental compositions of spring steels.

Material specification	% C	% Si	% Mn	% S	% P	%Cr	% V	% Al	% N
SAE92V45	0.49	1.24	1.27	0.013	0.015	0.51	0.15	0.006	0.010
SAE92V54	0.53	1.46	0.57	0.005	0.002	0.63	0.15	0.023	0.002

Specimens were prepared for heat treatment at long and short austenitising times of 90 seconds and 120 minutes at 900 ^{o}C. Quenched into oil and tempered for 90 seconds and 120 minutes. Besides standard metallography, tensile tests were conducted.

The metallographic investigation revealed that the SAE92V45 steel had finer prior austenite grain size after quenching than the SAE92V54 steel for both austenitising times. The mechanical properties of the steels revealed vast differences in UTS as shown in Figure 2.13.1 for 90-second and 60 minutes austenitising time with the same tempering time.
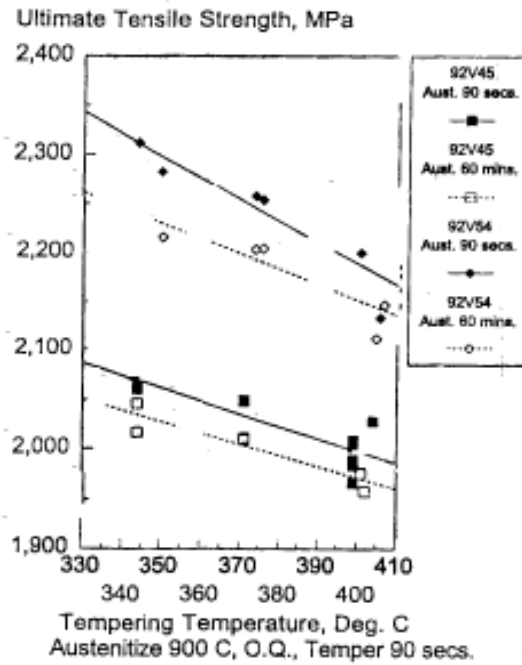
Figure 2.13.1: Spring steel austenitised at 900 °C for 90 seconds and 60 minutes, oil quenched, tempered for 90 seconds.

The reduction in UTS for longer austenitising time has been attributed to the dissolving of VN and V(C,N). A longer tempering time of 120 minutes shown in Figure 2.13.2 indicates lower UTS values combined with a steeper decline in tensile strength with increased tempering temperature. Longer tempering times result in more recovery and coarser carbides, which result in lower tensile strength [21].
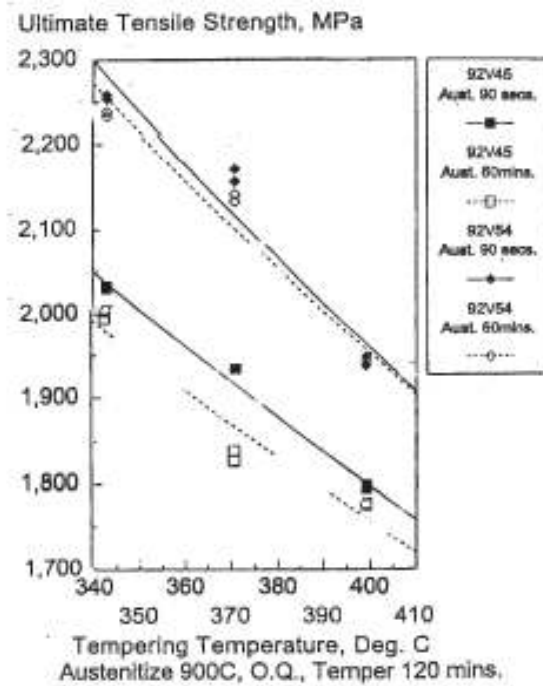
Figure 2.13.2: Spring steel austenitised at 900 °C for 90 seconds and 60 minutes, oil quenched, tempered for 120 minutes.

Comparative ductility results measured by the reduction in area of the tensiles for short austenitising and tempering times are given in Figure 2.13.3. The ductility of the SAE92V45 steel exhibited good ductility in all tests, whereas the SAE92V54 showed erratic results.
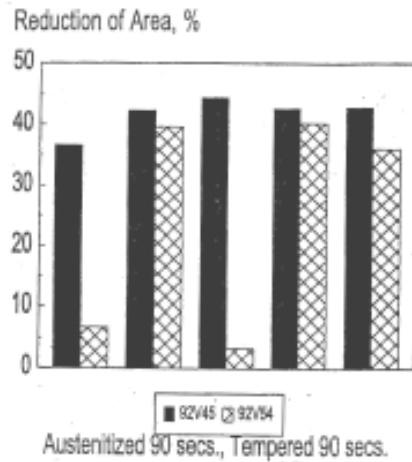
Figure 2.13.3: Reduction in area of spring steel austenitised at 900 °C for 90 seconds, oil quenched, tempered for 90 seconds.

Scanning electron micrographs of the fracture surfaces from the tensile specimens revealed the mode of failures. Figure 2.13.4 is a representation of the 92V45 steel fracture face showing microvoid coalescence.
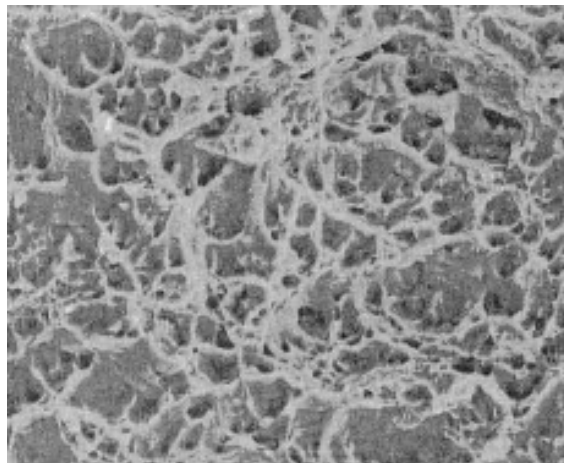
Figure 2.13.4: Fracture surface from tensile specimen of 92V45 steel austenitised at 900 °C for 90 sec, tempered for 90 sec. (3000X).

The analysis of the 92V54 steel with low ductility revealed intergranular fracture as shown in Figure 2.13.5.
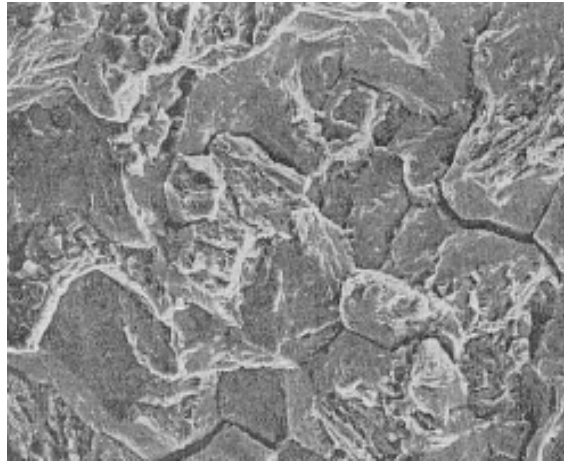
Figure 2.13.5: Fracture surface from tensile specimen of 92V54 steel austenitised at 900 ^{o}C for 90 sec, tempered for 90 sec. (3000X).

The fracture modes in the 92V54 steel varied from ductile to intergranular fracture characterised by variable reduction in area. Heitmann [21] discovered that the ductility varied even if several samples were identically heat treated. The variance in ductility of 92V54 has been attributed to the phenomenon of quench embrittlement.

This is a brittle fracture mechanism attributed to phosphorous segregation and cementite formation on austenite grain boundaries during the austenitising and quenching stages of hardening. The 92V54 steel is capable of reaching high tensile properties, but with an increased susceptibility to quench embrittlement.

2.14 COIL SPRINGS

Spring steels are defined as steels, which owing to their resilience in the quenched and tempered condition are suitable for the production of any type of springy component. The resilience of the steels results from their elastic deformability, which enables them to sustain loading to a specific limit without this causing permanent distortion after unloading. Figures 2.14.1 and 2.14.2 show typical coil spring for automotive applications.

Figure 2.14.1: Coil spring for automobiles.

Figure 2.14.2: Application of coil spring in a suspension system.

2.14.1 THE COIL SPRING MANUFACTURING PROCESS

The manufacture of automotive coil springs follows a definite route with special procedures set by the OEM's (Original Equipment Manufacturers). The quality of the end product cannot be compromised as the coil springs indirectly serve as safety devices in cars. If a coil spring failed while in operation, it would be equivalent to having a blow out on a tyre. Figure 2.14.3 gives a basic outline of a typical process.
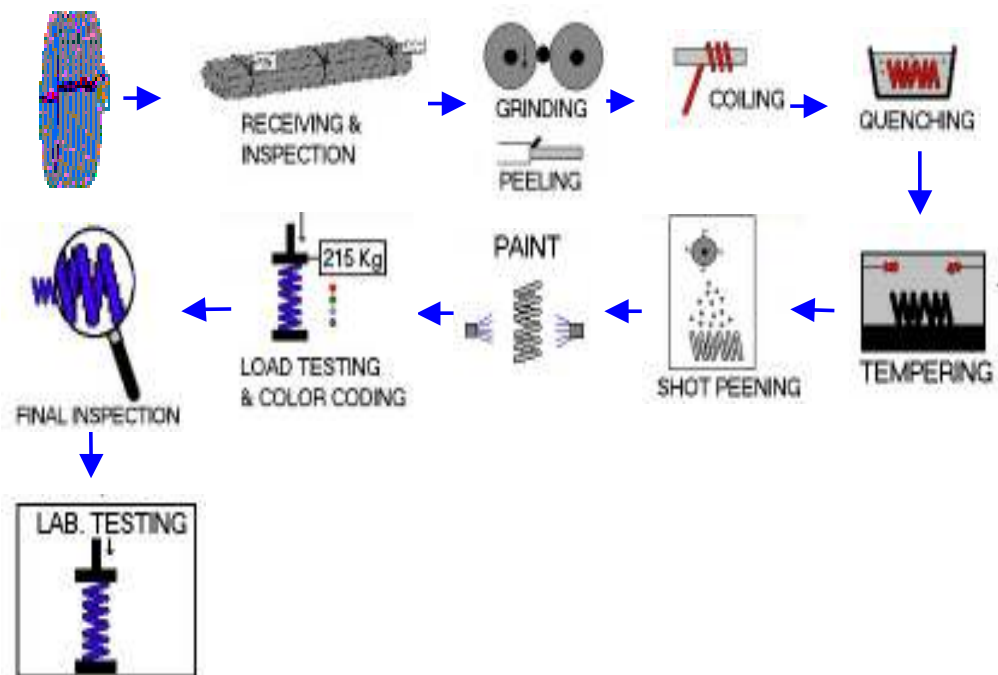
Figure 2.14.3: Typical coil spring manufacturing process.

The coil spring manufacturing process can be explained as follows:

Initial Processing

A 1-ton coil is supplied to the factory. The rod is decoiled, cut to length and straightened. The surface of the bars is then ground or peeled. The peeling or grinding operation is requirement of the OEM's for improved surface quality with respect to defects and decarburisation. Up to 3 % of the diameter per side is removed by

87

this operation. Figure 2.14.4 shows a typical bar in the as rolled condition. Figure 2.14.5 shows the same bar in the peeled condition. Figure 2.14.6 is a representation of the typical level of decarburisation on as-rolled material.

Figure 2.14.4: Bar in as rolled condition.

Figure 2.14.5: Bar in the peeled condition.
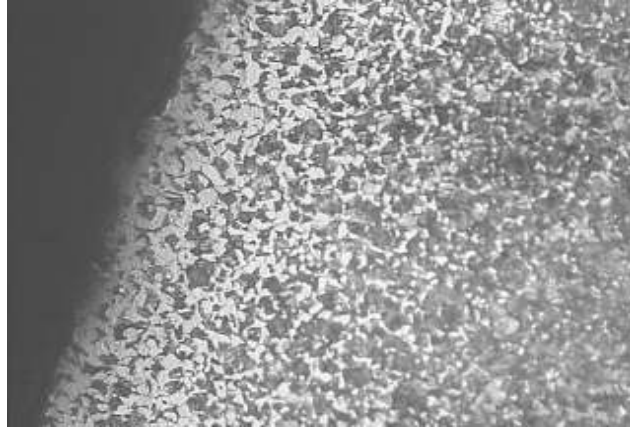
Figure 2.14.6: Decarburisation on as-rolled material. Etched in 2 % Nital, 100X.

Intermediate Processing

The peeled bars are inspected for surface defects by eddy current before coil spring manufacture. The coil springs are hot formed. Peeled bars are inserted into a furnace set at between 860 $^{\circ}$C to 890 $^{\circ}$C. Residence time in the furnace is typically set at 15 minutes to limit decarburisation. Figure 2.14.7 shows the typical level of decarburisation obtained during austenitisation. Decarburisation is unavoidable during the process and is allowable by the OEM's.
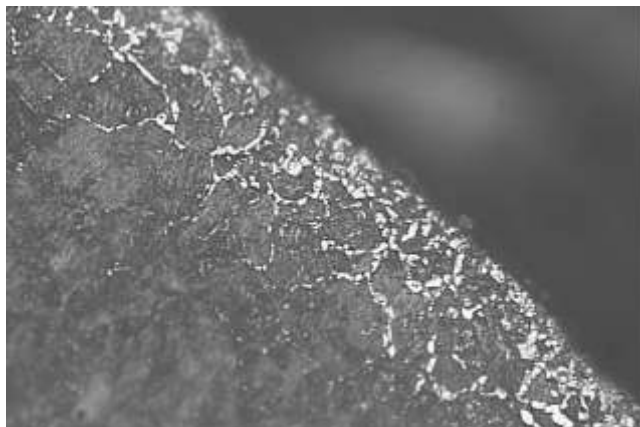
Figure 2.14.7: Decarburisation of peeled bar after austenitising and quenching. Etched in 2 % Nital, 500X

The hot bars are then coiled to the required dimensional specification. Quenching takes place in an oil bath. The springs are then tempered for 1.5 hours at between 420 ^{o}C and 440 ^{o}C. Typical hardness values are between 51 to 54 HRc. The tempered springs are then shot peened to improve the fatigue life of the final product. They are then subjected to a non-destructive load test. This serves as a final check of the heat treatment of the springs.

Final Processing

The final processing includes final inspection and fatigue testing. The fatigue testing forms an integral part of the requirements of coil springs. The springs are subjected to continuous loading and unloading during operation in a motor vehicle. The fatigue test is a severe method of simulating the actual operating conditions and is a strict requirement of the OEM's. The spring is compressed fully and allowed to return to its original position. This constitutes one cycle. A statistical sample is used per batch of coil springs (usually 4 tests per 100 springs). A typical fatigue-testing machine is shown in Figure 2.14.8:

Figure 2.14.8: Typical fatigue testing machine.

Figure 2.14.8 shows three springs in various stages of compression. The OEM's usually require the spring to be subjected to a minimum of 300000 cycles to pass the test. The technical specifications of the coil spring are presented in Table 2.14.1.

Table 2.14.1: Technical specification of the coil spring.

	Specification
Peeled diameter	10.8 mm ± 0.05 mm
Cut length	2695 mm ± 5 mm
Weight	1.94 Kg
Inspection	100 % eddy current
Length of coil	370 mm – 387 mm
Required hardness	51 – 54 HRc
Shot peening	90 % coverage minimum
Maximum allowable stress	1800 MPa
Allowable decarburisation	0.10 mm maximum
Fatigue test amplitude	191.5 mm
Fatigue test frequency	1 – 5 Hz
Minimum fatigue cycles to failure	300000

2.14.2 FATIGUE OF COIL SPRINGS

Fatigue occurs in structures that are subjected to cyclic stresses, and failures often occurs at a stress level, which is considerably lower than the yield stress of the material determined under static conditions [20]. The fatigue properties of metal components are important to designers because fatigue is the single largest cause of failure in service for metals, accounting for an estimated 90% of all failures.

Many failures can be attributed to poor design, but the majority occur at discontinuities such as spot welds. In a few cases, failure can be attributed to the surface condition of the material. Factors influencing the fatigue strength of a component include material properties, loading regime, residual stresses, surface condition and the presence of stress concentrations such as holes, welds, or severe changes in section.

The basic function of shot peening is to improve the fatigue life or strength of cyclically stressed metal components [22]. This is achieved by generating, via the peening process, a shell or skin of plastically deformed material around the peened part. This peened skin, which is in a state of high residual compressive stress (self-stress), resists the nucleation and propagation of micro-cracks at the part of the surface. Figure 2.14.9 shows a well-shot peened coil spring.
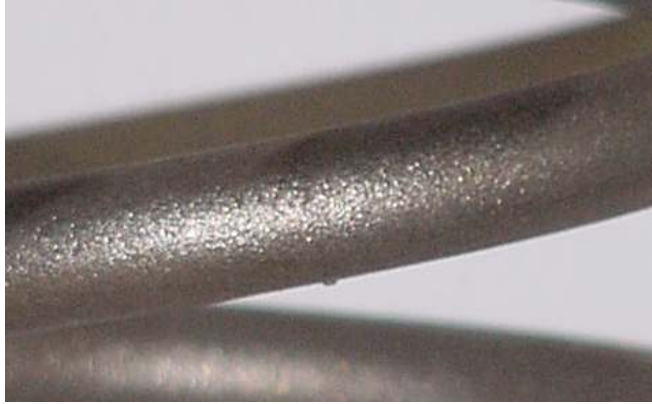
Figure 2.14.9: Well shot peened coil spring.

The fatigue strength of springs can be notably improved by shot peening [23]. After forming into coil spring, the inner surface of the spring exhibits tensile residual stress, $+\sigma_r$, which result in the decrease of fatigue strength. The tensile $+\sigma_r$, however can be changed into compressive residual stress, $-\sigma_r$, using shot peening from which the fatigue properties can be improved.

For high strength, high fatigue spring steels, especially good fatigue properties are required, which depend on their design as well as on the strength-ductility combination of the steel applied. High values of strength and ductility normally ensure excellent fatigue properties, but, unfortunately, ductility decreases with increasing strength level.

Therefore, today in the manufacture of automotive coil springs, a maximum strength of about 1750MPa is specified, because higher strength would lead to poor ductility and finally to worse fatigue properties [20]. The combination of hot rolling and subsequent thermo-mechanical treatment (TMT) appears to offer the promising possibility of improving both the strength and the toughness (ductility) and therefore the fatigue properties of the final springs.

However, the changes occurring in the austenite due to hot deformation, must be preserved until the start of the γ-α transformation. In this way, the changes in the microstructure of the austenite can influence the martensite formation in the quenched and tempered steel and improve mechanical properties.

Improved fatigue properties take two forms:

- Increase in the number of cycles to failure and,
- Increase in fatigue strength, which is defined as the load or stress below which, fatigue failure does not occur.

The fatigue resistance of metals may be quantified as the resistance to crack propagation offered by the material [24]. This resistance can be studied by examining the following two conditions:

- **Intensity and spacing of microstructural barriers**: If a crack is obstructed in its path by many closely packed barriers, which deflect the path of the crack, then the fatigue resistance is high. It follows that small grains offer a high resistance to crack advance in a material.
- **Crack tip plastic zone**: as a crack grows longer at a constant cyclic stress range its plastic zone size, which controls crack growth rate, increases.

The operation of coils springs is such that due to design, loading on the springs, induces torsional and bending forces. The coil springs normally fracture in a concoidal manner due to the forces acting on it.

2.14.3 THE EFFECT OF GRAIN SIZE ON FATIGUE

The fatigue fracture of materials containing flaws or cracks is caused by the growth of these defects under cyclic loading. For metallic materials, which are initially free of large flaws or cracks, slip motion leads to the formation of fatigue cracks, which eventually propagate to the critical length for final fracture [24]. The grain size of the metal can play an important role in slip motion, crack nucleation and growth of fatigue process.

To assess the influence of microstructural constituents such as grain size on fatigue strength, a quantitative understanding of the nature of the basic mechanism working in each stage of the fatigue process is essential. Taira *et al* [25] investigated the effect of grain size on crystal deformation, crack nucleation and crack growth in long life fatigue of a low carbon steel, by use of optical microscopy and SEM (Scanning electron microscopy).

The steel had composition of 0.2 % C, 0.92 % Mn, 0.26 Si, 0.11 P, 0.15 S, 0.009 N and was supplied in 8 mm thick hot rolled strip. Three different grain sizes were obtained by heat treating. The ferrite grain size measured 7.8, 20.5 and 55 μm. The material with each grain size was designated A, B and C respectively. The heat treatment condition and the mechanical properties derived from simple tensile tests are summarised in Table 2.14.2:

Table 2.14.2: Heat treatment condition and mechanical properties of material.

Material	Heat treatment	Grain size (μm)	YS (MPa)	UTS (MPa)
A	Annealed at 900 °C for 10 minutes followed by air cooling	7.8	366	528
B	Annealed at 1000 °C for 1 hour followed by furnace cooling	20.5	275	466
C	Annealed at 1200 °C for 5 hours followed by furnace cooling	55	194	433

The samples were machined after heat treatment for fatigue tests as shown in Figure 2.14.10.
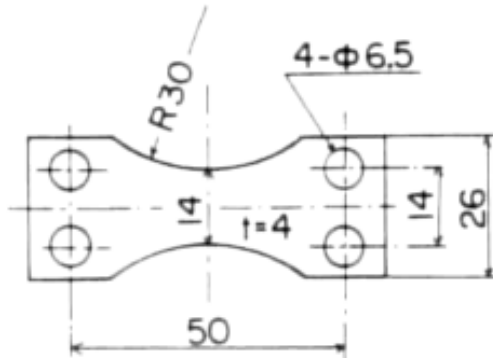
Figure 2.14.10: Machined specimen for fatigue tests. (Dimensions in mm).

The samples were etched in 3 % Nital prior to fatigue testing. The fatigue tests were performed in a resonance type bending test machine operated at a test speed of 33.3 Hz. In addition, fatigue crack propagation was performed on specimens machined after heat treatment as shown in Figure 2.14.11. A servo-hydraulic fatigue testing machine operating at 30 Hz was used. The length of the fatigue crack was monitored with a traveling microscope at 400 times magnification.
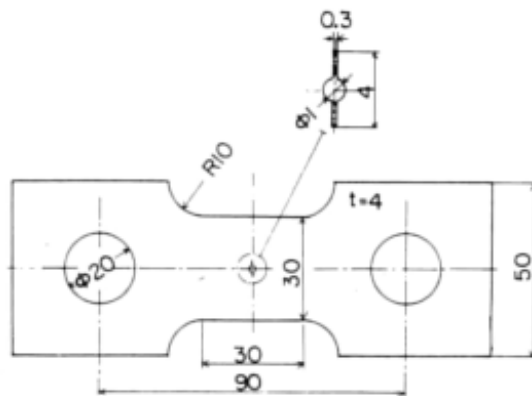
Figure 2.14.11: Machined specimen for fatigue crack propagation tests. (Dimensions in mm).

During fatigue tests, the machine was stopped and the specimen removed periodically. The microstructure and small cracks on the specimen surface was examined by optical microscopy and SEM. Figure 2.14.12 presents examples of micrographs, which were taken from the fatigued specimens. Figure 2.14.12(a) corresponds to the time when the slipband was first observed with stress amplitude (σ_a) of 245 MPa.

The number of stress cycles (N) is 1×10^4. The arrows in Figure 2.14.12(b) and 2.14.12(c) indicate the growth of fatigue cracks along directions not parallel to the slip plane, which is a characteristic feature of Stage II crack propagation.

The crack is nucleated along the grain boundary in the former case and along slipbands in the latter case. The σ_a was 245 MPa with N at 2.5×10^5 and 2.7×10^5 respectively. Figure 2.14.12(d) shows another crack nucleated along the grain boundary with the same σ_a as above and N of 3.0×10^5. Figures 2.14.12(e) and 2.14.12(f) were taken from specimens fatigued to 10^7 cycles.

Figure 2.14.12(e) corresponds to the microstructure of the specimen fatigued just below the fatigue limit. Figure 2.14.12(f) shows the microstructure of a specimen fatigued just above the limit of slipband formation.
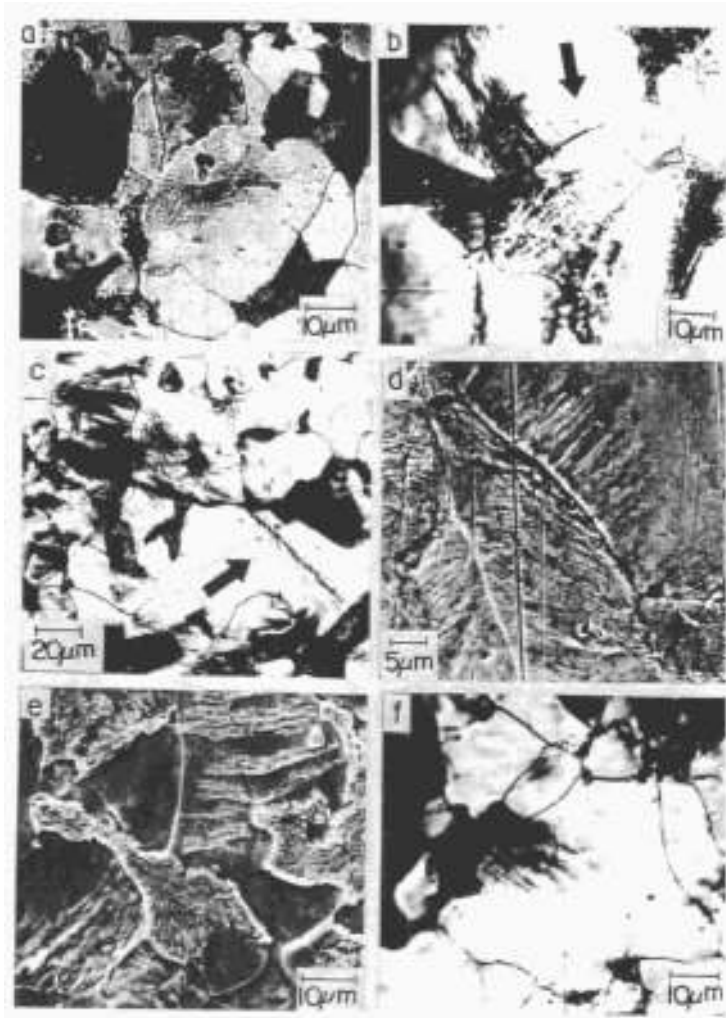
Figure 2.14.12: Optical micrographs and SEM taken from fatigued specimens of material B. (Stress axis is vertical).

The fractions of the number of cycles at slipband formation (N_s), at crack nucleation (N_c), and to the total life (N_f) were determined. The results are presented in Figures 2.14.13 to 2.14.15, corresponding to Materials A, B and C respectively.
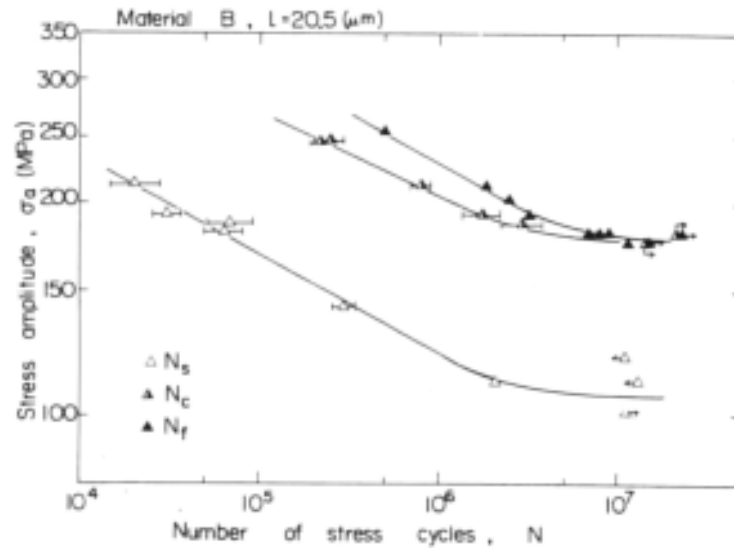
Figure 2.14.13: S-N curve for material A.
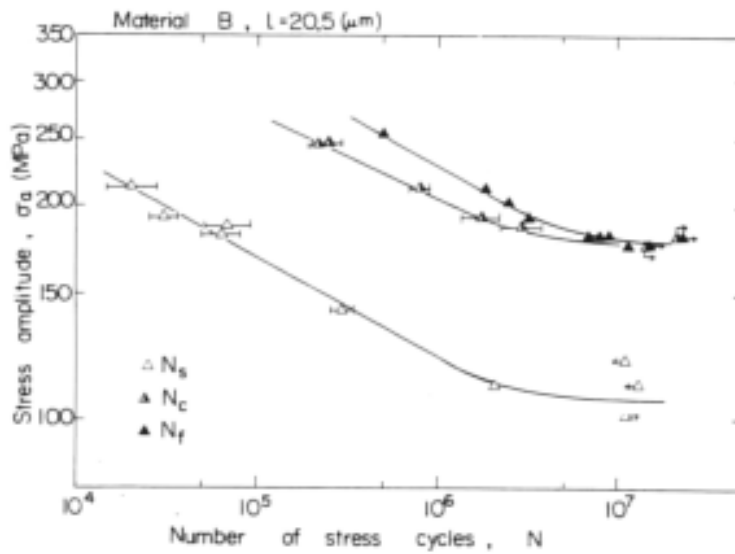
Figure 2.14.14: S-N curve for material B.

The relation between N_s and σ_a is independent of the grain size, and the limit of stress amplitude (σ_{wos}), for slipband formation is 107 MPa. The number of cycles to initiate a crack (N_c), is smaller in the larger grain size material and difference in N_c with different grain sizes diminishes for the cases of higher stress amplitude fatigue.

99
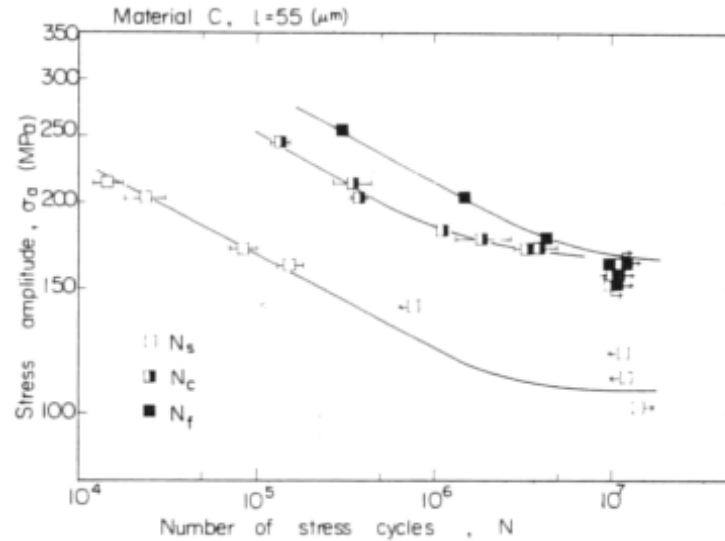
Figure 2.14.15: S-N curve for material B.

The number of cycles, N_p, spent for propagating a nucleated crack to final fracture is larger in smaller grain size material, when compared at the same stress amplitude. In conclusion, the grain size of low carbon steel does not affect either the limit of slipband formation or the relation between stress amplitude and number of cycles to slipband formation. The grain size has a significant influence on nucleation and propagation lives of cracks, and on the fatigue limit.

Precipitates such as VC or V(C,N) pin grain boundaries during heat treatment. The resulting fine grain size improves the fatigue life. Precipitates also increase tensile strength, which improves fatigue life.

3 EXPERIMENTAL PROCEDURE

3.1 HOT ROLLING OF STEEL

In order to assess the two steels on an equal basis, it was decided to hot roll them under the same conditions and to the same size. Two tons of steel in each grade was prepared for this investigation. The chemical analysis of the two steels are shown in Table 3.1.1:

Table 3.1.1: Chemical analysis and specification of steel grades used.

Material specification		%C	%Si	%Mn	%S	%P	%Cr	%Ni	%Mo	%V	%Al	%N
54SiCr6 Requirement	Min	0.51	1.20	0.60			0.60				0.020	
	Max	0.59	1.60	0.80	0.030	0.03	0.80				0.040	
Pit analysis		0.55	1.25	0.71	0.003	0.012	0.65	0.01	0.004	0.005	0.025	0.006
Sample		0.56	1.25	0.70	0.002	0.011	0.67	0.01	0.008	0.005	0.028	0.006
		Al : N = 4.2 : 1		V : N = 0.83 : 1								
SCV54/03 Requirement	Min	0.51	1.20	0.60			0.60			0.05		
	Max	0.59	1.60	0.80	0.030	0.030	0.80			0.15		
Pit analysis		0.56	1.31	0.69	0.002	0.011	0.65	0.08	0.016	0.056	0.016	0.007
Sample		0.56	1.31	0.69	0.002	0.011	0.66	0.08	0.019	0.056	0.016	0.007
		Al : N = 2.2 : 1		V : N = 7.7 : 1								

The typical processes in the hot rolling of the steel are shown in Figure 3.1.1.
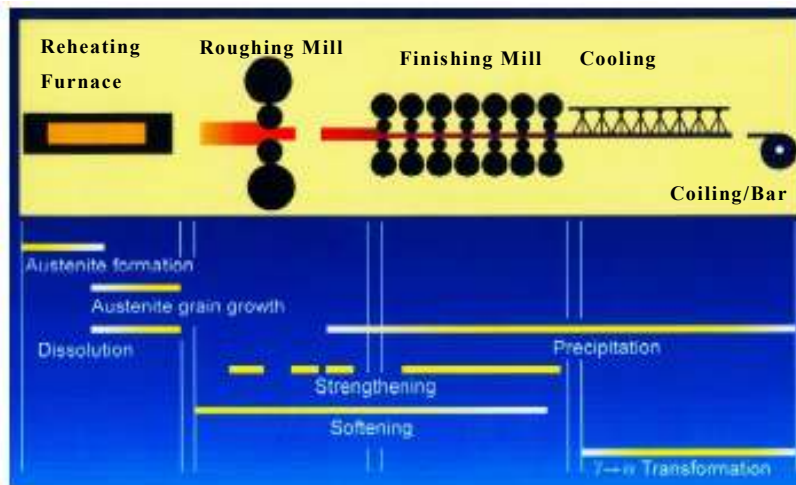
Figure 3.1.1: Hot rolling of steel.

The reheating furnace conditions were as follows:

- Soaking temperature in reheating furnace was set at 1300 ^{o}C.
- Billet temperature of SCV54/03 on exit from the furnace was 1103 ^{o}C.
- Billet temperature of 54SiCr6) on exit from the furnace was 1099 ^{o}C.
- Residence time of the billets in the furnace was 2 hours 20 minutes.
- Finishing temperature before cooling bench was about 900 ^{o}C for both steels.

The steels were rolled to a nominal diameter of 18.0 mm. Controlled cooling was applied on the cooling bench by means of insulated cooling hoods. The reason for the slow controlled cooling was to reduce the hardness of the material. Softer material facilitates easier straightening, cropping and peeling.

3.2 HEAT TREATMENT OF ROLLED PRODUCT FOR MECHANICAL PROPERTIES

Samples of 300 mm length were cut from the bundled 18.0 mm steel bars. These were subjected to austenitising at three different temperatures and quenched in oil. Tempering for several periods at multiple temperatures was then done. Two samples per steel grade were tempered at the same temperature for the preparation of tensile, metallographic, SEM and specimens. The heat treatment procedures are outlined in Table 3.2.1.

Table 3.2.1: Heat treatment of samples for determination of mechanical properties

Austenitising temperature °C	Tempering Temperature °C	Tempering Time			
		1 hour	2 hours	4 hours	8 hours
880	380	x			
	400	x			
	420	x			
	430	x	x	x	x
	440	x			
	460	x			
	480	x			
	500	x			
	530	x			
860	380	x			
	400	x			
	420	x			
	430	x	x	x	x
	440	x			
	460	x			
	480	x			
	500	x			
	530	x			
840	380	x			
	400	x			
	420	x			
	430	x	x	x	x
	440	x			
	460	x			
	480	x			
	500	x			
	530	x			

3.3   MANUFACTURE OF COIL SPRINGS

The manufacture of the coil springs was done in such a way as to minimise process variations. Fifty peeled bars of each steel grade were selected and loaded into the austenitising furnace. The SCV54/03 bars were loaded first. The 54SiCr6 bars were loaded immediately thereafter. The bars were austenitised at 890 $^{\circ}$C for 15 minutes. The short duration of the bars in the furnace limits the degree of decarburisation.

Decarburisation is an important factor in coil springs. It is important that input material to the coil spring manufacturing process has no decarburisation after the process of peeling. In turn, it is important that the hot rolled material must have minimal decarburisation

Coil samples were taken at quenching, after tempering and after shot peening. A portable pyrometer was used to measure bar temperatures at the furnace exit and prior to quenching the coil in oil (Shown in Table 3.3.1). The tempering of the coil springs was done at 430 $^{\circ}$C for 90 minutes.

Table 3.3.1: Temperature readings by pyrometer.

SCV54/03		54SiCr6	
Exit material temperature ($^{\circ}$C)	Into oil temperature ($^{\circ}$C)	Exit material temperature ($^{\circ}$C)	Into oil temperature ($^{\circ}$C)
891	802	893	803
892	798	894	800
891	797	894	803
893	801	897	793
892	798	895	797
891	797	895	803
890	795	897	802
892	793	897	797
890	800	895	802
891	796	894	795

A temperature loss of approximately 90 °C between the exit of the bars from the furnace and the quenching oil may be noted. This temperature loss occurs during the coiling operation.

3.4 METHODS OF MEASURING DECARBURISATION

Two international standards were used to measure the level of decarburisation in as rolled and heat treated steel, ASTM E1077[26] and SAEJ419[27]. The method used is dependant on the requirements of the customer. The accuracy of the method to be used depends on the degree of decarburisation, microstructure and base carbon content of the steel.

3.4.1 ASTM E1077

The decarburisation is measured by a microscopic method:

- Microscopic methods are most suitable for measuring the depth of decarburisation for as rolled, as forged, annealed, normalised or heat treated specimens.
- A transversal slice of the test piece is prepared metallographically and is etched in 2% Nital.
- Measurement of the depth of decarburisation is based on evaluation of the variation in microstructure at the surface due to the change in carbon content.
- Measurement is taken at 100 X magnification. The decarburisation is measured to the point where the microstructure becomes uniform.

The percentage decarburisation is calculated as follows:

$$\%Decarburisation = \frac{Decarburisation(mm)}{Diameter(mm)} \times 100 ....3.4.1$$

3.4.2 SAEJ419

As in the ASTM E1077 method, decarburisation analysis is done by microscopic methods. The difference in the SAEJ419 method is that an estimate of the point at which a 50 % carbon loss from the base metal to the surface is measured. This point is defined as the depth of decarburisation.

3.5 HARDNESS TESTS

Rockwell hardness tests were performed in accordance with ASTM E18 – 84[28].

3.6 GRAIN SIZE MEASUREMENT

The grain size of steel was measured in accordance with ASTM E112 – 85[29].

3.6.1 THE OXIDATION METHOD

The oxidation method is used to determine the resistance to grain growth.

- This method is good for carbon and alloy steels with a 0.35 – 0.60 % C-contents for determining prior austenite grain size and for performing grain growth tests.
- Polish the sample to the final stage.
- Place it in a furnace with the polished side up.
- Heat at 857 $^{\circ}$C ± 14 $^{\circ}$C for one hour. Cool the sample in water.
- Final polish the original polished surface and etch in 10 % HCL-alcohol solution for 5 – 10 minutes. The grain size, which is oxidised by high temperature, is now visible.

3.7   TENSILE TESTING

Tensile testing were carried out according to the ASTM E8M[30] specification. The test method covers tensile testing of metallic materials in any form at room temperature, specifically the methods of determination of yield strength, yield point, tensile strength, elongation and reduction in area.

3.8   FATIGUE TESTING

The coil springs were fatigue tested according to the following settings:

Fatigue test amplitude	191.5 mm
Fatigue test frequency	4 Hz
Minimum fatigue cycles to failure	300000

4   RESULTS

4.1   MATERIAL IN THE HOT ROLLED CONDITION

4.1.1   MICROSTRUCTURE OF HOT ROLLED MATERIAL

Approximately 2 tons of the SCV54/03 and 54SiCr6 were rolled under standard practice to 18.0 mm diameter bar. Samples were taken for metallurgical evaluation. Figure 4.1.1 shows the as rolled microstructure of SCV54/03. The microstructure consisted of ferrite and pearlite, which is typical of hot rolled steel of this composition.
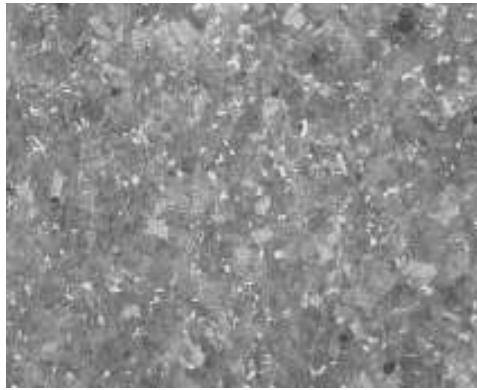
Figure 4.1.1: Microstructure of hot rolled SCV54/03. Etched in 2 % Nital, 200X.

Figure 4.1.2 shows the same sample at higher magnification. Note the well defined pearlite colonies.
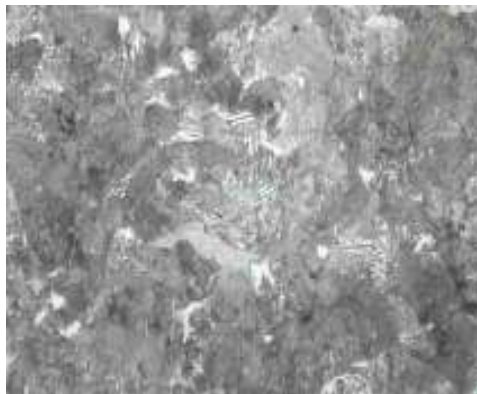
Figure 4.1.2: Microstructure of hot rolled SCV54/03. Etched in 2 % Nital, 500X.

The as rolled microstructure of the 54SiCr6 steel (Figure 4.1.3) is comparable to the SCV54/03 steel shown in Figure 4.1.1.
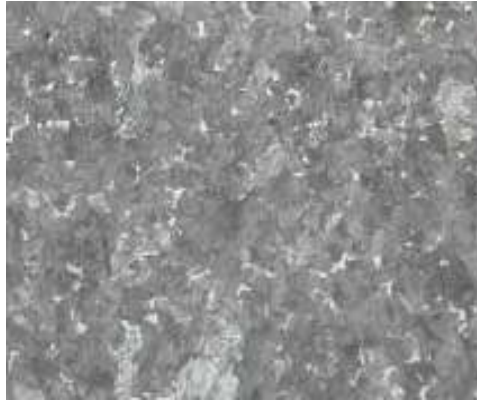
Figure 4.1.3: Microstructure of hot rolled 54SiCr6. Etched in 2 % Nital, 200X.

Figure 4.1.4: Microstructure of hot rolled 54SiCr6. Etched in 2 % Nital, 500X.

Due to the minor differences in chemical composition of the two steels, the as rolled microstructures are comparable. The grain size measured by the ASTM E112 method was ASTM 8 and finer.

4.1.2 DECARBURISATION ON HOT ROLLED MATERIAL

Figures 4.1.5 and 4.1.6 shows the decarburisation on an as rolled sample of SCV54/03 and 54SiCr6 respectively. The two methods of measuring decarburisation always give different results. The decarburisation on SCV54/03 is 0.10 mm when measured according to SAE J419 and 0.17 mm when measured according to ASTM E1077. The measurements for 54SiCr6 were 0.14 and 0.20 mm respectively.
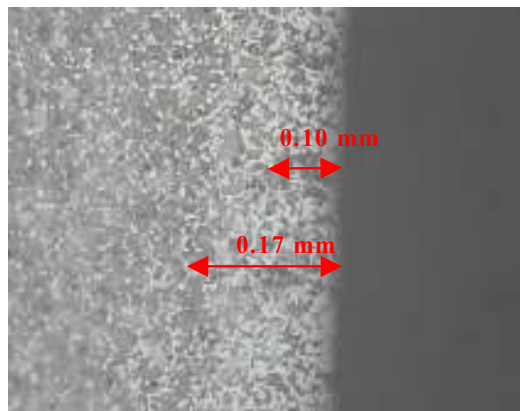
Figure 4.1.5: Decarburisation on SCV54/03 in the as rolled condition. Etched in 2 % Nital, 100X.
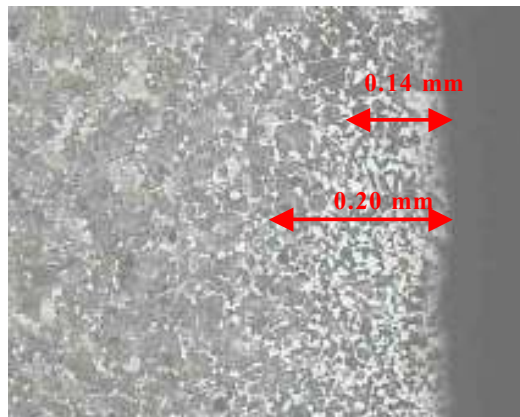
Figure 4.1.6: Decarburisation on SCV54/03 in the as rolled condition. Etched in 2 % Nital, 100X.

Table 4.1.1 shows the decarburisation readings of random as rolled experimental samples.

Table 4.1.1: Decarburisation readings on SCV54/03 and 54SiCr6 from the mill.

Method of Measurement		Decarburisation			
		ASTM E1077		SAE J419	
		Depth in			
		mm	Percentage	mm	Percentage
Steel Grade	SCV54/03	0.17	0.94 %	0.10	0.56 %
		0.16	0.89 %	0.09	0.50 %
		0.19	1.06 %	0.10	0.56 %
		0.18	1.00 %	0.11	0.61 %
		0.16	0.89 %	0.08	0.44 %
	Average	**0.17**	**0.96 %**	**0.10**	**0.53 %**
	54SiCr6	0.20	1.11 %	0.14	0.78 %
		0.18	1.00 %	0.11	0.61 %
		0.16	0.89 %	0.10	0.56 %
		0.15	0.83 %	0.10	0.56 %
		0.16	0.89 %	0.08	0.44 %
	Average	**0.17**	**0.94 %**	**0.11**	**0.59 %**

N.B: Percentage decarburisation based on nominal diameter of 18.0 mm.

The results shown in Table 4.1.1 are on Figures 4.1.7 and 4.1.8 for methods ASTM E1077 and SAE J419 respectively. It can be seen that the decarburisation on the samples of the two steels are comparable.
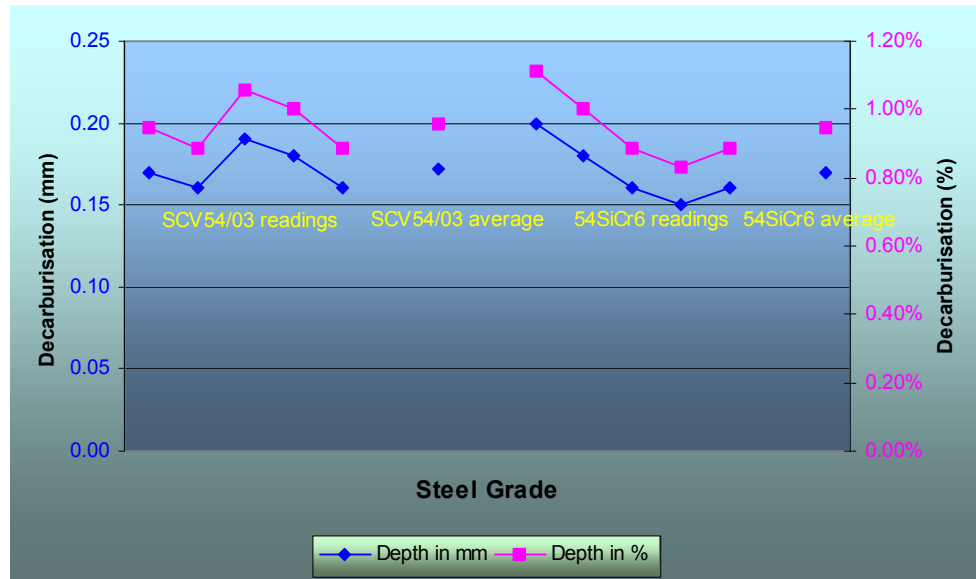
Figure 4.1.7: Graph of decarburisation on SCV54/03 and 54SiCr6 in the as rolled condition. According to ASTM E1077.
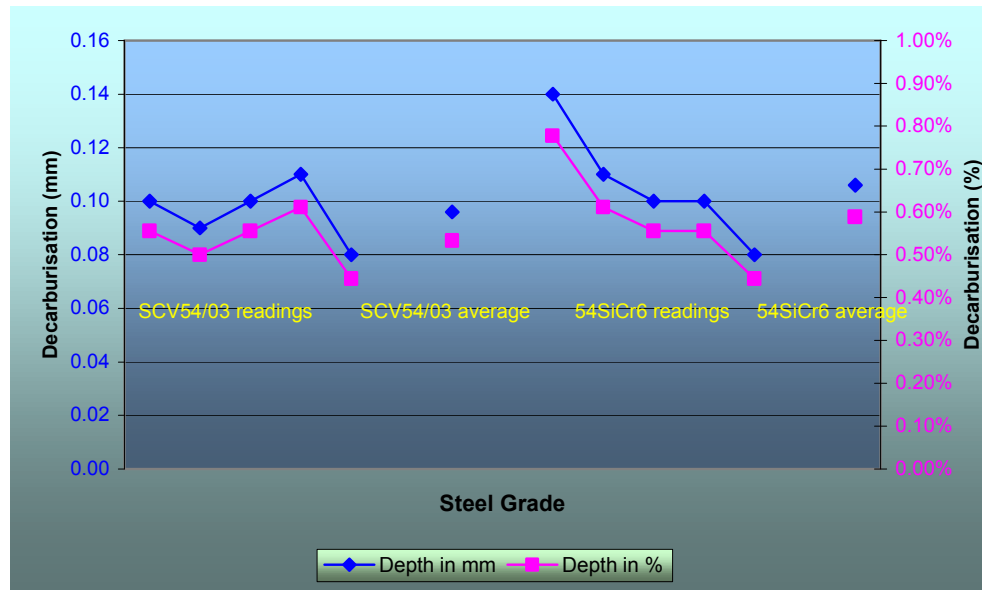
Figure 4.1.8: Graph of decarburisation on SCV54/03 and 54SiCr6 in the as rolled condition according to SAE J419.

4.1.3 MECHANICAL PROPERTIES OF HOT ROLLED MATERIAL

The results of hardness and tensile tests on the hot rolled material are presented in Table 4.1.2 and 4.1.3:

Table 4.1.2: Hardness of hot rolled material

Steel Grade	Average Hardness
SCV54/03	30.9
54SiCr6	29.9

Table 4.1.3: Mechanical properties of hot rolled material

Steel Grade	UTS (MPa)	YS (MPa)	Elongation (%)	Reduction in Area (%)
SCV54/03	873.2	794.4	16.4	22.1
54SiCr6	866.8	807.1	22.9	42.1

The mechanical properties of as rolled material depend on the rolling and cooling conditions. The UTS and YS are marginally different for the two steels. However, the reduction in area indicates that 54SiCr6 had superior ductility to SCV54/03.

4.2 HEAT TREATMENT OF ROLLED PRODUCT TO DETERMINE MECHANICAL PROPERTIES

4.2.1 GENERAL MICROSTRUCTURE OF AS QUENCHED MATERIAL

The as quenched microstructure of each steel grade at the three austenitising temperatures was examined after quenching in oil. Figures 4.2.1 and 4.2.2 show the as quenched microstructure of SCV54/03 and 54SiCr6 after austenitising at 880°C.
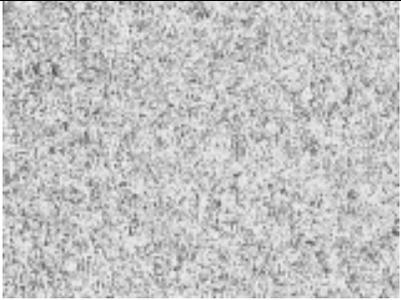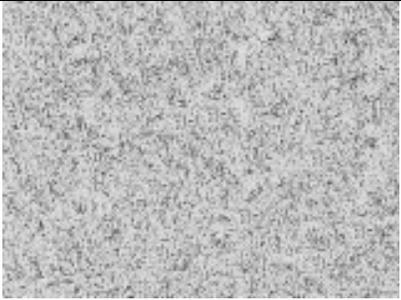
880 $^{\circ}$C quench	Figure 4.2.1: As quenched microstructure of SCV54/03. Etched in 2 % Nital, 100X.	Figure 4.2.2: As quenched microstructure of 54SiCr6. Etched in 2 % Nital, 100X.

The as quenched microstructures showed negligible differences between the steels at the 860 and 840 $^{\circ}$C austenitising temperatures. Refer to Appendix 1: Part 7.3 for micrographs. At 880 $^{\circ}$C, the grain structure of the SCV54/03 samples was coarser than the 54SiCr6 samples.

4.2.2 PRIOR AUSTENITE GRAIN SIZE OF AS QUENCHED MATERIAL

The grain size was evaluated at the three austenitising temperatures after quenching as shown in Figures 4.2.3 to 4.2.8. It can be seen that at austenitising temperatures of 860 and 840 $^{\circ}$C, the grain size is comparable between the steels. However, at 880 $^{\circ}$C, the grain size of the SCV54/03 sample was larger than the 54SiCr6 sample.

114
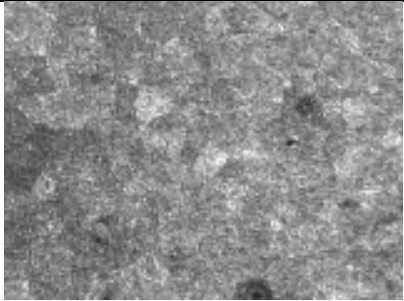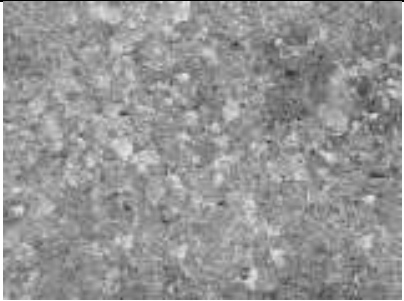
880 °C quench		
	Figure 4.2.3: As quenched microstructure of SCV54/03. Etched in FeCl$_3$:HCl solution, 100X.	Figure 4.2.4: As quenched microstructure of 54SiCr6. Etched in FeCl$_3$:HCl solution, 100X.
860 °C quench		
	Figure 4.2.5: As quenched microstructure of SCV54/03. Etched in FeCl$_3$:HCl solution, 100X.	Figure 4.2.6: As quenched microstructure of 54SiCr6. Etched in FeCl$_3$:HCl solution, 100X.
840 °C quench		
	Figure 4.2.7: As quenched microstructure of SCV54/03. Etched in FeCl$_3$:HCl solution, 100X.	Figure 4.2.8: As quenched microstructure of 54SiCr6. Etched in FeCl$_3$:HCl solution, 100X.
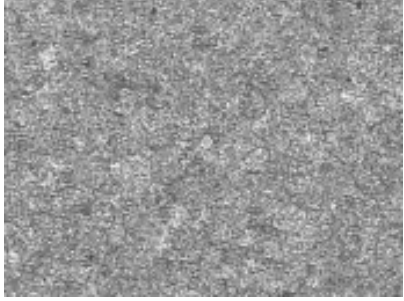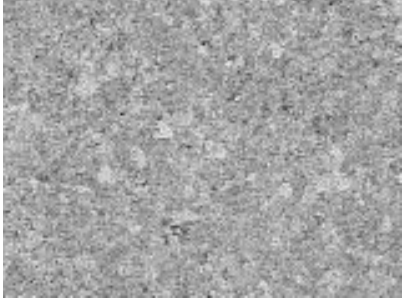
4.2.3 MICROSTRUCTURE OF MATERIAL QUENCHED AND TEMPERED AT 530 °C.

The microstructure of the SCV54/03 revealed slightly coarser martensite than 54SiCr6 at the 860 and 880 °C austenitising

115

temperatures after tempering at 530 $^{\circ}$C as shown in Figures 4.2.9 to 4.2.14. Additional micrographs are shown in Appendix 1: Part 7.4 to 7.11 for tempering temperatures between 380 $^{\circ}$C to 500 $^{\circ}$C.
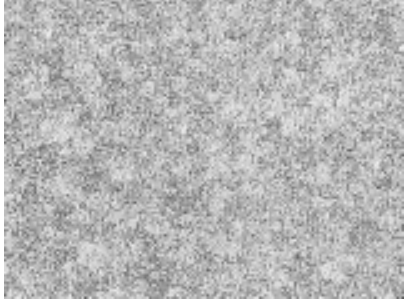
880 $^{\circ}$C Quench	 Figure 4.2.9: Microstructure of SCV54/03 tempered at 530 $^{\circ}$C. Etched in 2 % Nital, 100X.	 Figure 4.2.10: Microstructure of 54SiCr6 tempered at 530 $^{\circ}$C. Etched in 2 % Nital, 100X.
860 $^{\circ}$C Quench	 Figure 4.2.11: Microstructure of SCV54/03 tempered at 530 $^{\circ}$C. Etched in 2 % Nital, 100X.	 Figure 4.2.12: Microstructure of 54SiCr6 tempered at 530 $^{\circ}$C. Etched in 2 % Nital, 100X.
840 $^{\circ}$C Quench	 Figure 4.2.13: Microstructure of SCV54/03 tempered at 530 $^{\circ}$C. Etched in 2 % Nital, 100X.	 Figure 4.2.14: Microstructure of 54SiCr6 tempered at 530 $^{\circ}$C. Etched in 2 % Nital, 100X.
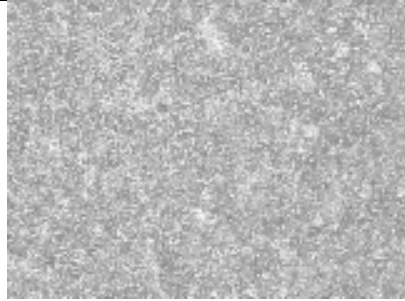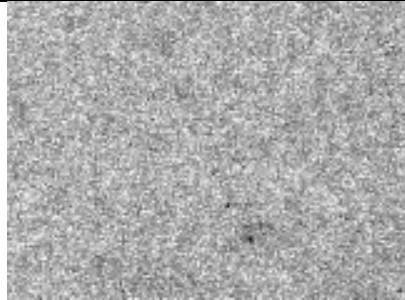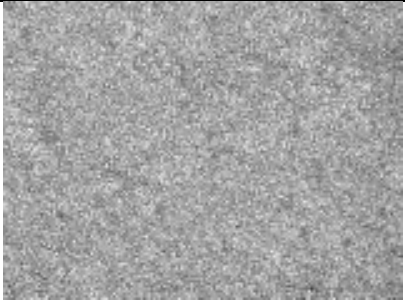
In general, the microstructures of the two steels at the 840 $^{\circ}$C and 860 $^{\circ}$C austenitising temperatures were similar after tempering.

116

4.3 MICROSTRUCTURAL EVOLUTION OF VANADIUM FINE GRAINED SPRING STEEL

The tempering of the SCV54/03 samples at 430 ^{o}C was varied from 1 to 8 hours. Slight coarsening of the microstructures was observed. Figures 4.3.1 to 4.3.6 shows the microstructures of the SCV54/03 samples.
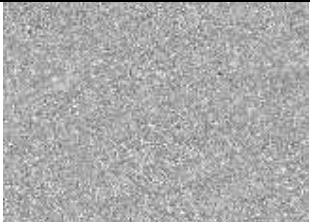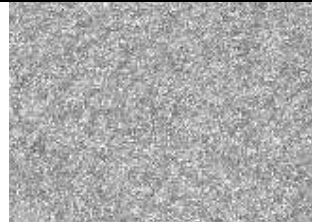
	840 ^{o}C quench	860 ^{o}C quench	880 ^{o}C quench
1 Hour	Figure 4.3.1: Microstructure of SCV54/03 tempered at 430 ^{o}C for 1 hour. Etched in 2 % Nital, 100X.	Figure 4.3.2: Microstructure of SCV54/03 tempered at 430 ^{o}C for 1 hour. Etched in 2 % Nital, 100X.	Figure 4.3.3: Microstructure of SCV54/03 tempered at 430 ^{o}C for 1 hour. Etched in 2 % Nital, 100X.
8 Hours	Figure 4.3.4: Microstructure of SCV54/03 tempered at 430 ^{o}C for 8 hour. Etched in 2 % Nital, 100X.	Figure 4.3.5: Microstructure of SCV54/03 tempered at 430 ^{o}C for 8 hour. Etched in 2 % Nital, 100X.	Figure 4.3.6: Microstructure of SCV54/03 tempered at 430 ^{o}C for 8 hour. Etched in 2 % Nital, 100X.
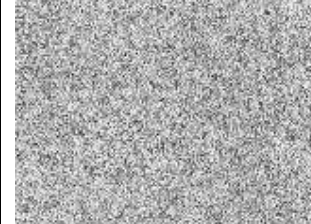
117

4.4 MICROSTRUCTURAL EVOLUTION OF ALUMINIUM FINE GRAINED SPRING STEEL

The same process of increasing the tempering time was done on the 54SiCr6 samples. Slight coarsening of the microstructures was observed. Figures 4.4.1 to 4.4.6 shows the microstructures of the 54SiCr6 samples.
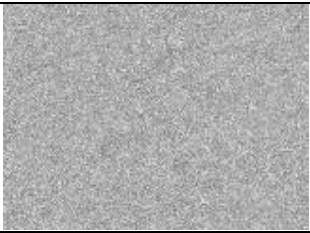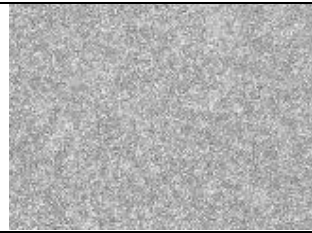
	840 ^{o}C quench	860 ^{o}C quench	880 ^{o}C quench
1 Hour	Figure 4.4.1: Microstructure of 54SiCr6 tempered at 430 ^{o}C for 1 hour. Etched in 2 % Nital, 100X.	Figure 4.4.2: Microstructure of 54SiCr6 tempered at 430 ^{o}C for 1 hour. Etched in 2 % Nital, 100X.	Figure 4.4.3: Microstructure of 54SiCr6 tempered at 430 ^{o}C for 1 hour. Etched in 2 % Nital, 100X.
8 Hours	Figure 4.4.4: Microstructure of 54SiCr6 tempered at 430 ^{o}C for 8 hour. Etched in 2 % Nital, 100X.	Figure 4.4.5: Microstructure of 54SiCr6 tempered at 430 ^{o}C for 8 hour. Etched in 2 % Nital, 100X.	Figure 4.4.6: Microstructure of 54SiCr6 tempered at 430 ^{o}C for 8 hours. Etched in 2 % Nital, 100X.

4.5 MECHANICAL PROPERTIES OF ROLLED AND HEAT TREATED MATERIAL

4.5.1 HARDNESS OF MATERIAL QUENCHED AND TEMPERED FOR ONE HOUR

The average hardness of the samples was measured after quenching in oil and tempering for one hour. A summary of the results is shown in Table 4.5.1.

Table 4.5.1: Hardness results of material quenched from 880, 860 and 840 ^{o}C and tempered for one hour

Austenitising temperature ^{0}C	Tempering Temperature ^{0}C	SCV54/03 Average HRc	54SiCr6 Average HRc
880	380	56.5	56.5
	400	55.0	55.0
	420	54.0	53.8
	430	52.7	52.7
	440	51.1	50.9
	460	50.0	49.9
	480	48.1	47.9
	500	45.5	44.1
	530	42.1	42.0
Average Hardness Difference = 0.24 HRc			
860	380	55.8	55.2
	400	53.0	53.3
	420	51.3	51.2
	430	49.7	49.2
	440	48.9	48.7
	460	48.5	47.9
	480	47.2	46.3
	500	45.8	45.1
	530	43.2	41.8
Average Hardness Difference = 0.51 HRc			
840	380	55.7	55.3
	400	53.5	53.5
	420	52.4	52.0
	430	51.8	51.2
	440	50.3	50.2
	460	49.3	49.0
	480	48.0	47.8
	500	46.3	46.5
	530	45.7	45.3
Average Hardness Difference = 0.26 HRc			

It can be seen that the two steels react quite comparably during heat treatment. The average hardness difference between SCV54/03 and 54SiCr6 at 880 $^{\circ}$C, 860 $^{\circ}$C and 840 $^{\circ}$C is 0.2, 0.5 and 0.3 HRC respectively, which is insignificant. Plots of hardness against tempering temperature are shown in Figures 4.5.1 to 4.5.3.
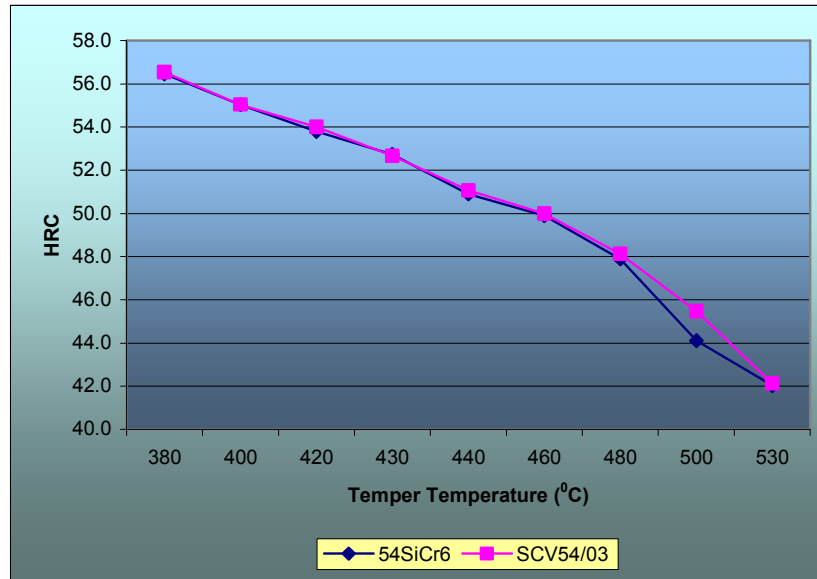
Figure 4.5.1: Plot of hardness against tempering temperature for SCV54/03 and 54SiCr6 austenitised at 880 $^{\circ}$C.
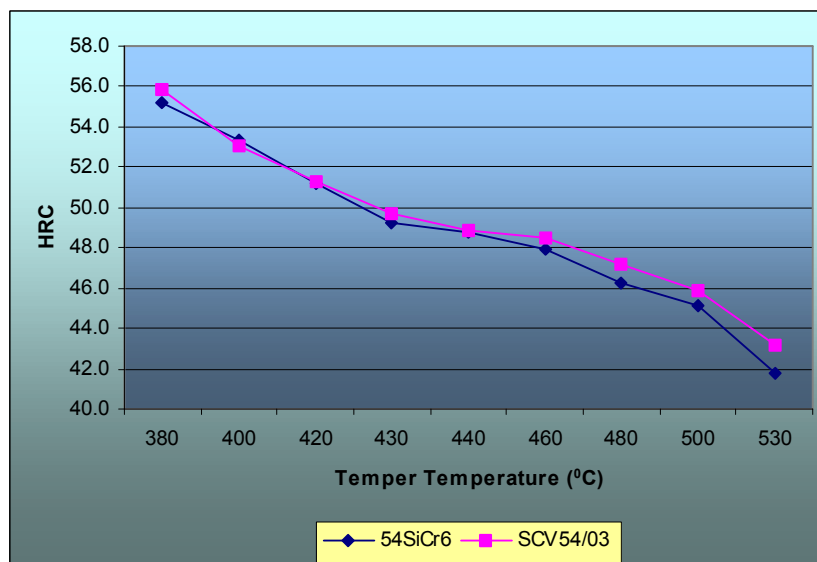
Figure 4.5.2: Plot of hardness against tempering temperature for SCV54/03 and 54SiCr6 austenitised at 860 $^{\circ}$C.
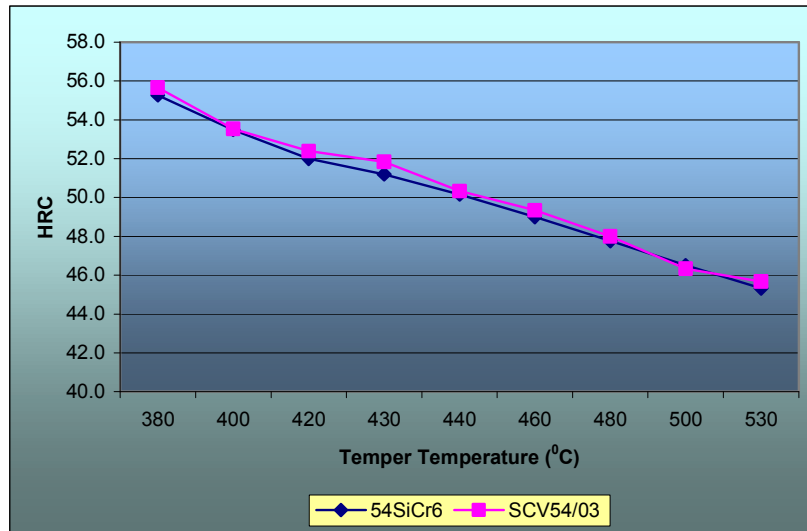
Figure 4.5.3: Plot of hardness against tempering temperature for SCV54/03 and 54SiCr6 austenitised at 840 $^\circ$C.

The above data were superimposed on to a single graph, Figure 4.5.4 to show differences in behaviour between the two steels.
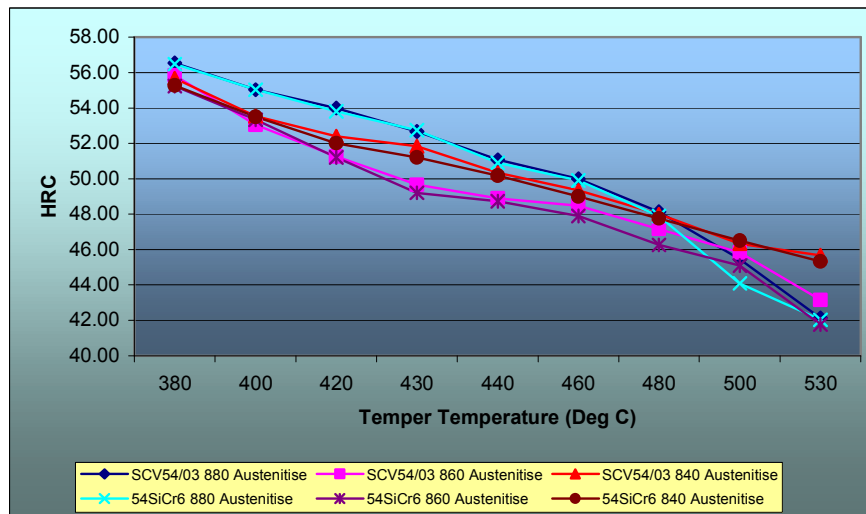
Figure 4.5.4: Superimposed temper curves.

It is quite noticeable that higher austenitising temperatures promote higher hardness after tempering.

4.5.2 HARDNESS OF MATERIAL QUENCHED AND TEMPERED FOR ONE, TWO, FOUR AND EIGHT HOURS

The hardness of the samples was measured after tempering for one, two, four and eight hours. The summary is shown in Table 5.4.2.

Table 4.5.2: Hardness of material quenched and tempered for one to eight hours at 430 ^{o}C.

Austenitising temperature	Tempering Temperature	Tempering Hours	SCV54/03	54SiCr6
^{0}C	^{0}C		Average	Average
880	430	1	52.7	52.7
		2	50.1	49.5
		4	48.7	48.5
		8	48.3	48.0
860	430	1	49.7	49.2
		2	49.0	49.0
		4	48.6	48.3
		8	48.3	48.2
840	430	1	51.8	51.2
		2	50.7	50.4
		4	49.8	49.8
		8	49.5	49.3

Extending the tempering time generally decreased the hardness. Plots of hardness against tempering temperature are shown in Figures 4.5.5 to 4.5.7.
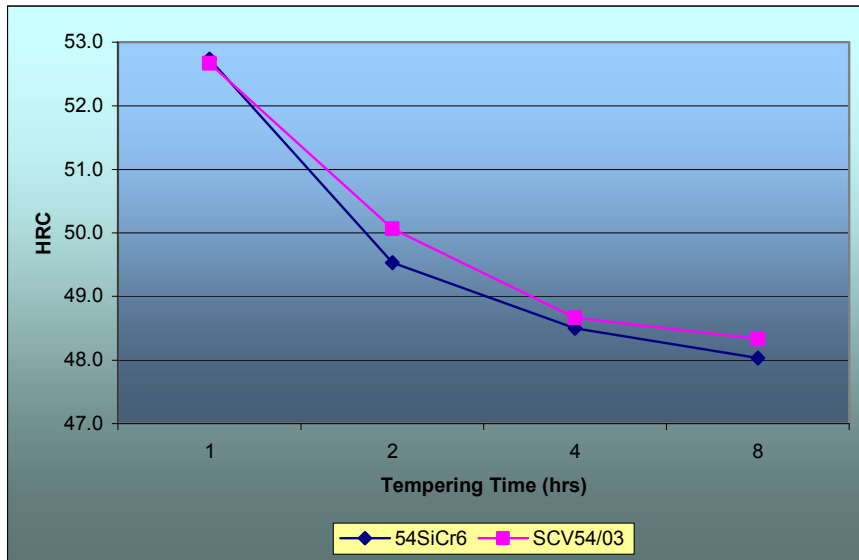
Figure 4.5.5: Plot of hardness against tempering temperature for SCV54/03 and 54SiCr6 austenitised at 880 ^{o}C and tempered for 1 to 8 hours at 430 ^{o}C.
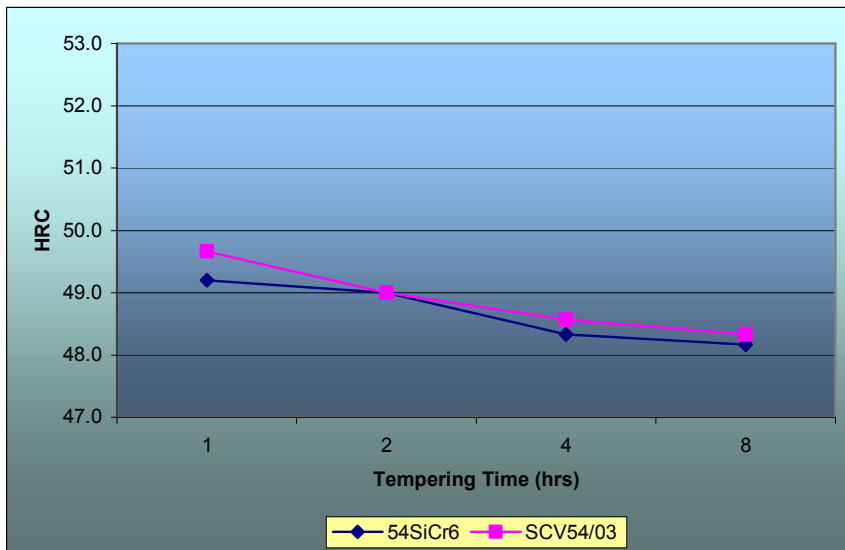
Figure 4.5.6: Plot of hardness against tempering temperature for SCV54/03 and 54SiCr6 austenitised at 860 ^{o}C and tempered for 1 to 8 hours at 430 ^{o}C.
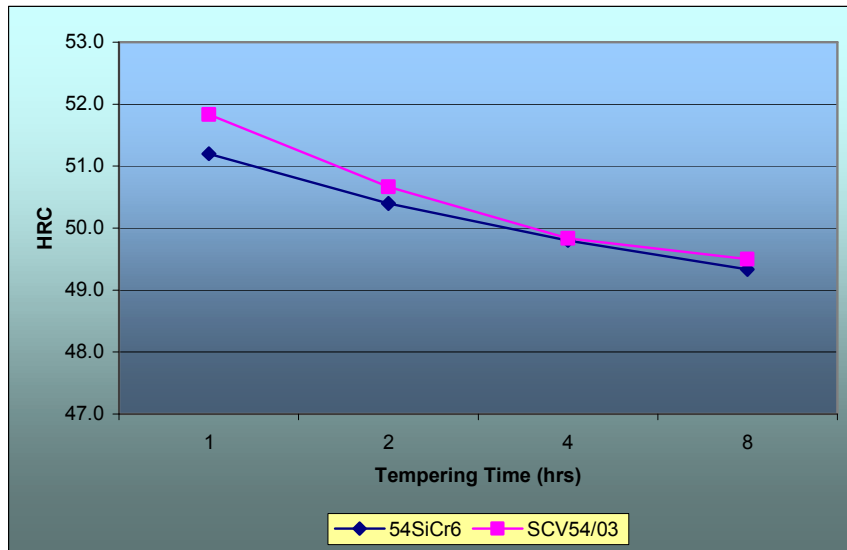
Figure 4.5.7: Plot of hardness against tempering temperature for SCV54/03 and 54SiCr6 austenitised at 840 $^{\circ}$C and tempered for 1 to 8 hours at 430 $^{\circ}$C.

The data was superimposed onto a single graph, Figure 4.5.8.
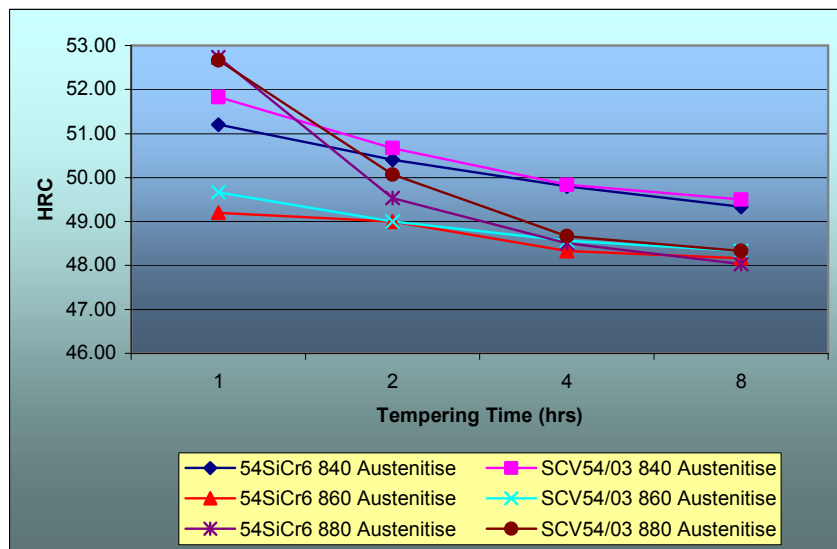
Figure 4.5.8: Plot of hardness against tempering time for SCV54/03 and 54SiCr6 austenitised at 840 $^{\circ}$C, 860 $^{\circ}$C and 880 $^{\circ}$C and tempered for 1 to 8 hours at 430 $^{\circ}$C.

4.5.3 TENSILE PROPERTIES MATERIAL TEMPERED FOR ONE HOUR

Tensile tests were conducted on the samples at the various austenitising and tempering temperatures. The summary is shown in Table 4.5.3. (Refer to Appendix 2: Part 8.1 for all results).

Table 4.5.3: Tensile results of quenched material tempered for one hour.

Austenitising temperature °C	Tempering Temperature °C	SCV54/03			54SiCr6			Average difference in		
		UTS (MPa)	YS (MPa)	Elongation (%)	UTS (MPa)	YS (MPa)	Elongation (%)	UTS (MPa)	YS (MPa)	Elongation (%)
880	380	2115.9	2039.8	4.0%	2074.8	1978.4	9.9%	41.1	61.4	-5.9%
	400	1995.2	1818.0	6.6%	1953.9	1741.3	10.4%	41.2	76.7	-3.8%
	420	1860.5	1634.6	7.6%	1800.3	1595.4	11.1%	60.2	39.2	-3.5%
	430	1791.6	1621.2	6.2%	1728.5	1567.2	12.8%	63.1	54.0	-6.6%
	440	1630.1	1450.7	8.0%	1628.7	1468.0	12.8%	1.4	-17.3	-4.8%
	460	1528.4	1385.9	8.3%	1491.0	1351.2	13.6%	37.4	34.7	-5.4%
	480	1507.3	1341.5	9.2%	1494.8	1321.1	16.0%	12.5	20.4	-6.8%
	500	1487.8	1353.9	10.0%	1444.8	1304.6	16.3%	43.0	49.4	-6.3%
	530	1447.1	1299.0	11.8%	1365.3	1223.1	17.3%	81.8	75.8	-5.5%
							Average	42.4	43.8	
860	380	2098.8	1871.8	3.5%	2049.5	1826.2	8.7%	49.4	45.5	-5.3%
	400	1940.7	1715.5	7.0%	1951.3	1725.3	10.6%	-10.6	-9.8	-3.7%
	420	1888.2	1709.5	7.0%	1838.0	1664.7	11.3%	50.2	44.8	-4.3%
	430	1784.7	1606.8	6.8%	1731.7	1571.8	12.7%	53.0	34.9	-5.9%
	440	1692.5	1537.4	8.7%	1664.9	1512.4	13.1%	27.6	25.1	-4.4%
	460	1598.0	1430.2	8.1%	1543.7	1381.6	13.6%	54.3	48.6	-5.4%
	480	1520.7	1452.0	9.4%	1462.6	1396.0	15.9%	58.1	56.1	-6.5%
	500	1495.7	1363.9	10.7%	1415.3	1290.7	16.8%	80.5	73.2	-6.0%
	530	1464.6	1391.0	12.3%	1341.4	1272.4	17.5%	123.2	118.6	-5.2%
							Average	54.0	48.6	
840	380	2140.4	1909.0	3.4%	2098.4	1869.9	10.0%	42.0	39.0	-6.6%
	400	2006.7	1774.3	5.0%	1957.6	1730.9	10.7%	49.1	43.3	-5.7%
	420	1888.9	1710.7	6.4%	1867.5	1691.4	11.7%	21.4	19.3	-5.3%
	430	1776.3	1599.4	7.0%	1763.1	1600.3	12.7%	13.2	-0.9	-5.7%
	440	1699.0	1543.3	8.2%	1658.7	1506.7	12.9%	40.3	36.6	-4.7%
	460	1647.0	1474.1	8.8%	1555.5	1392.2	13.3%	91.5	81.9	-4.5%
	480	1534.1	1465.0	9.3%	1500.0	1432.0	14.3%	34.1	33.0	-5.0%
	500	1509.5	1376.5	11.0%	1429.0	1303.1	15.9%	80.6	73.4	-4.9%
	530	1455.1	1311.6	12.9%	1409.3	1283.7	18.1%	45.8	27.9	-5.2%
							Average	46.4	39.3	

Note: Negative values in the average difference are to the advantage of 54SiCr6 and vice versa.

In all cases, the SCV54/03 material had superior tensile strength. The 54SiCr6 steel had superior elongation in all cases. An SCV54/03 specimen, austenitised at 880 °C and tempered at 430 °C failed prematurely due to an inclusion as will be seen at a later stage. When discarding this result, the UTS of SCV54/03 was on average about 48 MPa higher than that of 54SiCr6. The data presented in Table 4.5.3 of UTS are plotted on Figures 4.5.9, 4.5.10 and 4.5.11 as a function of tempering temperature.
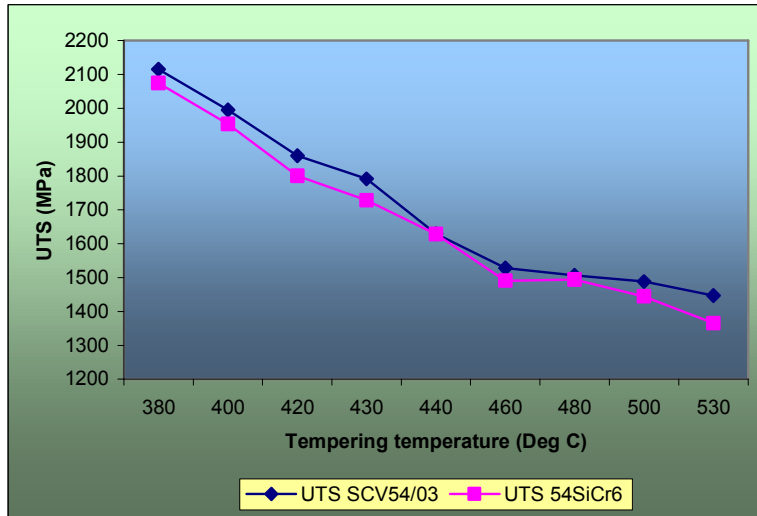
Figure 4.5.9: UTS curves for SCV54/03 and 54SiCr6 austenitised at 880 ^{o}C and tempered for 1 hour.

Figure 4.5.10: UTS curves for SCV54/03 and 54SiCr6 austenitised at 860 ^{o}C and tempered for 1 hour.
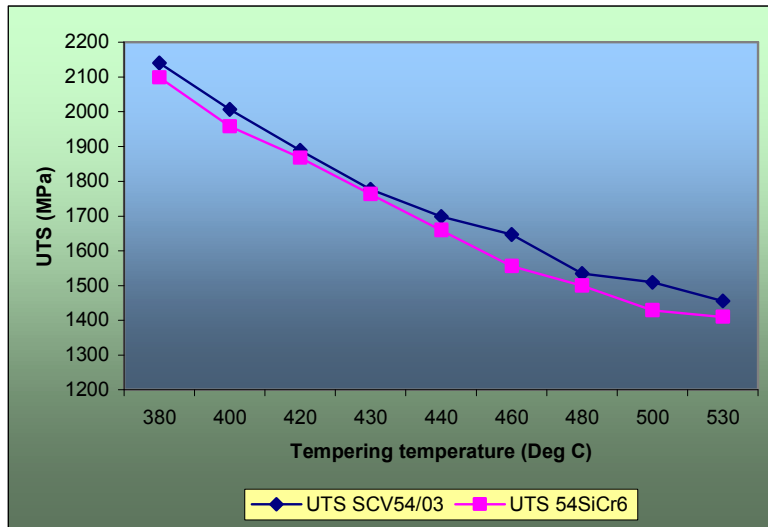
Figure 4.5.11: UTS curves for SCV54/03 and 54SiCr6 austenitised at 840 ^{o}C and tempered for 1 hour.

The data is compared in Figure 4.5.12.
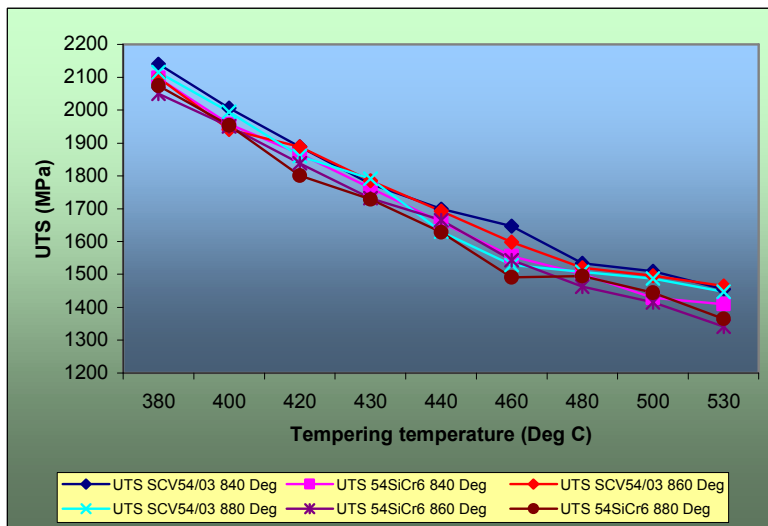
Figure 4.5.12: UTS curves for SCV54/03 and 54SiCr6 austenitised at 840 ^{o}C, 860 ^{o}C and 880 ^{o}C and tempered for 1 hour.

The ductility of the tensile specimens measured as reduction in area is presented in Table 4.5.4 (complete results in Table 8.1.3: Appendix 2, Part 8.1). In general, 54SiCr6 had superior ductility while SCV54/03 displayed some erratic ductility particularly in material austenitised at 860 °C and 840 °C. The ductility of 54SiCr6 was relatively consistent.

Table 4.5.4: Reduction in area of material tempered for one hour.

Austenitising temperature	Tempering Temperature	SCV54/03	54SiCr6
		Average reduction in area (%)	Average reduction in area (%)
°C	°C	Average	Average
	380	10.6%	31.2%
	400	14.0%	34.6%
	420	17.9%	36.4%
	430	13.9%	39.9%
880	440	19.3%	40.6%
	460	19.8%	39.9%
	480	23.6%	43.8%
	500	30.3%	46.5%
	530	37.1%	46.9%
	380	7.6%	30.8%
	400	10.1%	31.8%
	420	16.5%	32.3%
	430	19.9%	36.7%
860	440	21.2%	39.7%
	460	21.3%	41.5%
	480	20.7%	41.7%
	500	28.2%	45.4%
	530	31.2%	47.4%
	380	5.5%	29.3%
	400	11.2%	32.3%
	420	15.9%	33.4%
	430	20.5%	33.3%
840	440	19.1%	35.4%
	460	16.0%	37.6%
	480	12.1%	41.3%
	500	14.7%	42.8%
	530	21.8%	45.5%

The values in Table 4.5.4 are plotted in Figures 4.5.13 and 4.5.14.
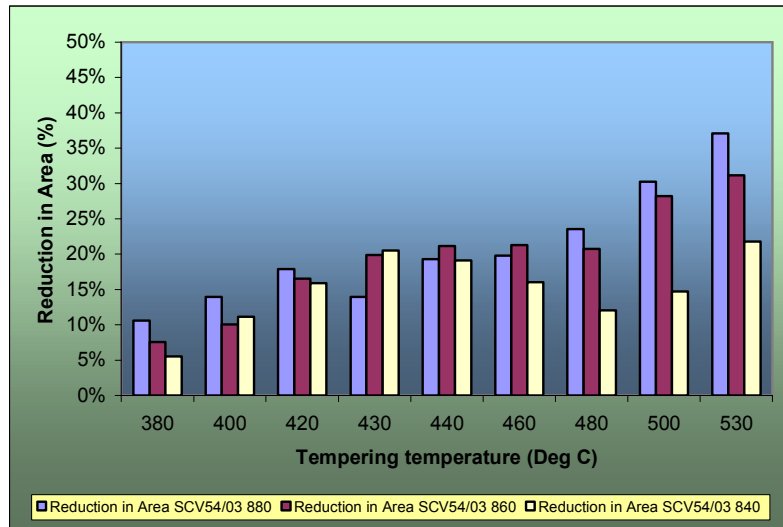
Figure 4.5.13: Reduction in area of SCV54/03 for the three austenitising temperatures.

The scatter in values of area reduction for the SCV54/03 steel was mainly noted in material austenitised 840 ^{o}C.
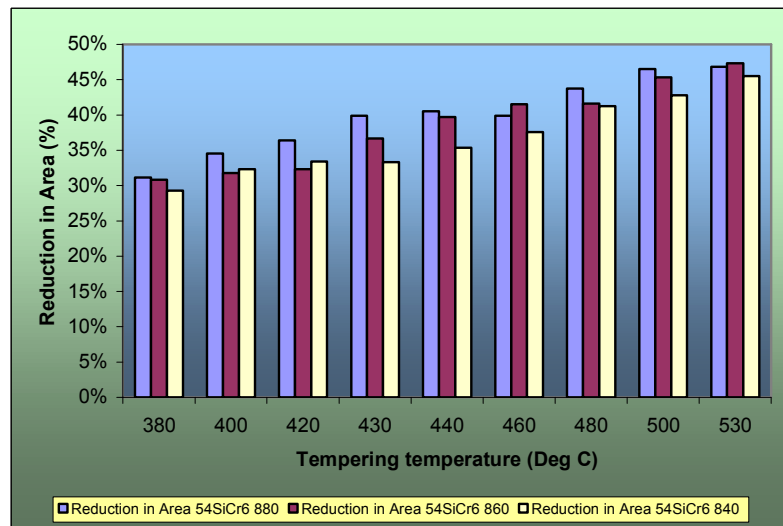
Figure 4.5.14: Reduction in area of 54SiCr6 for the three austenitising temperatures.

All results on the 54SiCr6 material are relatively consistent when compared to SCV54/03. 54SiCr6 has superior ductility to SCV54/03.

4.5.4 TENSILE PROPERTIES OF MATERIAL TEMPERED FOR 1, 2, 4 AND 8 HOURS

Tensile tests were conducted on the samples austenitised at the various temperatures and tempered for extended periods of time at 430 $^{\circ}$C. The summary is shown in Table 4.5.5. (Refer to Appendix 2: Part 8.2 for complete results).

Table 4.5.5: Tensile test results of quenched material tempered for one, two, four and eight hours.

Austenitising temperature	Tempering Temperature	Tempering Hours	SCV54/03			54SiCr6		
^{0}C	^{0}C		Average UTS (MPa)	Average YS (MPa)	Average Elongation (%)	Average UTS (MPa)	Average YS (MPa)	Average Elongation (%)
880	430	1	1791.6	1621.2	6.2%	1728.5	1567.2	12.8%
		2	1767.7	1608.8	6.8%	1727.0	1553.4	13.7%
		4	1700.5	1556.3	6.6%	1685.6	1528.3	14.8%
		8	1573.4	1450.3	7.0%	1556.1	1408.0	15.7%
860	430	1	1784.7	1606.8	6.0%	1731.7	1571.8	12.7%
		2	1777.1	1617.3	6.9%	1692.7	1559.0	14.0%
		4	1650.0	1510.1	7.0%	1655.3	1531.1	14.6%
		8	1576.5	1441.8	7.0%	1601.4	1456.5	15.9%
840	430	1	1776.3	1612.6	5.8%	1750.7	1589.2	12.7%
		2	1730.6	1586.7	6.7%	1734.8	1572.5	13.6%
		4	1692.4	1529.8	7.1%	1669.6	1529.7	14.5%
		8	1656.4	1503.9	7.1%	1635.3	1524.3	15.3%

Table 4.5.5 shows that the tensile strength of the samples decreased with increasing tempering time. Figures 4.5.15, 4.5.16, 4.5.17, and 4.5.18 show the graphs of UTS versus tempering time for the two steels.
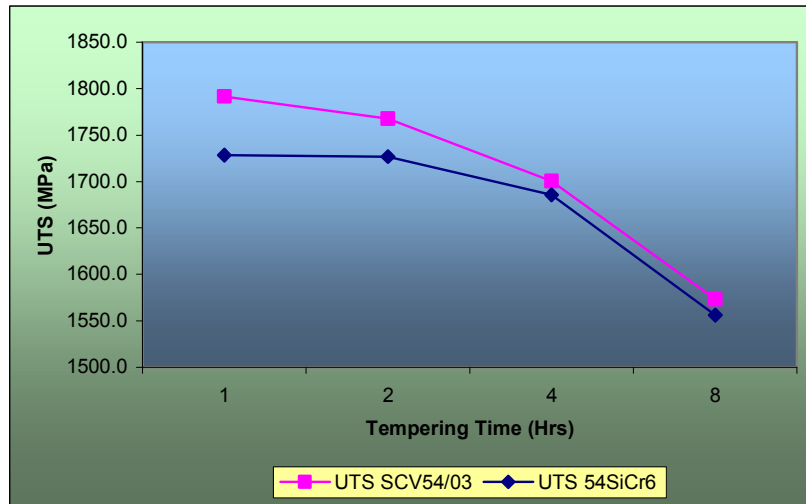
Figure 4.5.15: UTS as a function of tempering time at 430 ^{o}C after austenitising at 880 ^{o}C.
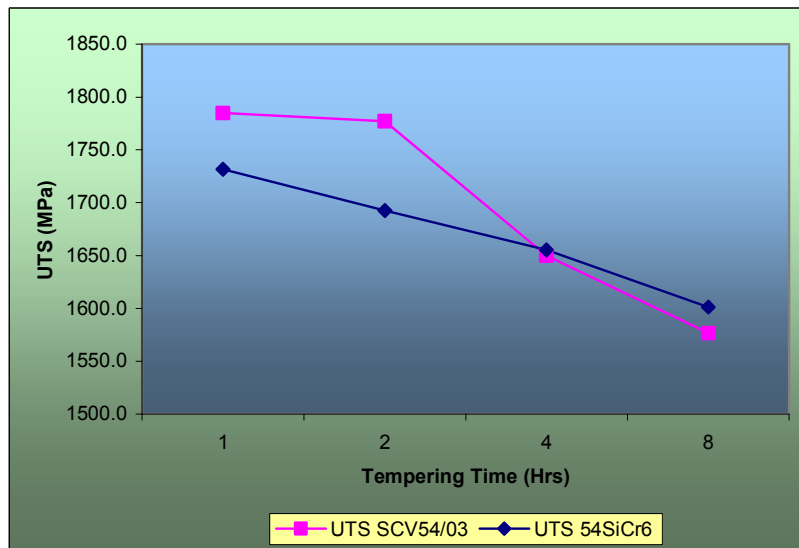
Figure 4.5.16: UTS as a function of tempering time at 430 ^{o}C after austenitising at 860 ^{o}C.
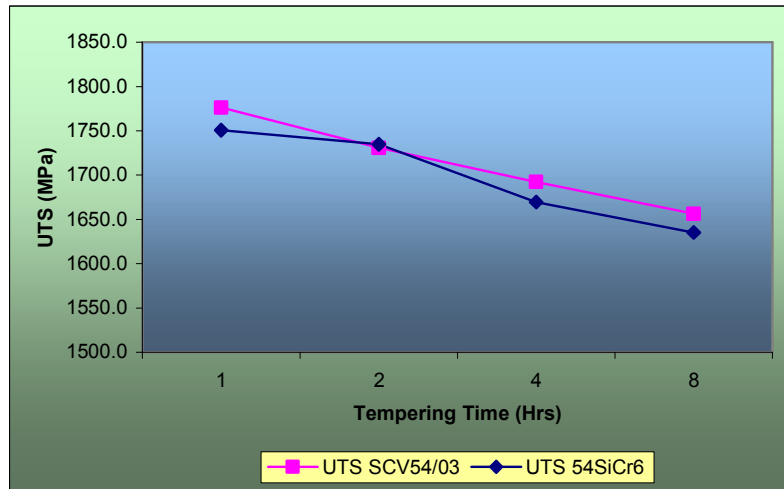
Figure 4.5.17: UTS as a function of tempering time at 430 °C after austenitising at 840 °C.
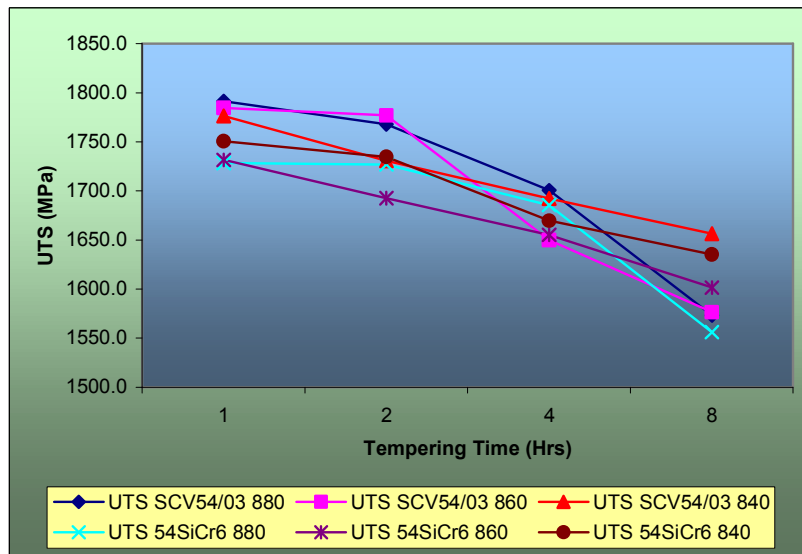
Figure 4.5.18: UTS as a function of tempering time at 430 °C after austenitising at 880 °C, 860 °C and 840 °C.

In general, after longer tempering times the tensile strength of the two steels decreased.

The ductility of these samples showed an increase for longer tempering times (Table 4.5.6, complete results in Table 8.2.2: Appendix 2, Part 8.2). As previously noted, the ductility of 54SiCr6 was superior to that of SCV54/03.

Table 4.5.6: Reduction in area of quenched material tempered for one, two, four and eight hours.

Austenitising temperature	Tempering Temperature	Tempering Time	SCV54/03	54SiCr6
^{0}C	^{0}C	Hrs	Reduction in area (%)	Reduction in area (%)
880	430	1	21.0%	39.9%
		2	22.1%	41.8%
		4	23.3%	46.4%
		8	24.8%	49.6%
860	430	1	20.7%	36.7%
		2	22.0%	39.1%
		4	23.3%	42.4%
		8	23.8%	46.1%
840	430	1	18.8%	33.3%
		2	19.0%	35.6%
		4	19.4%	37.4%
		8	20.8%	42.6%

The graphs (Figures 4.5.19 and 4.5.20) show a slight fall off in ductility for the lower austenitising temperatures of 860 ^{o}C and 840 ^{o}C. In all cases, the ductility of the two steels increases for tempering times from 1 to 8 hours. The results on the 54SiCr6 steel are consistently higher than the SCV54/03 steel.
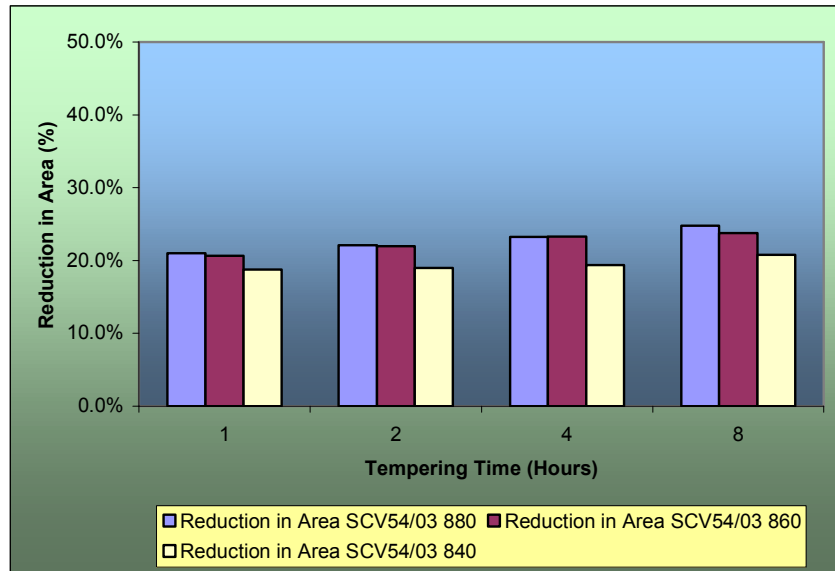
Figure 4.5.19: Reduction in area as a function of tempering time at 430 ^{o}C after austenitising SCV54/03 at different temperatures.
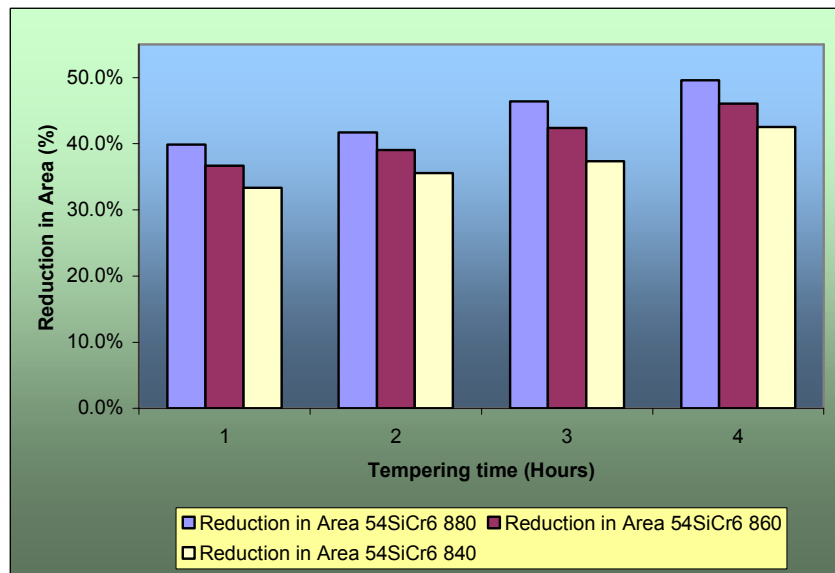
Figure 4.5.20: Reduction in area as a function of tempering time at 430 ^{o}C after austenitising 54SiCr6 at different temperatures.

4.5.5 SEM ANALYSIS OF TENSILE FRACTURE SURFACES

The fracture surfaces of the tensile specimens were examined with the aid of an SEM. Several examples are presented in this section. The samples examined are outlined in Table 4.5.7:

Table 4.5.7: Fractured tensile specimens examined by SEM.

Austenitising temperature	Tempering Temperature	SCV54/03		54SiCr6	
^{0}C	^{0}C	Tempering Time (Hrs)		Tempering Time (Hrs)	
		1	8	1	8
880	430	X			
	530	X		X	
860	380			X	
	530	X			
840	430		X		
	530	X			

An SCV54/03 tensile specimen austenitised at 880 ^{o}C and tempered for one hour at 430 ^{o}C failed at a UTS of 1426 MPa compared to a second sample of 1792 MPa. Close examination of the fracture surface by SEM revealed an inclusion at the fracture initiation as shown in Figure 4.5.21.
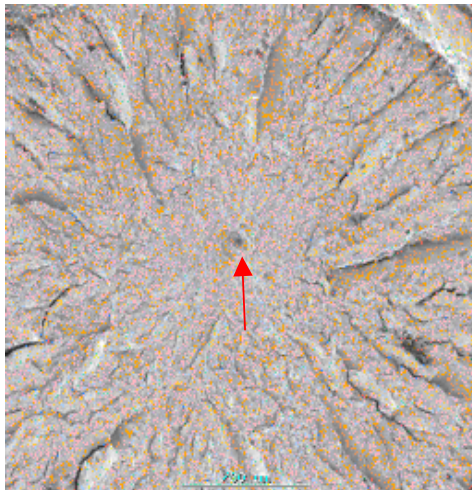
Figure 4.5.21: SEM fractograph of SCV54/03 austenitised at 880 ^{o}C, tempered at 430 ^{o}C. The failure originated from the inclusion denoted by the arrow.

135

The inclusion was analysed by Electron Microprobe, Figure 4.5.22.
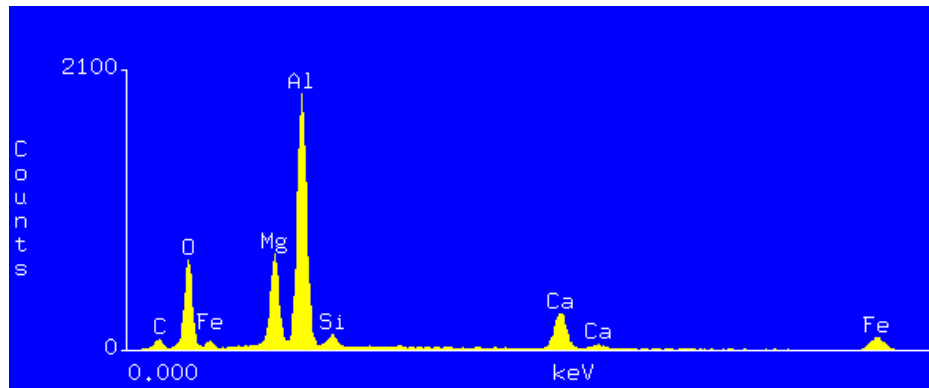
Figure 4.5.22: Electron Microprobe analysis of the inclusion.

The non-metallic inclusion consisted mainly of alumina (68%), with some minor constituents of magnesium oxide (28%), calcium oxide (9%), silica (2%) and iron oxide (3%).

A SCV54/03 sample austenitised at 880 ^{o}C and tempered at 530 ^{o}C for one hour was examined by an SEM. Close examination of the fracture surface as seen in Figure 4.5.23, shows the failure to be by cleavage with some microvoids suggesting ductility.
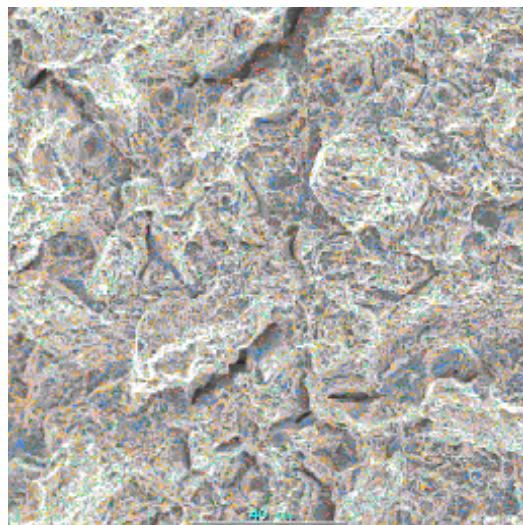
Figure 4.5.23: High magnification SEM fractograph of SCV54/03 austenitised at 880 ^{o}C, tempered at 530 ^{o}C showing cleavage and some microvoids.

136

A sample of 54SiCr6 austenitised at 880 ^{o}C and tempered for one hour at 530 ^{o} showed numerous fine microvoids as seen in Figure 4.5.24. The reduction in area was 49 % and UTS of 1361 MPa.
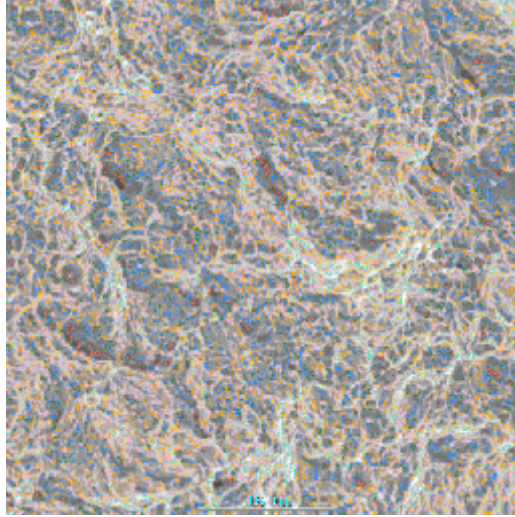
Figure 4.5.24: SEM fractograph of 54SiCr6 austenitised at 880 ^{o}C, tempered at 530 ^{o}C, numerous microvoids present.

A sample of SCV54/03 austenitised at 860 ^{o}C and tempered for one hour at 530 ^{o}C shown in Figure 4.5.25 displayed cleavage with some microvoids.
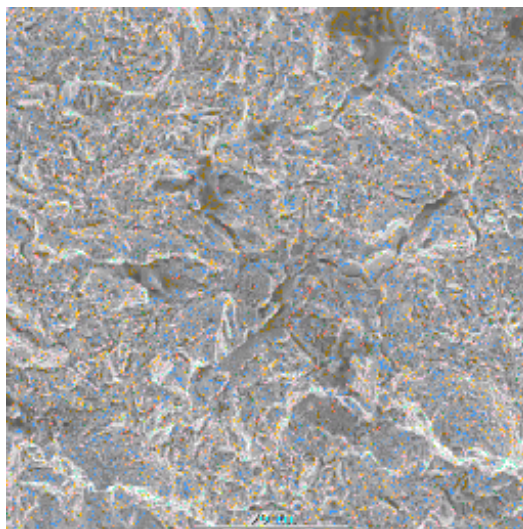
Figure 4.5.25: SEM fractograph of SCV54/03 austenitised at 860 ^{o}C, tempered at 530 ^{o}C, numerous microvoids present.

A sample of 54SiCr6 austenitised at 860 ^{o}C and tempered for one hour at 380 ^{o}C fractured in a ductile manner showed a fracture face with microvoids (Figure 4.5.26) with a UTS of 2037 MPa and reduction in area of 32 %.
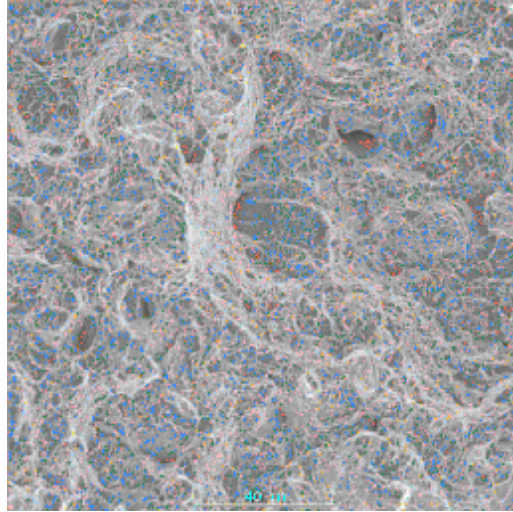
Figure 4.5.26: SEM fractograph of 54SiCr6 austenitised at 860 ^{o}C, tempered at 380 ^{o}C, numerous microvoids present.

Figure 4.5.27 shows the fracture surface of a SCV54/03 specimen austenitised at 840 ^{o}C and tempered at 530 ^{o}C for one hour.
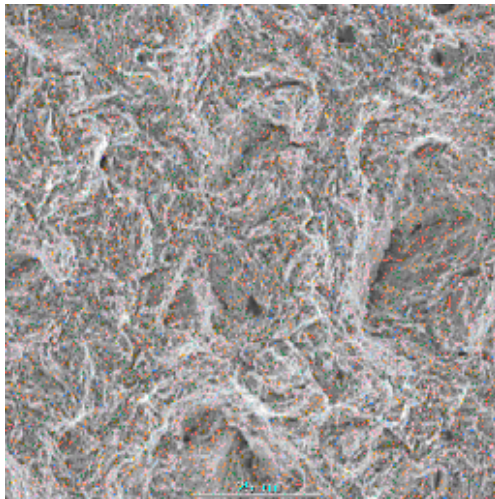
Figure 4.5.27: SEM fractograph of SCV54/03 austenitised at 840 ^{o}C, tempered at 530 ^{o}C.

This sample with UTS of 1487 MPa, revealed no intergranular fracture. The sample was relatively ductile with reduction in area of 22 %. The fracture was mixed consisting of mainly dimple fracture with some cleavage.

A sample of SCV54/03 austenitised at 840 ^{o}C and tempered for eight hours at 430 ^{o}C fractured with by microvoid coalescence but with some intergranular fracture (Figure 4.5.28). The longer tempering time increased the UTS from 1447 MPa to 1674 MPa.
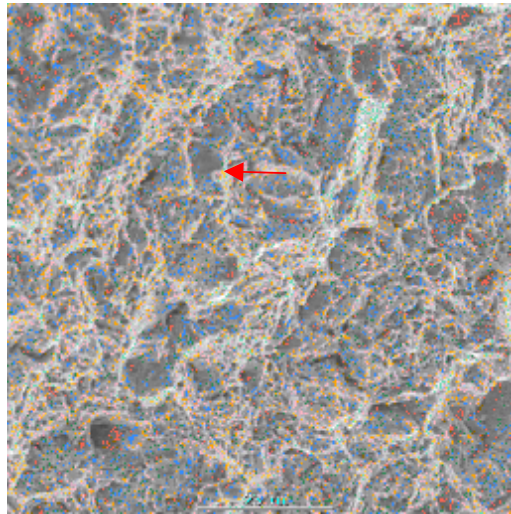
Figure 4.5.28: SEM fractograph of SCV54/03 austenitised at 840 ^{o}C, tempered at 530 ^{o}C, numerous microvoids present. Note the intergranular fracture denoted by arrow.

It can be concluded from the SEM investigation on the tensile fracture faces that the 54SiCr6 steel fails in a ductile manner as seen by the microvoid coalescence. However, the fractures on the SCV54/03 steel was mixed. The failure modes were a mixture of microvoid coalescence, cleavage and intergranular.

4.5.6 GRAIN GROWTH TESTS ON ROLLED PRODUCT

An important aspect of spring steels is that the final grain size be well controlled for improved toughness. Figures 4.5.29 and 4.5.30 show the as rolled microstructure of hot rolled SCV54/03 and 54SiCr6 respectively. It is evident that the grain size of the two steels are very fine and in the order of grain size ASTM 7 to 8.
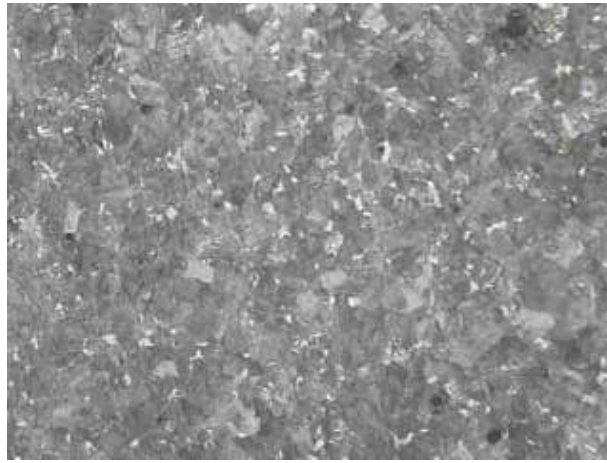
Figure 4.5.29: As rolled microstructure of SCV54/03. Etched in 2 % Nital, 200X.
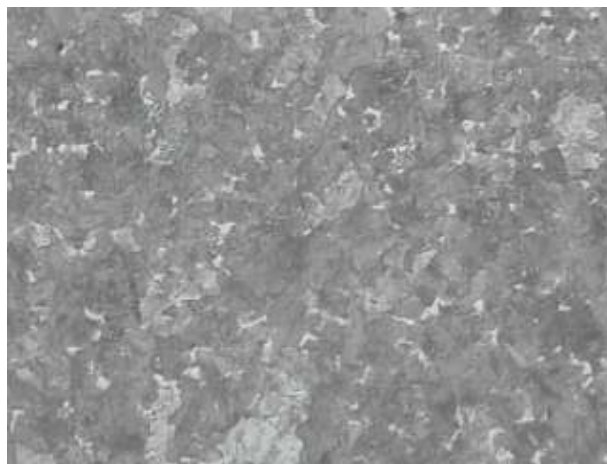
Figure 4.5.30: As rolled microstructure of 54SiCr6. Etched in 2 % Nital, 200X.

The as rolled samples shown previously were subjected to the oxidation method of determining grain growth. Figures 4.5.31 and 4.5.32 show the grain growth patterns of SCV54/03 and 54SiCr6 respectively.
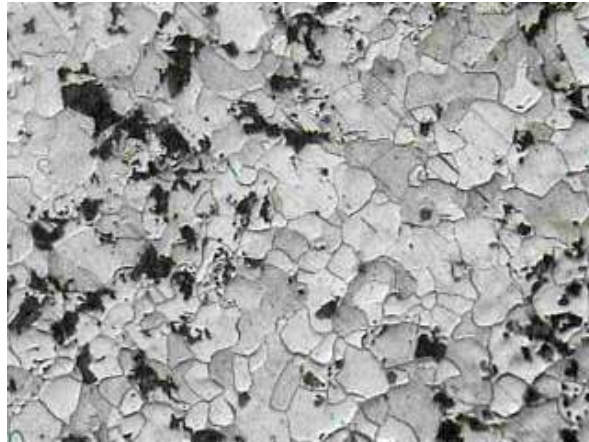
Figure 4.5.31: Grain growth of SCV54/03 when subjected to the oxidation method of determining grain growth. Grain Size 5 – 7. Etched in 10 % HCl-alcohol solution, 200X.
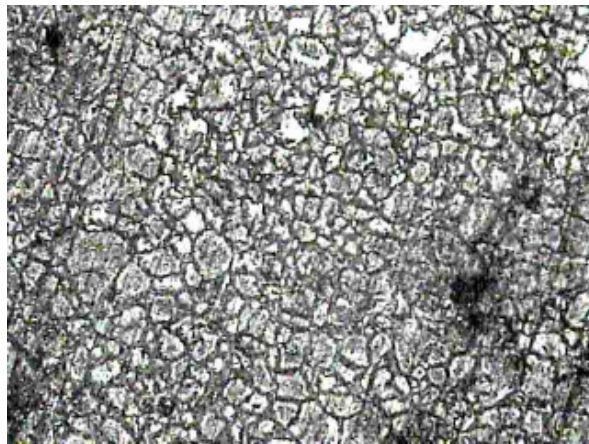
Figure 4.5.32: Grain growth of 54SiCr6 when subjected to the oxidation method of determining grain growth. Grain size 8 and finer. Etched in 10 % HCl-alcohol solution, 200X.

It is evident that in SCV54/03 sample, the grain size has increased by about 2 orders of magnitude while the 54SiCr6 sample was unaffected.

4.6 PROPERTIES OF COIL SPRINGS

4.6.1 AS QUENCHED COIL SPRINGS

The coil springs produced industrially were examined metallographically. Figures 4.6.1 and 4.6.2 show the as quenched microstructure of SCV54/03 and 54SiCr6 respectively. The microstructure of the two steels is relatively fine and not distinguishable. Austenitising time was in the order of 15 minutes.
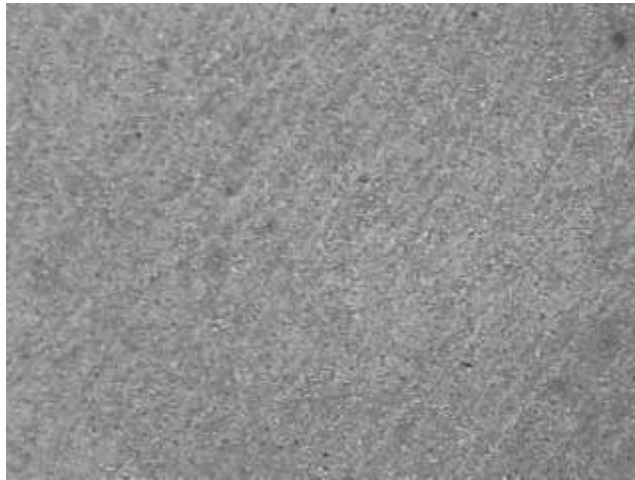
Figure 4.6.1: As quenched microstructure of SCV54/03 in a coil spring. Etched in 2% Nital, 100X.
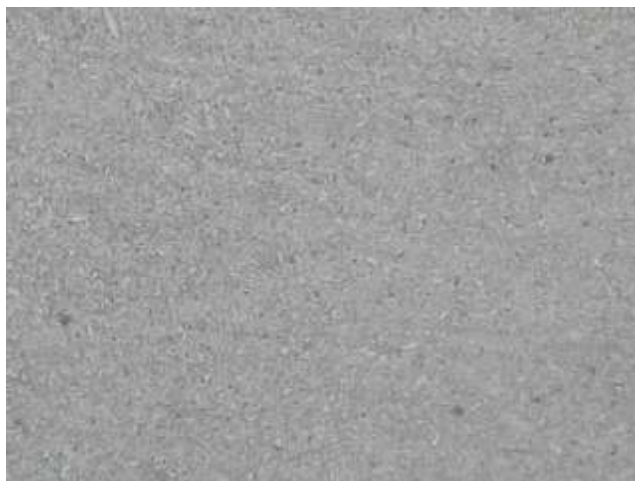
Figure 4.6.2: As quenched microstructure of 54SiCr6 in a coil spring. Etched in 2% Nital, 100.

4.6.2 TEMPERED COIL SPRINGS

The microstructure of the tempered coil springs did not reveal any significant differences (Figures 4.6.3 and 4.6.4).
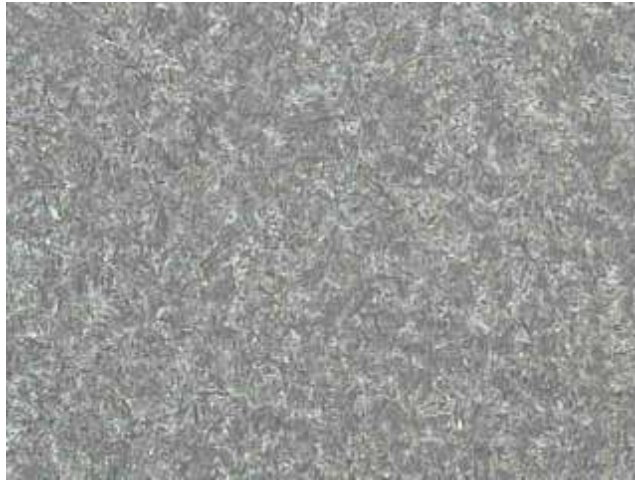
Figure 4.6.3: Microstructure of tempered SCV54/03 steel. Etched in 2% Nital, 100X.
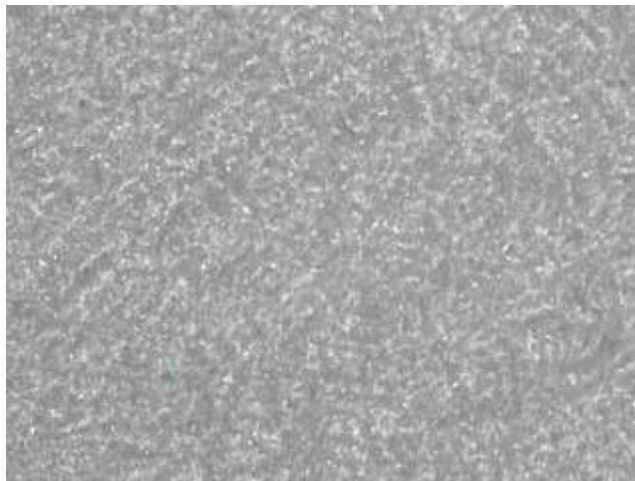
Figure 4.6.4: Microstructure of tempered 54SiCr6 steel. Etched in 2% Nital, 100X.

4.7 FATIGUE TESTING

Fatigue testing was conducted on coil springs of each steel grade. The fatigue-testing machine can test up to 4 coil springs at a time. In order to minimise process deviations during testing, two coil springs per steel grade were mounted onto the fatigue testing machine. The fatigue cycles at failure were measured in each case. The coil springs have to reach 300000 cycles for acceptance. The machine is equipped with an automatic cut out when a failure occurs. A fatigue testing rig is shown in Figure 4.7.1.

Figure 4.7.1: Test layout on fatigue testing machine.

4.8   FATIGUE TESTING RESULTS

The results of the fatigue testing of SCV54/03 and 54SiCr6 are shown in Table 4.8.1 and 4.8.2 respectively:

Table 4.8.1: Fatigue results on SCV54/03

Fatigue results on	Sample	Fatigue cycles achieved	Removed from machine without failure or failed	Percentage of failures below 300000 cycles
SCV54/03	1	2278000	Removed	40 %
	2	1856716	Removed	
	3	1052570	Removed	
	4	332981	Removed	
	The above coil springs passed the minimum fatigue cycles and did not fail the test.			
	5	162199	Failed	
	6	177124	Failed	
	7	189000	Failed	
	8	210600	Failed	
	9	421284	Failed	
	10	896710	Failed	

Four of the ten SCV54/03 coil springs passed the minimum 300000 cycles without failure. These were removed from the fatigue testing machine to speed up the testing phase. A total of six of the SCV54/03 coil springs failed of which four were below the minimum of 300000 cycles.

Table 4.8.2: Fatigue results on 54SiCr6

Fatigue results on	Sample	Fatigue cycles achieved	Removed from machine without failure or failed	Percentage of failures below 300000 cycles
54SiCr6	1	2895606	Removed	0 %
	2	2278000	Removed	
	3	1856716	Removed	
	4	1229964	Removed	
	5	1052570	Removed	
	6	899245	Removed	
	7	645891	Removed	
	The above coil springs passed the minimum fatigue cycles and did not fail the test.			
	8	340200	Failed	
	9	351000	Failed	
	10	441023	Failed	

All of the 54SiCr6 coil springs passed the minimum required 300000 cycles. In fact, the three failures that did occur were due to poor handling of the springs resulting in surface defects, which eventually contributed to failure. It is evident that the 54SiCr6 coil springs are less susceptible to failure compared to the SCV54/03 coil springs.

4.9 ANALYSIS OF FATIGUE FAILURES

The analysis of the coil spring fracture faces are presented below in Figures 4.9.1 to 4.9.4: (See Appendix 3: Part 9.1 for more photographs)

Figure 4.9.1: Failure in 54SiCr6 at 340200 cycles.	Figure 4.9.2: Failure in 54SiCr6 at 351000 cycles.
Figure 4.9.3: Failure on SCV54/03 at 210600 cycles.	Figure 4.9.4: Failure on SCV54/03 at 189000 cycles.

The failures on the 54SiCr6 coil springs were in a ductile manner. The failures on the SCV54/03 coil springs was concoidal in nature indicating the torsional load on the spring during compression in the fatigue testing rig.

4.9.1   SEM ANALYSIS OF FATIGUE FAILURES OF SCV54/03

In order to ascertain the cause of failure in the coil springs. SEM work was done on the fracture faces. The fracture face of the SCV54/03 spring which failed at 210600 cycles was analysed in an SEM. Figures 4.9.5 and 4.9.6 shows the mode of failure.
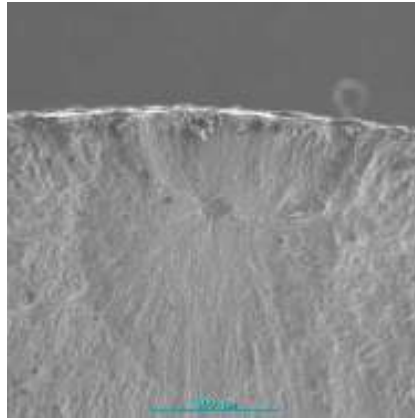
Figure 4.9.5: Failure on SCV54/03 spring at 210600 cycles.
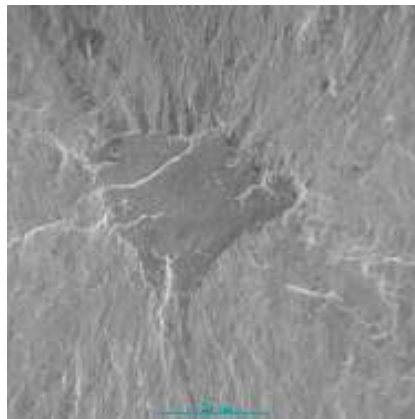
Figure 4.9.6: Origin of failure at 210600 cycles.

A clear sub-surface micro-crack was evident approximately 0.4 mm below the surface. In coil springs, this is not the normal mode of failure. In general, the failures originate from the surface (poor shot peening, mechanical damage or tool marks).

The sub surface defect does not originate from decarburisation. The decarburisation in this coil spring was less then 0.1 mm. Note the radial markings emanating from the sub-surface crack showing that the crack extended up to about 0.8 mm before final fracture. This equates to 0.5 % of the cross sectional area of the coil spring.

Examination by SEM of the failure at 189000 cycles, revealed a non-metallic inclusion (of which only a small portion still remained on the fracture surface), which served as a source of failure. The inclusion is shown in Figure 4.9.7.
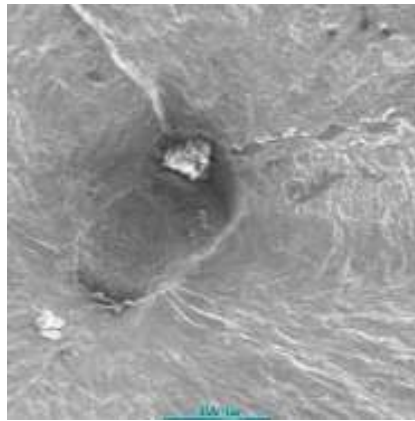
Figure 4.9.7: Origin of failure at 189000 cycles.

Electron microprobe analysis of the non-metallic inclusion as shown in Figure 4.9.8 revealed that it consisted of mainly alumina (50%), with some minor constituents of calcium oxide (26%), magnesium oxide (11%), silica (6%) and iron oxide (6%)
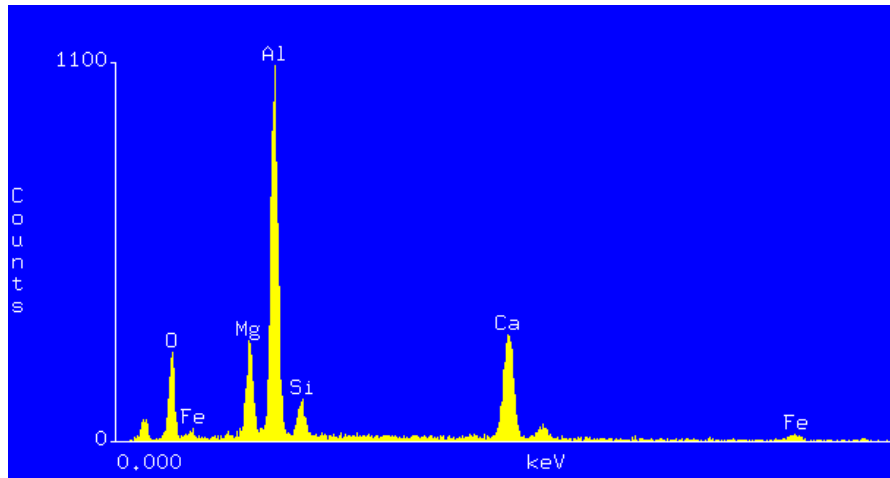
Figure 4.9.8: Electron Microprobe analysis of the inclusion.

The failure at 421284 cycles was due to a sub-surface micro-crack approximately 0.5 mm under the surface as shown in Figure 4.9.9. This failure did not originate from decarburisation, which was less than 0.15 mm in the coil spring.
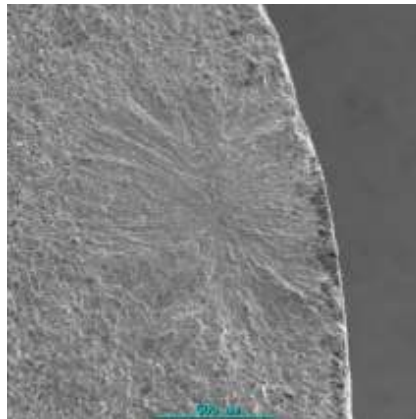
Figure 4.9.9: Origin of failure at 421284 cycles.

The three failures outlined in this section indicate that the SCV54/03 coil springs are susceptible to failure from subsurface cracks and defects. Under normal conditions, a coil spring would fail from the surface.

4.10 SEM ANALYSIS OF FATIGUE FAILURES OF 54SICR6

The origin of the fatigue failures in the 54SiCr6 coil springs was from the surface. Figures 4.10.1 and 4.10.2 indicate the origin of failure.
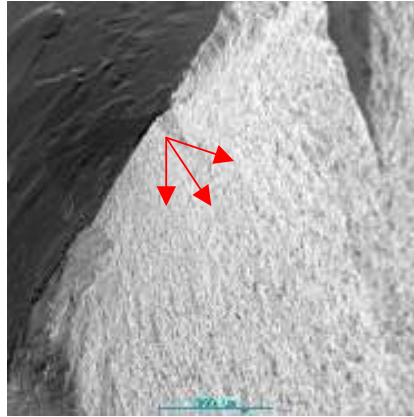
Figure 4.10.1: Failure of 54SiCr6 at 340200 cycles.
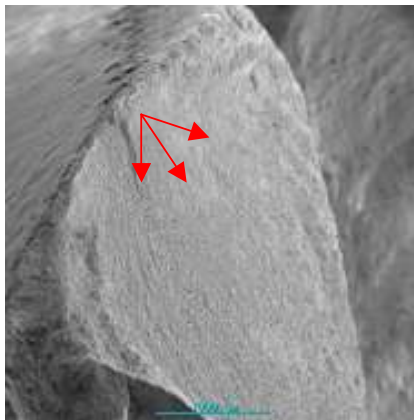
Figure 4.10.2: Failure of 54SiCr6 at 351000 cycles.

Failures from the surface are considered to be the normal mode of failure. When the failures on the 54SiCr6 coil springs are compared to the failures on the SCV54/03 coil springs, it is evident that the 54SiCr6 steel is more tolerant to the extreme stresses in the fatigue testing operation. If any sub surface defects were present, they did not contribute to the failures in 54SiCr6 coil springs.

151

5   DISCUSSION

5.1   PROPERTIES OF AS ROLLED SCV54/03 AND 54SICR6

The hot rolling behaviour of SCV54/03 and 54SiCr6 was similar. Both steels are easy to roll and show similar levels of decarburisation. The main contribution to decarburisation in steel is the level of C and Si. Due to the similarity in C and Si of the two steels no significant difference in the levels of decarburisation was observed. The essential difference in the chemical composition was the presence of V in SCV54/03 and Al in 54SiCr6.

The mechanical properties of the as rolled material were similar. The differences in hardness, UTS and YS were negligible. The most noticeable difference was the elongation and reduction in area of the two steels. The elongation of the as rolled SCV54/03 and 54SiCr6 steel was 16 and 23 % respectively. At the same time, the reduction in area was 22 % for SCV54/03 and 42 % for 54SiCr6 steel. The ductility of the two steels are relatively low but they are considered satisfactory for high strength materials.

As mentioned in the literature survey [2], V does not precipitate readily during hot rolling. However, the difference in ductility between the two steels suggests the precipitation of Al and V compounds may have contributed to this difference. It is probable that minor degrees of precipitation hardening took place, rendering the SCV54/03 less ductile than 54SiCr6. The scope of this study did not cover TEM examination therefore a thorough analysis was not possible.

The grain size of hot rolled steel is mainly determined by the finishing temperature, the amounts of reduction in the last few passes (particularly in the last pass) and cooling conditions. The type of steel will determine the grain size through its precipitation, recrystallisation and grain growth characteristics. The literature survey [1] indicated that V steels are susceptible to grain growth when the final passes have low reduction and when the finishing temperature is too high.

During the hot rolling of the two steels, the exit temperature of the billets from the furnace was about 1100 $^{\circ}$C while the finishing temperature was about 900 $^{\circ}$C. In addition, the high reduction from a 140 mm square billet to an 18 mm round was sufficient for a fine grain size. A slow cooling process was adopted to reduce the hardness of the material for downstream processing. It is possible that during this phase, grain growth could have occurred. However, the grain size was measured as ASTM 8 and finer in both steels in the as rolled condition. This grain size is considered fine and satisfactory for the materials involved.

Aluminium nitrides, VN and V(C,N) do not precipitate readily during hot rolling. It is apparent that any precipitation of V compounds in SCV54/03 or Al compounds in 54SiCr6 had similar effects on grain size. It is more likely that high reduction during hot rolling was the overriding factor in controlling grain size.

5.2 EFFECT OF AUSTENITISING TEMPERATURE ON GRAIN SIZE

The aim of using three austenitising temperatures in heat treatment was to determine if V was effective in controlling grain growth. It has been shown that higher austenitising temperatures promote grain growth in SCV54/03, when austenitised for one hour at

153

temperatures of 860 and 880 $^{\circ}$C. The 54SiCr6 did not suffer from any grain growth at the same austenitising temperatures.

The effects of heat treatment on the two steels may be expected to be similar in certain temperature ranges. However, when the austenitising temperature exceeds a certain limit, the two steels may be expected to respond differently due to differences in the stability of the precipitates, which control grain growth. In the present case, it has been shown that austenitising temperatures of 860 $^{\circ}$C or higher result in grain growth in steel SCV54/03.

This effect can be expected to be exacerbated by long austenitising periods of time. These findings are in agreement with previous findings[21] and show clearly that the stability of V compounds is limited and probably dissolve at temperatures of 860 $^{\circ}$C and higher. The higher stability of AlN resulted in finer grain size. This compound tends to go into solution at temperatures of 1050 $^{\circ}$C or higher.

The grain size of SCV54/03 worsened from ASTM 8 grain size number to ASTM 5 grain size number over a one hour period above 860 $^{\circ}$C. Grain size control was better in 54SiCr6 due to the stability of the AlN precipitates. It has been seen [25] that larger grains reduce the fatigue life of steel and would therefore be completely undesirable in automotive coil springs.

5.3   MECHANICAL PROPERTIES AFTER HEAT TREATMENT

Both V and Al compounds tend to either precipitate or coarsen during a tempering process [2]. The tensile strength and hardness of SCV54/03 improved due to precipitation of V compounds during tempering. This was evident in the slight increase in hardness of tempered SCV54/03 steel. 54SiCr6 did not show this tendency

154

under similar conditions. Grain refinement is unique in that it adds both strength and toughness to the steel whereas precipitation increases strength at the expense of ductility. This was the probable reason for the lower reduction in area of steel SCV54/03.

The differences in tensile strength between SCV54/03 and 54SiCr6 were 42.4, 54.0 and 46.4 MPa for austenitising temperatures of 880 ^{o}C, 860 ^{o}C and 840 ^{o}C respectively, SCV54/03 being the stronger steel. This result appears to be due solely to the effect of precipitation. However, the slightly higher strength of steel SCV54/03 (less than 3 %) is of little significance given the high strength (about 2100 Mpa) of the materials investigated.

The elongation and reduction in area of 54SiCr6 was superior to that of SCV54/03. The improved ductility of steel 54SiCr6 led to higher reduction in area in the tensile tests and ductile fractures in the coil springs. It has been seen that these values were consistent for 54SiCr6 while the results for SCV54/03 were be erratic. The reduction in area of SCV54/03 after austenitising at 880 ^{o}C exceeded the values at the remaining austenitising temperatures.

This may be due to the fact that the dissolution of V precipitates at 880 ^{o}C resulted in more finely distributed precipitate particles in a tempered product. The reverse would apply for samples austenitised at 840 ^{o}C, since the precipitates would not be dissolved and therefore would be expected to coarsen during tempering.

The maximum operating stresses of the coil spring manufactured from the two steels is 1800 Mpa. Both steels reach this strength level easily when tempered at about 420 ^{o}C. The reduction in area of the steel 54SiCr6 tempered at this temperature, exceeded 30 %

155

irrespective of austenitising temperature. The SCV54/03 steel was only able to achieve a maximum of 17.9 %.

The unpredictability of the SCV54/03 steel extended to the fatigue testing of the coil springs. The SCV54/03 steel does not allow for deviations in the heat treatment, particularly when austenitising, which is normal during heat treatment in a production process. Austenitising temperatures of below 860 $^{\circ}$C can have a marked effect on the ductility of this steel due to the dynamics of the V precipitation.

It can be seen that precipitation effects increase the tensile strength slightly but reduce the ductility. The samples austenitised at 860 $^{\circ}$C or lower temperatures tend to have lower ductility when compared to the marginal increase in tensile strength. As a result, austenitising temperatures in excess of 860 $^{\circ}$C should be used for heat treating SCV54/03 steel. The precipitation effects of the V compounds are thus reduced. The ductility of the 54SiCr6 steel poses no problem for coil springs, as the levels are well above 30 % for the reduction in area.

The general appearance of tensile fracture surfaces under the SEM showed that fracture in SCV54/03 could be by cleavage, intergranular, or microvoid coalescence. Tensile failures by cleavage or intergranular mechanisms are obviously unacceptable in automotive coil springs, which are submitted to fluctuating stresses over long periods of time. Such failures are unpredictable; they occur with minimum energy absorption and can result in serious accidents. The 54SiCr6 steel failed by microvoid coalescence irrespective of material condition. This steel would make a good candidate for coil springs.

The effect of longer tempering times was reduced tensile strength with an increase in ductility for both steels. The longer tempering times decreased the tensile strength of the two steels by up to 220 MPa over an 8 hour tempering period. Closer examination of the results revealed that for three austenitising temperatures, the ductility of SCV54/03 increased by only 3 % after tempering for 8 hours. While, the ductility of 54SiCr6 increased by as much as 10%. The 54SiCr6 steel was still able to maintain ductility values in excess of 30 %. It is clear that V precipitates have contributed to the marginal increase in ductility of SCV54/03. The coarser particles contribute to reduced mechanical properties.

It is important to keep in mind that the V content of SCV54/03 was 0.06% while the Al content of 54SiCr6 was 0.02%. The difference is of the order of 200 %. Yet it can be concluded that the higher V content was of no significance to the SCV54/03 steel. In fact except for UTS and YS, the more significant property of ductility has been reduced.

5.4 FATIGUE PROPERTIES

Perhaps the most important test conducted on the two steel grades was the fatigue test of the coil springs. The conditions of manufacture of the coil springs were made as similar as possible for consistency. The fatigue testing results would therefore be indicative of the field performance of the two steels.

The loading on coil springs is in the form of a torsional bending force. During loading, the maximum stress occurs at the surface. Failure could therefore be expected to initiate at the surface. Coil springs are shot peened to induce compressive stresses in the surface, which oppose tensile stresses induced by the load. However, excessive shot peening can result in surface defects,

which serve as sites for crack initiation. An important factor would be the level of decarburisation on the coil spring, which is basically a soft layer. Shot peening would result in a rough surface layer with several stress raisers. These stress raisers are ideal for crack initiation and eventual fatigue failure.

The fatigue life of springs in SCV54/03 was very erratic with springs failing between 162199 and 897710 stress cycles. A further anomaly was that failure tended to initiate from sub-surface defects. Forty percent of the SCV54/03 springs tested did not pass the minimum 300000 cycles. The spread of failures on SCV54/03 demonstrates the unpredictability of this steel as a coil spring material. Similar results were displayed in the mechanical testing.

The manufacture of coil springs is not a perfect process. The coil springs tend to have decarburisation, shot peening defects and tool marks on the surface. Normally, failure of a coil spring would originate from these defects. Internal defects in steel such as inclusions are normal and may also trigger fatigue failure depending on their size, position and shape. The effects of inclusions and other internal defects was more pronounced in steel SCV54/03 than steel 54SiCr6. This may be attributed to the lower ductility of the steel, which made it more sensitive to such defects.

Springs in steel 54SiCr6 failed in a narrow range of cycles (340200 to 441023), failure invariably initiating at shot peening defects on the surface. The consistency of the results and the fact that none of the samples failed below the minimum requirement of 300000 cycles, make this material highly suitable for the application. Automotive coil springs are safety critical components and their behaviour in use has to be highly predictable.

The notch sensitivity of the steel SCV54/03 appears to be higher than steel 54SiCr6. Although fracture toughness values were not determined, it can be deduced that the 54SiCr6 steel would allow for a larger defect than SCV54/03 for failure to occur at the same number of fatigue cycles. This is a testament to the efficacy of Al grain refinement, which improves the toughness of the steel. The inconsistent fatigue results in SCV54/03 coupled with the fact that several failures were below the minimum 300000 cycles do not permit confidence in this material.

6   CONCLUSION

- Steels SCV54/03 and 54SiCr6 had similar mechanical properties except for ductility, steel 54SiCr6 showing significantly higher ductility than steel SCV54/03.

- Steel SCV54/03 was susceptible to grain growth at austenitising temperatures exceeding 860 $^\circ$C. Steel 54SiCr6 was not prone to grain growth at normal heat treatment temperatures.

- The fatigue properties of steel 54SiCr6 were consistent and satisfactory in all cases making this material a suitable candidate for the manufacture of automotive coil springs.

- The fatigue properties of steel SCV54/03 were erratic and did not always meet the requirement of a minimum of 300000 cycles to failure making this material unsuitable for the automotive coil springs.

7 APPENDIX 1

7.1 PHOTOMICROGRAPHS OF DECARBURISATION ON SCV54/03 (AS ROLLED)

Figure 7.1.1: Decarburisation on SCV54/03, 0.09 mm (SAEJ419), 0.16 mm (ASTM E1077), 100X.	Figure 7.1.2: Decarburisation on SCV54/03, 0.10 mm (SAEJ419), 0.19 mm (ASTM E1077), 100X.
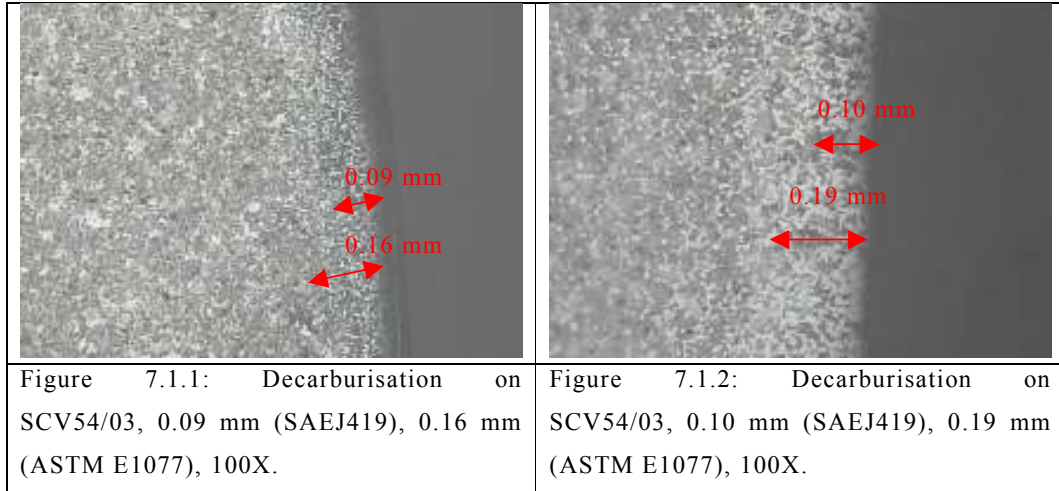
7.2 PHOTOMICROGRAPHS OF DECARBURISATION ON 54SICR6 (AS ROLLED)
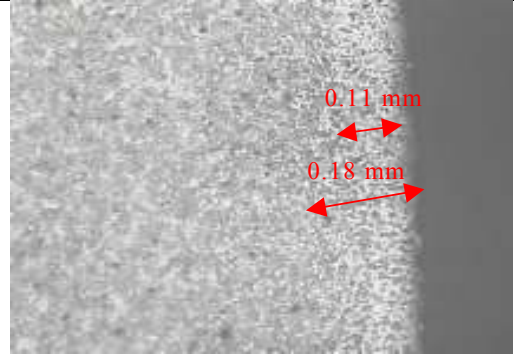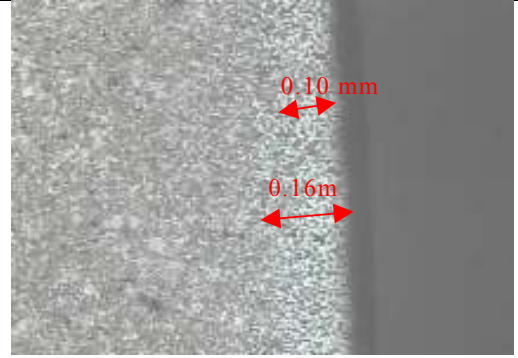
Figure 7.2.1: Decarburisation on 54SiCr6, 0.11 mm (SAEJ419), 0.18 mm (ASTM E1077), 100X.

Figure 7.2.2: Decarburisation on 54SiCr6, 0.10 mm (SAEJ419), 0.16 mm (ASTM E1077), 100X.
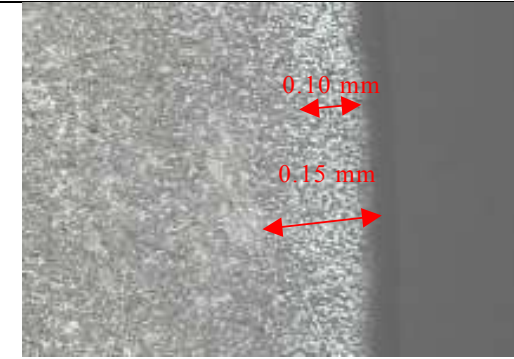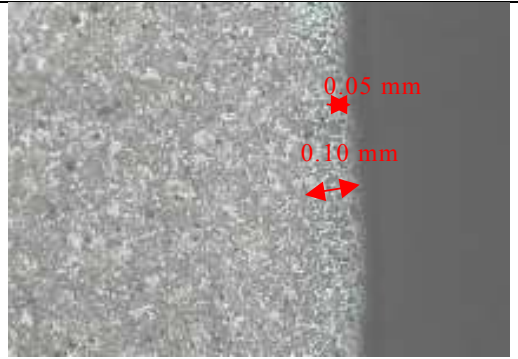
Figure 7.2.3: Decarburisation on 54SiCr6, 0.10 mm (SAEJ419), 0.15 mm (ASTM E1077), 100X.

Figure 7.2.4: Decarburisation on 54SiCr6, 0.05 mm (SAEJ419), 0.10 mm (ASTM E1077), 100X.

7.3 PHOTOMICROGRAPHS OF AS QUENCHED ROLLED PRODUCT

As quenched micrographs of SCV54/03 and 54SiCr6 at 100 X magnification.
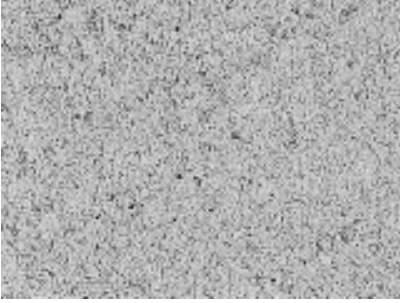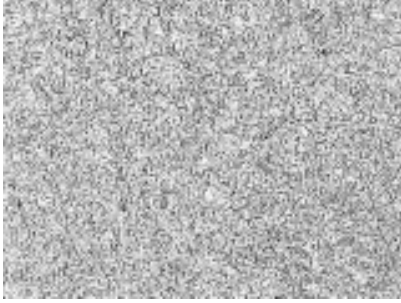
860 °C quench	Figure 7.3.1: As quenched microstructure of SCV54/03. Etched in 2 % Nital, 100X	Figure 7.3.2: As quenched microstructure of 54SiCr6. Etched in 2 % Nital, 100X
840 °C quench	Figure 7.3.3: As quenched microstructure of SCV54/03. Etched in 2 % Nital, 100X	Figure 7.3.4: As quenched microstructure of 54SiCr6. Etched in 2 % Nital, 100X
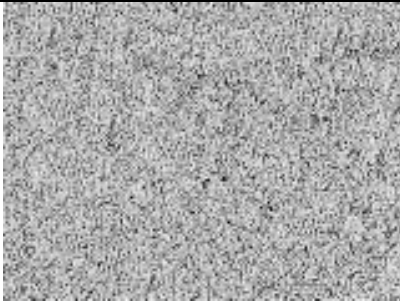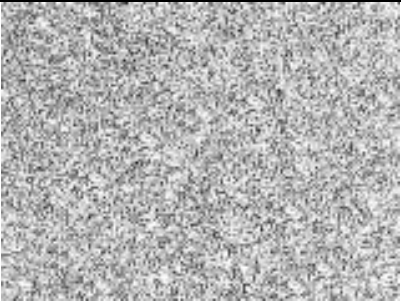
As quenched micrographs of SCV54/03 and 54SiCr6 at 500 X magnification.
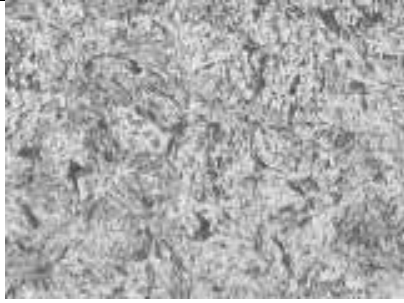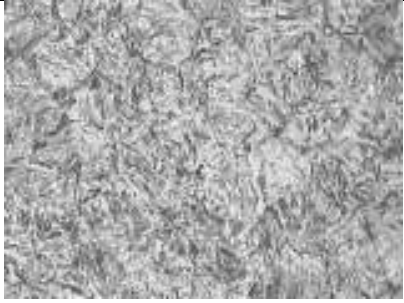
880 °C quench		
	Figure 7.3.5: As quenched microstructure of SCV54/03. Etched in 2 % Nital, 500X	Figure 7.3.6: As quenched microstructure of 54SiCr6. Etched in 2 % Nital, 500X
860 °C quench		
	Figure 7.3.7: As quenched microstructure of SCV54/03. Etched in 2 % Nital, 500X	Figure 7.3.8: As quenched microstructure of 54SiCr6. Etched in 2 % Nital, 500X
840 °C quench		
	Figure 7.3.9: As quenched microstructure of SCV54/03. Etched in 2 % Nital, 500X	Figure 7.3.10: As quenched microstructure of 54SiCr6. Etched in 2 % Nital, 500X
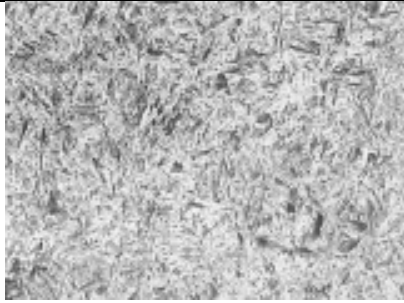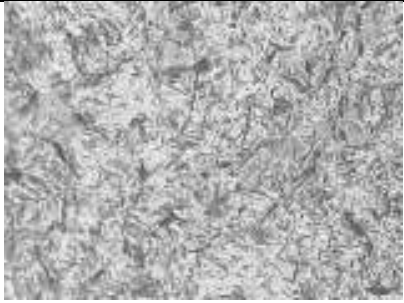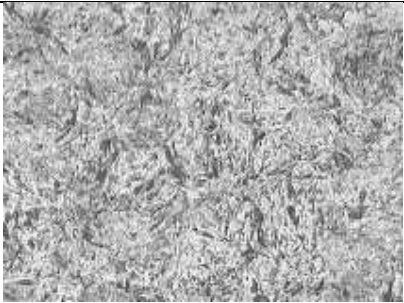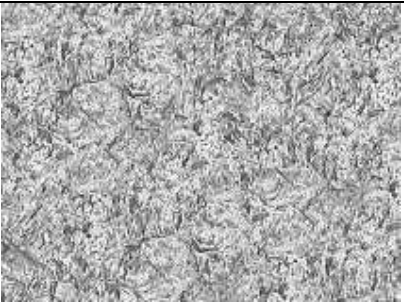
7.4 ADDITIONAL PHOTOMICROGRAPHS OF SAMPLES QUENCHED AND TEMPERED AT 500 ^{o}C
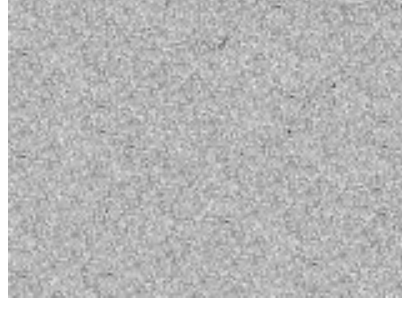
880 ^{o}C Quench	Figure 7.4.1: Microstructure of SCV54/03 tempered at 500 ^{o}C. Etched in 2 % Nital, 100X.	Figure 7.4.2: Microstructure of 54SiCr6 tempered at 500 ^{o}C. Etched in 2 % Nital, 100X.
860 ^{o}C Quench	Figure 7.4.3: Microstructure of SCV54/03 tempered at 500 ^{o}C. Etched in 2 % Nital, 100X.	Figure 7.4.4: Microstructure of 54SiCr6 tempered at 500 ^{o}C. Etched in 2 % Nital, 100X.
840 ^{o}C Quench	Figure 7.4.5: Microstructure of SCV54/03 tempered at 500 ^{o}C. Etched in 2 % Nital, 100X.	Figure 7.4.6: Microstructure of 54SiCr6 tempered at 500 ^{o}C. Etched in 2 % Nital, 100X.
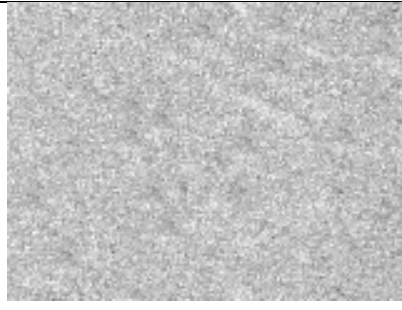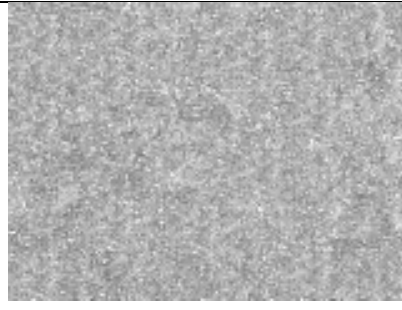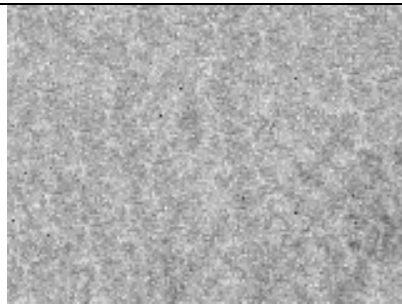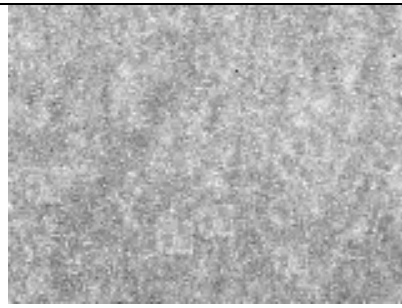
7.5 ADDITIONAL PHOTOMICROGRAPHS OF SAMPLES QUENCHED AND TEMPERED AT 480 ^{o}C

880 ^{o}C Quench		
	Figure 7.5.1: Microstructure of SCV54/03 tempered at 480 ^{o}C. Etched in 2 % Nital, 100X.	Figure 7.5.2: Microstructure of 54SiCr6 tempered at 480 ^{o}C. Etched in 2 % Nital, 100X.
860 ^{o}C Quench		
	Figure 7.5.3: Microstructure of SCV54/03 tempered at 480 ^{o}C. Etched in 2 % Nital, 100X.	Figure 7.5.4: Microstructure of 54SiCr6 tempered at 480 ^{o}C. Etched in 2 % Nital, 100X.
840 ^{o}C Quench		
	Figure 7.5.5: Microstructure of SCV54/03 tempered at 480 ^{o}C. Etched in 2 % Nital, 100X.	Figure 7.5.6: Microstructure of 54SiCr6 tempered at 480 ^{o}C. Etched in 2 % Nital, 100X.
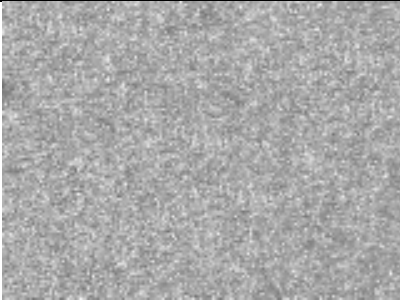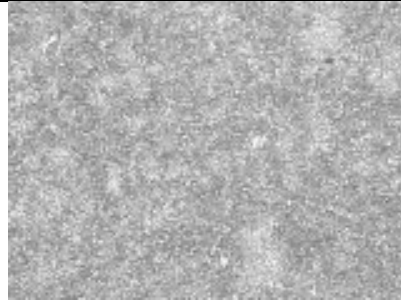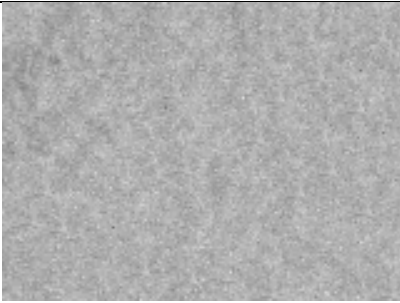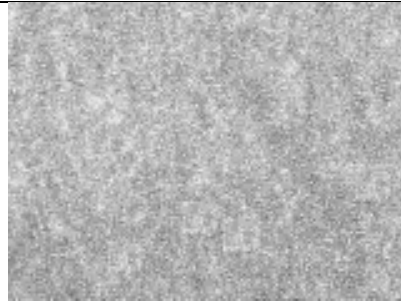
7.6 ADDITIONAL PHOTOMICROGRAPHS OF SAMPLES QUENCHED AND TEMPERED AT 460 ^{o}C

Figure 7.6.1: Microstructure of SCV54/03 tempered at 460 ^{o}C. Etched in 2 % Nital, 100X.

Figure 7.6.2: Microstructure of 54SiCr6 tempered at 460 ^{o}C. Etched in 2 % Nital, 100X.
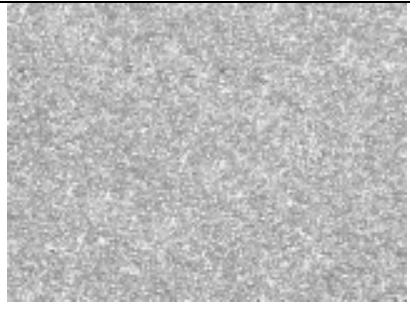
Figure 7.6.3: Microstructure of SCV54/03 tempered at 460 ^{o}C. Etched in 2 % Nital, 100X.

Figure 7.6.4: Microstructure of 54SiCr6 tempered at 460 ^{o}C. Etched in 2 % Nital, 100X.
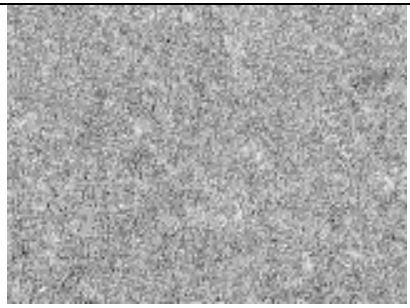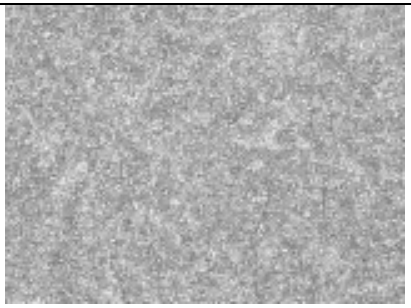
Figure 7.6.5: Microstructure of SCV54/03 tempered at 460 ^{o}C. Etched in 2 % Nital, 100X.

Figure 7.6.6: Microstructure of 54SiCr6 tempered at 460 ^{o}C. Etched in 2 % Nital, 100X.

(880 ^{o}C Quench; 860 ^{o}C Quench; 840 ^{o}C Quench)

7.7 ADDITIONAL PHOTOMICROGRAPHS OF SAMPLES QUENCHED AND TEMPERED AT 440 ^{o}C

880 ^{o}C Quench	Figure 7.7.1: Microstructure of SCV54/03 tempered at 440 ^{o}C. Etched in 2 % Nital, 100X.	Figure 7.7.2: Microstructure of 54SiCr6 tempered at 440 ^{o}C. Etched in 2 % Nital, 100X.
860 ^{o}C Quench	Figure 7.7.3: Microstructure of SCV54/03 tempered at 440 ^{o}C. Etched in 2 % Nital, 100X.	Figure 7.7.4: Microstructure of 54SiCr6 tempered at 440 ^{o}C. Etched in 2 % Nital, 100X.
840 ^{o}C Quench	Figure 7.7.5: Microstructure of SCV54/03 tempered at 440 ^{o}C. Etched in 2 % Nital, 100X.	Figure 7.7.6: Microstructure of 54SiCr6 tempered at 440 ^{o}C. Etched in 2 % Nital, 100X.
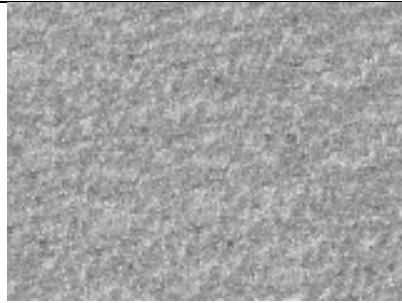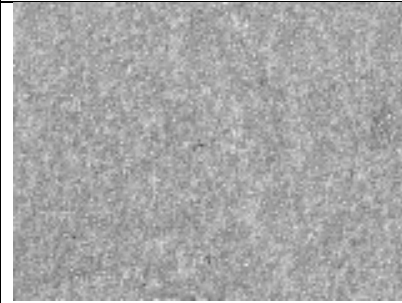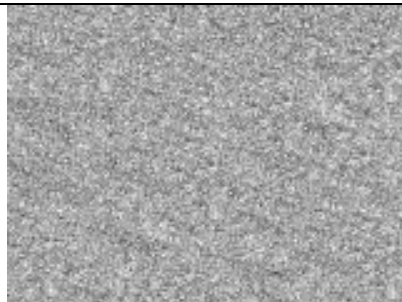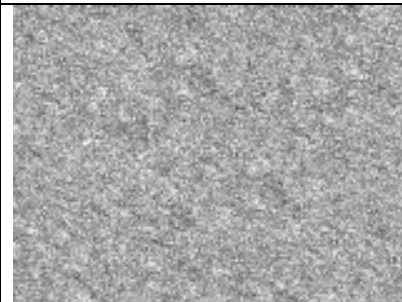
7.8 ADDITIONAL PHOTOMICROGRAPHS OF SAMPLES QUENCHED AND TEMPERED AT 430 ^{o}C
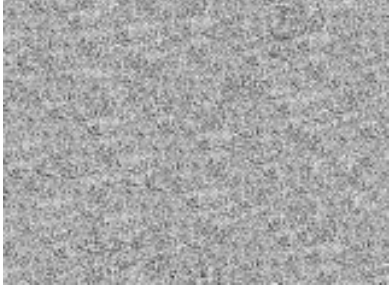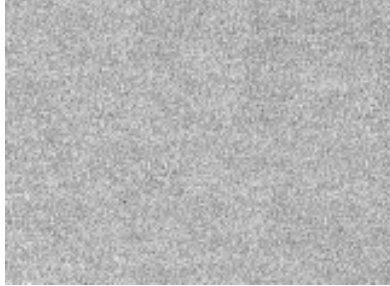
880 ^{o}C Quench		
	Figure 7.8.1: Microstructure of SCV54/03 tempered at 430 ^{o}C. Etched in 2 % Nital, 100X.	Figure 7.8.2: Microstructure of 54SiCr6 tempered at 430 ^{o}C. Etched in 2 % Nital, 100X.
860 ^{o}C Quench		
	Figure 7.8.3: Microstructure of SCV54/03 tempered at 430 ^{o}C. Etched in 2 % Nital, 100X.	Figure 7.8.4: Microstructure of 54SiCr6 tempered at 430 ^{o}C. Etched in 2 % Nital, 100X.
840 ^{o}C Quench		
	Figure 7.8.5: Microstructure of SCV54/03 tempered at 430 ^{o}C. Etched in 2 % Nital, 100X.	Figure 7.8.6: Microstructure of 54SiCr6 tempered at 430 ^{o}C. Etched in 2 % Nital, 100X.
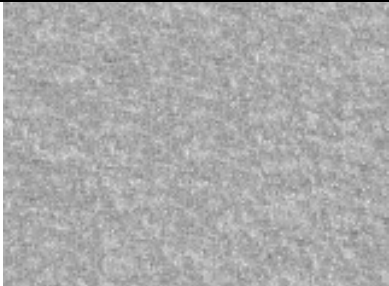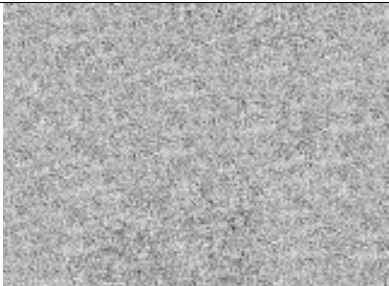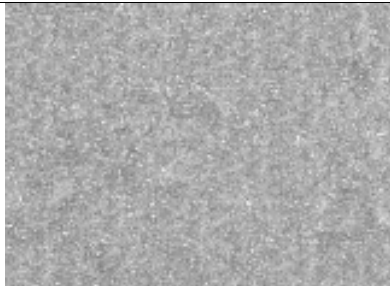
7.9   ADDITIONAL   PHOTOMICROGRAPHS   OF   SAMPLES QUENCHED AND TEMPERED AT 420 ^{o}C

880 ^{o}C Quench	Figure 7.9.1: Microstructure of SCV54/03 tempered at 420 ^{o}C. Etched in 2 % Nital, 100X.	Figure 7.9.2: Microstructure of 54SiCr6 tempered at 420 ^{o}C. Etched in 2 % Nital, 100X.
860 ^{o}C Quench	Figure 7.9.3: Microstructure of SCV54/03 tempered at 420 ^{o}C. Etched in 2 % Nital, 100X.	Figure 7.9.4: Microstructure of 54SiCr6 tempered at 420 ^{o}C. Etched in 2 % Nital, 100X.
840 ^{o}C Quench	Figure 7.9.5: Microstructure of SCV54/03 tempered at 420 ^{o}C. Etched in 2 % Nital, 100X.	Figure 7.9.6: Microstructure of 54SiCr6 tempered at 420 ^{o}C. Etched in 2 % Nital, 100X.
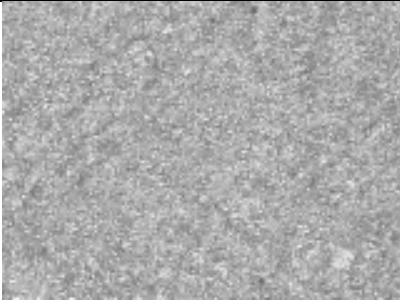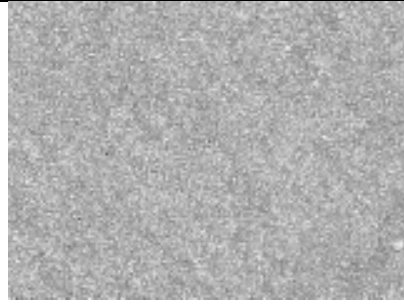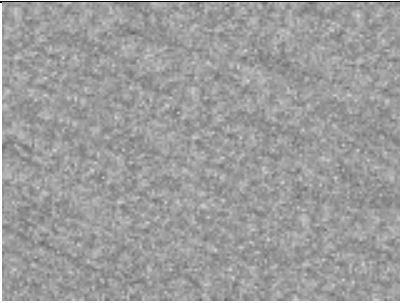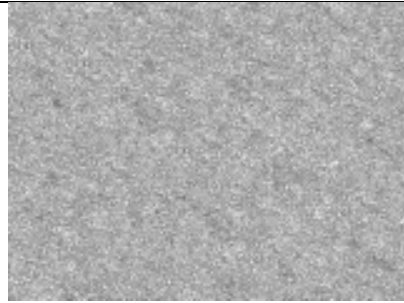
7.10 ADDITIONAL PHOTOMICROGRAPHS OF SAMPLES QUENCHED AND TEMPERED AT 400 ^{o}C

880 ^{o}C Quench	Figure 7.10.1: Microstructure of SCV54/03 tempered at 400 ^{o}C. Etched in 2 % Nital, 100X.	Figure 7.10.2: Microstructure of 54SiCr6 tempered at 400 ^{o}C. Etched in 2 % Nital, 100X.
860 ^{o}C Quench	Figure 7.10.3: Microstructure of SCV54/03 tempered at 400 ^{o}C. Etched in 2 % Nital, 100X.	Figure 7.10.4: Microstructure of 54SiCr6 tempered at 400 ^{o}C. Etched in 2 % Nital, 100X.
840 ^{o}C Quench	Figure 7.10.5: Microstructure of SCV54/03 tempered at 400 ^{o}C. Etched in 2 % Nital, 100X.	Figure 7.10.6: Microstructure of 54SiCr6 tempered at 400 ^{o}C. Etched in 2 % Nital, 100X.
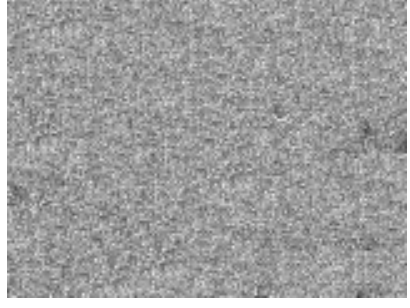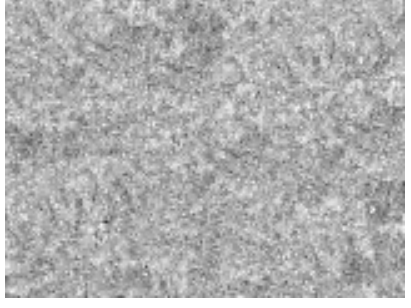
7.11 ADDITIONAL PHOTOMICROGRAPHS OF SAMPLES QUENCHED AND TEMPERED AT 380 ^{o}C

880 ^{o}C Quench
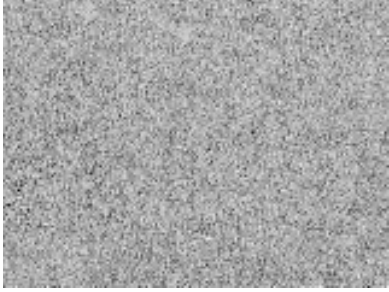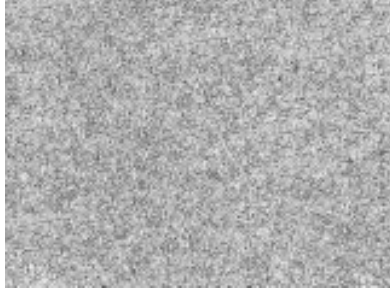
Figure 7.11.1: Microstructure of SCV54/03 tempered at 380 ^{o}C. Etched in 2 % Nital, 100X.

Figure 7.11.2: Microstructure of 54SiCr6 tempered at 380 ^{o}C. Etched in 2 % Nital, 100X.

860 ^{o}C Quench
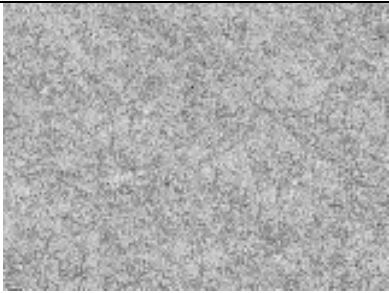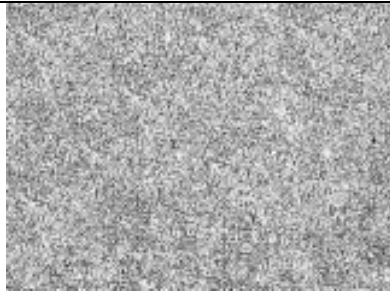
Figure 7.11.3: Microstructure of SCV54/03 tempered at 380 ^{o}C. Etched in 2 % Nital, 100X.

Figure 7.11.4: Microstructure of 54SiCr6 tempered at 380 ^{o}C. Etched in 2 % Nital, 100X.

840 ^{o}C Quench
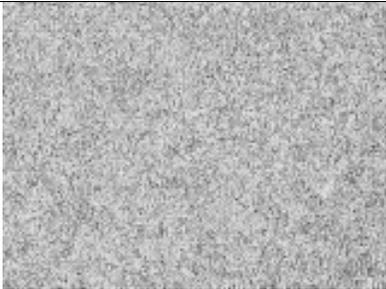
Figure 7.11.5: Microstructure of SCV54/03 tempered at 380 ^{o}C. Etched in 2 % Nital, 100X.

Figure 7.11.6: Microstructure of 54SiCr6 tempered at 380 ^{o}C. Etched in 2 % Nital, 100X.

8.1 TENSILE RESULTS OF MATERIAL TEMPERED FOR ONE HOUR

Table 8.1.1: Tensile results of samples tempered for 1 hour.

Austenitising Temperature	Tempering Temperature	Hardness (HRc)		SCV54/03						54SiCr6					
				UTS (MPa)		YS (MPa)		Elongation (%)		UTS (MPa)		YS (MPa)		Elongation (%)	
°C	°C	SCV54/03	54SiCr6	Test 1	Test 2	Test 1	Test 2	Test 1	Test 2	Test 1	Test 2	Test 1	Test 2	Test 1	Test 2
880	380	56.5	56.5	2137.7	2094.1	2096.3	1983.2	3.5%	4.5%	2098.6	2051.0	1989.5	1967.3	10.0%	9.9%
	400	55.0	55.0	1969.8	2020.6	1813.7	1822.4	6.3%	6.9%	1952.2	1955.7	1757.0	1725.6	10.2%	10.6%
	420	54.0	53.8	1861.3	1859.7	1769.3	1499.9	7.6%	7.6%	1801.3	1799.3	1567.1	1623.6	11.2%	11.0%
	430	52.7	52.7	1791.6	1425.9	1621.2	1258.4	6.2%	4.1%	1723.4	1733.6	1562.5	1572.0	12.7%	12.9%
	440	51.1	50.9	1621.6	1638.7	1459.4	1442.0	8.1%	7.9%	1652.3	1605.1	1497.0	1439.0	13.0%	12.6%
	460	50.0	49.9	1554.8	1502.0	1432.0	1339.8	8.5%	8.0%	1502.4	1479.7	1367.1	1335.2	13.6%	13.7%
	480	48.1	47.9	1502.4	1512.1	1322.1	1360.9	8.8%	9.5%	1489.3	1500.2	1310.6	1331.6	16.0%	16.0%
	500	45.5	44.1	1486.0	1489.7	1337.4	1370.5	10.0%	10.0%	1457.0	1432.7	1290.9	1318.2	16.1%	16.6%
	530	42.1	42.0	1432.8	1461.4	1297.3	1300.6	11.5%	12.0%	1361.2	1369.4	1212.2	1234.1	17.7%	16.9%
860	380	55.8	55.2	2102.3	2095.3	1894.7	1848.8	3.5%	3.4%	2037.6	2061.3	1833.6	1818.8	7.9%	9.6%
	400	53.0	53.3	1889.3	1992.0	1687.2	1743.9	6.8%	7.1%	1945.7	1956.9	1737.5	1713.1	11.0%	10.2%
	420	51.3	51.2	1876.2	1900.2	1727.4	1691.6	6.0%	8.0%	1852.3	1823.7	1706.0	1623.5	11.5%	11.1%
	430	49.7	49.2	1810.2	1759.2	1621.3	1592.3	6.6%	6.9%	1710.5	1753.0	1557.0	1586.7	12.8%	12.6%
	440	48.9	48.7	1699.5	1685.6	1546.9	1528.0	8.8%	8.5%	1684.5	1645.2	1533.3	1491.4	13.6%	12.6%
	460	48.5	47.9	1594.2	1601.8	1424.7	1435.7	8.1%	8.2%	1526.3	1561.0	1364.0	1399.2	13.5%	13.6%
	480	47.2	46.3	1529.2	1512.1	1530.1	1374.0	9.6%	9.3%	1456.9	1468.3	1457.8	1334.2	15.8%	16.0%
	500	45.8	45.1	1500.6	1490.9	1356.1	1371.8	10.9%	10.6%	1402.7	1427.9	1267.6	1313.8	16.5%	17.0%
	530	43.2	41.8	1446.9	1482.3	1298.8	1483.2	11.0%	13.6%	1356.7	1326.1	1217.8	1327.0	17.4%	17.6%
840	380	55.7	55.3	2156.3	2124.5	1943.4	1874.6	3.6%	3.1%	2101.2	2095.5	1890.9	1849.0	9.7%	10.3%
	400	53.5	53.5	2001.2	2012.1	1787.1	1761.5	5.0%	5.0%	1958.3	1956.9	1748.8	1713.1	11.2%	10.2%
	420	49.4	49.4	1910.5	1867.3	1759.0	1662.4	6.9%	5.8%	1878.0	1857.0	1729.7	1653.1	11.9%	11.4%
	430	47.3	47.5	1757.0	1795.7	1573.6	1625.3	6.9%	7.2%	1756.3	1769.9	1598.7	1601.9	12.4%	13.0%
	440	45.4	45.5	1695.4	1702.7	1543.2	1543.5	8.2%	8.2%	1669.0	1648.4	1519.2	1494.3	13.1%	12.8%
	460	44.3	44.5	1612.8	1681.2	1441.3	1506.9	8.7%	8.9%	1548.7	1562.4	1384.0	1400.4	13.1%	13.5%
	480	43.9	43.8	1545.6	1522.7	1546.5	1383.6	9.3%	9.3%	1502.4	1497.6	1503.3	1360.8	14.6%	14.0%
	500	42.9	42.9	1512.6	1506.4	1367.0	1386.1	11.1%	11.0%	1421.6	1436.3	1284.7	1321.6	15.7%	16.0%
	530	40.7	40.2	1486.5	1423.7	1317.9	1305.2	13.3%	12.5%	1403.0	1415.7	1264.7	1302.6	18.0%	18.2%

Note: Blocks marked in yellow indicate failure from inclusion.

Table 8.1.2: Average difference in UTS between SCV54/03 and 54SiCr6, tempered for 1 hour over 2 tensile tests.

Austenitising temperature	Tempering Temperature	SCV54/03	54SiCr6
°C	°C	Average difference	
		in UTS (MPa)	
880	380	39.1	43.1
	400	17.6	64.9
	420	60.0	60.4
	430	68.1	-307.6
	440	-30.7	33.6
	460	52.4	22.3
	480	13.1	11.9
	500	29.0	57.0
	530	71.6	92.0
	Average	35.6	8.6
860	380	64.7	34.0
	400	-56.3	35.2
	420	23.9	76.6
	430	99.8	6.2
	440	15.0	40.3
	460	67.9	40.8
	480	72.3	43.8
	500	97.9	63.0
	530	90.2	156.2
	Average	52.8	55.1
840	380	55.1	28.9
	400	42.9	55.2
	420	32.5	10.3
	430	0.7	25.8
	440	26.3	54.3
	460	64.1	118.8
	480	43.2	25.1
	500	91.0	70.1
	530	29.8	8.0
	Average	42.9	44.1

Table 8.1.3: Reduction in area of tensiles after tempering for 1 hour.

Austenitising temperature	Tempering Temperature	SCV54/03			54SiCr6		
		Reduction in area (%)			Reduction in area (%)		
^{0}C	^{0}C	Test 1	Test 2	Average	Test 1	Test 2	Average
880	380	10.0%	11.2%	10.6%	32.1%	30.3%	31.2%
	400	14.1%	13.8%	14.0%	36.2%	32.9%	34.6%
	420	17.6%	18.2%	17.9%	34.6%	38.3%	36.4%
	430	19.2%	8.6%	13.9%	39.6%	40.2%	39.9%
	440	19.9%	18.7%	19.3%	39.9%	41.2%	40.6%
	460	21.5%	18.1%	19.8%	41.2%	38.6%	39.9%
	480	22.6%	24.6%	23.6%	44.0%	43.6%	43.8%
	500	29.0%	31.6%	30.3%	46.5%	46.5%	46.5%
	530	37.0%	37.2%	37.1%	48.5%	45.2%	46.9%
860	380	8.2%	7.0%	7.6%	29.6%	32.0%	30.8%
	400	11.0%	9.2%	10.1%	31.1%	32.6%	31.8%
	420	16.5%	16.5%	16.5%	34.5%	30.2%	32.3%
	430	18.3%	21.6%	19.9%	37.3%	36.1%	36.7%
	440	20.7%	21.7%	21.2%	38.7%	40.8%	39.7%
	460	18.7%	24.0%	21.3%	42.1%	40.9%	41.5%
	480	15.6%	25.9%	20.7%	40.8%	42.5%	41.7%
	500	26.9%	29.6%	28.2%	45.1%	45.7%	45.4%
	530	30.2%	32.1%	31.2%	48.5%	46.2%	47.4%
840	380	6.5%	4.6%	5.5%	28.0%	30.6%	29.3%
	400	12.5%	9.9%	11.2%	32.8%	31.9%	32.3%
	420	16.2%	15.6%	15.9%	30.4%	36.5%	33.4%
	430	19.6%	21.5%	20.5%	31.8%	34.8%	33.3%
	440	16.6%	21.7%	19.1%	36.5%	34.2%	35.4%
	460	16.6%	15.4%	16.0%	36.0%	39.2%	37.6%
	480	6.5%	17.6%	12.1%	41.0%	41.5%	41.3%
	500	16.9%	12.6%	14.7%	43.5%	42.1%	42.8%
	530	22.0%	21.6%	21.8%	44.6%	46.4%	45.5%

8.2 TENSILE RESULTS OF MATERIAL TEMPERED FOR 1,2,4 AND 8 HOURS

Table 8.2.1: Tensile results of samples tempered for 1, 2, 4 and 8 hours.

Austenitising temperature	Tempering Temperature	Tempering Hours	SCV54/03						54SiCr6					
			UTS (MPa)		YS (MPa)		Elongation (%)		UTS (MPa)		YS (MPa)		Elongation (%)	
°C	°C		Test 1	Test 2	Test 1	Test 2	Test 1	Test 2	Test 1	Test 2	Test 1	Test 2	Test 1	Test 2
880	430	1	1791.6	1425.9	1621.2	1258.4	6.2%	4.1%	1723.4	1733.6	1562.5	1572.0	12.7%	12.9%
		2	1754.3	1781.0	1588.8	1628.8	6.4%	7.1%	1721.6	1732.5	1543.1	1563.8	13.3%	14.1%
		4	1705.4	1695.6	1580.3	1532.3	6.5%	6.6%	1685.6	1685.7	1556.9	1499.7	14.2%	15.4%
		8	1598.2	1548.6	1475.7	1424.9	7.2%	6.8%	1546.9	1565.3	1396.3	1419.6	15.6%	15.9%
860	430	1	1810.2	1759.2	1621.3	1592.3	6.1%	5.9%	1710.5	1753.0	1557.0	1586.7	12.8%	12.6%
		2	1768.9	1785.2	1602.0	1632.7	6.8%	6.9%	1700.2	1685.2	1541.3	1576.6	13.8%	14.1%
		4	1658.0	1642.0	1536.4	1483.8	7.1%	7.0%	1652.3	1658.3	1481.4	1580.7	14.3%	14.8%
		8	1548.0	1605.0	1413.9	1469.6	7.1%	6.8%	1602.4	1600.5	1479.6	1433.5	15.6%	16.2%
840	430	1	1757.0	1795.7	1585.4	1639.9	5.5%	6.2%	1756.3	1745.2	1598.7	1579.6	12.4%	13.0%
		2	1735.8	1725.4	1583.7	1589.7	6.6%	6.9%	1727.0	1742.6	1558.7	1586.2	13.6%	13.6%
		4	1705.2	1679.6	1556.3	1503.4	7.2%	7.0%	1655.0	1684.2	1483.8	1575.7	14.4%	14.7%
		8	1658.5	1654.2	1513.0	1494.8	7.0%	7.2%	1635.2	1635.4	1524.3	1524.3	15.3%	15.3%

Table 8.2.2: Reduction in area of tensiles for material tempered for 1, 2, 4 and 8 hours.

Austenitising temperature	Tempering Temperature	Tempering Time	SCV54/03			54SiCr6		
			Reduction in area (%)			Reduction in area (%)		
°C	°C	Hrs	Test 1	Test 2	Average	Test 1	Test 2	Average
880	430	1	21.0%	8.6%	14.8%	39.6%	40.2%	39.9%
		2	21.6%	22.6%	22.1%	41.0%	42.5%	41.8%
		4	23.5%	23.0%	23.3%	46.0%	46.8%	46.4%
		8	24.6%	25.0%	24.8%	49.0%	50.2%	49.6%
860	430	1	19.8%	21.6%	20.7%	37.3%	36.1%	36.7%
		2	21.0%	23.0%	22.0%	38.6%	39.5%	39.1%
		4	24.6%	22.0%	23.3%	41.2%	43.5%	42.4%
		8	24.0%	23.5%	23.8%	46.9%	45.2%	46.1%
840	430	1	18.5%	19.0%	18.8%	31.8%	34.8%	33.3%
		2	18.9%	19.0%	19.0%	35.6%	35.5%	35.6%
		4	19.6%	19.2%	19.4%	36.2%	38.5%	37.4%
		8	20.6%	21.0%	20.8%	41.5%	43.6%	42.6%

9 APPENDIX 3

9.1 ADDITIONAL PHOTOGRAPHS OF FATIGUE FAILURES

Figure 9.1.1: Fatigue failure on SCV54/03 at 162199 cycles	Figure 9.1.2: Fatigue failure on SCV54/03 at 298023 cycles.
Figure 9.1.3: Fatigue failure on SCV54/03 at 421284 cycles.	Figure 9.1.4: Fatigue failure on SCV54/03 at 897710 cycles.

10 REFERENCES

1   R.Lagneborg, T.Siwekki, S.Zajac and B.Hutchinson. The role of vanadium in microalloyed steels, Scandinavian Journal of Metallurgy, Vol. 28, No 2, 1999, pp 186 – 241.

2   A.M.Sage. An overview of the use of microalloys in HSLA steels with particular reference to vanadium and titanium. *Proceedings of HSLA Steels `90*, Beijing, October 1990.

3   W.Roberts, A.Sandberg and T.Siwecki. Precipitation of V(C,N) in HSLA steels microalloyed with vanadium, *Proceedings of International Conference on Vanadium Steels*, Krakow, October 1980.

4   F.G.Wilson and T.Gladman. Aluminium nitride in steel, *International Materials Review*, Vol. 33, No 5, 1988, pp 221 – 286.

5   T.Gladman. The physical metallurgy of microalloyed steels, The Institute of Materials, London, 1997.

6   M.Korchynsky. A new role for microalloyed steels – adding economic value, *Proceedings of Vanitec International Symposium*, 13-14 October 2001, Beijing, China.

7   I.Chikushi, M.Kozaki, R.Kurahashi, M.Takahashi, A.Adachi and S.Takaoka. Ultrafine grained steel production at the New Nakayama hot strip mill, *AISI Steel Technology*, pp 42 – 48.

8   J.Majta, A.K.Zurek, M.Cola, P.Hochanadel and M.Pietrzyk. An integrated computer model with applications for austenite-to-ferrite transformation during hot deformation of Nb-microalloyed steels, *Metallurgical and Materials Transactions*, Vol. 33A, May 2002, pp 1509 – 1520.

9   M.Korchynsky. The growing role for vanadium in HSLA steels for thin-slab casting, *Metal Producing*, Vol. 11, 1998, pp 70 – 72.

10   S.Zajac. Precipitation and grain refinement in vanadium containing steels, *Proceedings of Vanitec International Symposium*, 13-14 October 2001, Beijing, China.

11   S.Zajac and R.Lagneborg, Thermodynamic model for the precipitation of carbonitrides in microalloyed steels, Swedish Institute for Metals Research, Internal Report, 1998.

12   D.T.Llewellyn. Nitrogen in steels, *Ironmaking and Steelmaking*, Vol. 20, No 1, 1993, pp 35 – 41.

13   R.Lagneborg and S.Zajac. A model for interphase precipitation in v-microalloyed structural steels, *Metallurgical and Materials Transactions*, Vol.31A, 2000, pp 261 – 273.

14   A.T.Davenport and R.W.K.Honeycombe. Precipitation of carbides at austenite/ferrite boundaries in alloy steels, *Proceedings of Royal Society*, London, 1971.

15   E.E.Blum, A.V.Grin and M.I.Goldshteyn. Dissolution and precipitation of aluminium nitride in low alloy steel, *Physics of Metals and Metallography*, Vol 21, Part 3, 1966, pp 75 – 89.

16   S.Zajac, T.Siwecki, W.B.Hutchinson and R.Lagneborg. Strengthening mechanisms in vanadium microalloyed steels intended for long products, *ISIJ International*, Vol. 38, No 10, 1998, pp 1130 – 1139.

17   W.Roberts. Hot deformation studies on a V-microalloyed steel, Swedish Institute for Metals Research, Internal Report, 1978.

18   W.Roberts, A.Sandberg and T.Siwecki. Precipitation of V(C,N) in HSLA steels microalloyed with v, *Proceedings of Conference on Vanadium Steels*, Krakow, October 1980, Vanitec, pp D1 – D12.

19   R.W.K.Honeycombe, Steels microstructure and properties, Edward Arnold Publishers, 1981.

20   C.Lewis. Simulating the rocky road with fatigue testing, *Materials World*, Vol. 12, March 1999, pp 139 – 141.

21   W.E.Heitmann, T.G.Oakwood and G.Krauss. Continuous heat treatment of automotive suspension spring steels, *Microalloyed Bar and Forging Steels*, The Minerals, Metals & Materials Society, Vol. 2, 1996, pp 431 – 453.

22   M.C.Sharma and A.Mubeen. Effect of shot size on peening intensity for local peening of different thickness samples, Maulana Azad College of Technology, Bhopal, India.

23   W.Baao, G.Zhenhuan, W.Zhunling and W.Renzhi. Effect of shot peening on fatigue behaviour of compressive coil springs, *Metal Progress*, No 6, 1952, pp 97 – 106.

24   K.J.Miller. Materials science perspective of metal fatigue resistance, *Materials Science and Technology*, June 1993, Vol. 9, pp 453 – 462.

25   S.Taira, K.Tanaka and M.Hoshina. Grain size effect on crack nucleation and growth in long-life fatigue of low-carbon steel, *Proceedings of Conference on Fatigue*, Kansas City, May 1978, ASTM STP 675 Publication, pp 135 - 162.

26   ASTM E1077 – 01. Standard test methods for estimating the depth of decarburisation of steel specimens, *Annual Book of ASTM Standards*, June 2001, pp768 – 777.

27   SAEJ419. Methods of measuring decarburisation, December 1983.

28   ASTM E18 – 84. Standard test method for Rockwell and Rockwell superficial hardness of metallic materials, *Annual Book of ASTM Standards*, 1988, pp 167 – 183.

29   ASTM E112 – 85. Standard methods for determining the average grain size, *Annual Book of ASTM Standards*, 1988, pp 277 – 301.

30   ASTM E8M – 87. Standard test methods of tension of metallic materials, *Annual Book of ASTM Standards*, 1988, pp 137 – 151.

31   ASTM A370 – 91a. Standard test methods and definitions for mechanical testing of steel products, *Annual Book of ASTM Standards*, 1992, pp 170 – 215.

32   R.W.K.Honeycombe. Transformation from austenite in alloy steels, *Metal Transformation*, Vol 7, 1976.

33   DIN 17221. Hot rolled steels for springs suitable for quenching and tempering, December 1988.

34   H.Adrian. A mechanism for effect of vanadium on hardenability of medium carbon manganese steel, *Materials Science and Technology*, Vol 15, April 1999.

35   A.P.Singh A.Prasad, K.Prakash, D.Sengupta, G.M.D.Murty and S.Jha. Influence of thermo-mechanical processing and accelerated cooling on microstructures and mechanical properties of plain carbon and microalloyed steels, *Materials Science and Technology*, Vol. 15, February 1999, pp 121 – 126.

36   P.Mitchell and T.Gladman. Vanadium in interstitial free steels, *Proceedings of 39th MWSP Conference*, Vol. 35, 1998, pp 37 – 48.

37   O.Girina and D.Bhattacharya. Effect of vanadium on mechanical properties and bake hardenability in ULC steels, *Proceedings of 41st ISS Mechanical Working and Steel Processing Conference*, October 1999, Baltimore, pp 89 – 94.

38   T.Yamamoto, R.Kobayashi, T.Ozone and M.Kurimoto. Precipitation strengthened spring steel for automotive suspensions, *Proceedings of Steels, Technology and Processing Conference*, October 1993, Philadelphia, pp 1017 – 1023.

39   J.D.Boyd, T.F.Mallis and G.Nadkami. Tempering of microalloyed spring steels, *Proceedings of SPEICH Symposium*, 1992, pp 92 – 100.

40　A.A.Karpov. Experience of v-containing spring steels production at OAO "ChMZ", *Proceedings of Conference on Vanadium Steels*, Moscow, September 2002, Vanitec, pp 34 – 42.

41　K.G.Budinski. Engineering materials, 4th Edition, Prentice-Hall, 1992.

42　G.E.Dieter. Mechanical Metallurgy, 2nd Edition, McGraw-Hill, 1982.